Alma Mater Studiorum – Università di Bologna

DOTTORATO DI RICERCA IN
MECCANICA E SCIENZE AVANZATE DELL'INGEGNERIA

Ciclo XXXV

Settore Concorsuale: 09/C2

Settore Scientifico Disciplinare: ING-IND/18

STUDY AND IMPLEMENTATION OF CONTROL STRATEGIES FOR POLYMERIZATION PROCESSES ASSISTED BY ATMOSPHERIC PRESSURE PLASMA JETS

Presentata da: Giulia Laghi

Coordinatore Dottorato

Prof. Lorenzo Donati

Supervisore

Prof. Matteo Gherardi

Esame finale anno 2023

“Happiness can be found even in the darkest of times,
if one only remembers to turn on the light.”

Albus Dumbledore

Table of contents

Abstract

In recent years, polymerization processes assisted by atmospheric pressure plasma jets (APPJs) have received increasing attention in numerous industrially relevant sectors since they allow to coat complex 3D substrates without requiring expensive vacuum systems. Therefore, advancing the comprehension of these processes has become a high priority topic of research. In this perspective, my PhD dissertation is focused on the study and the implementation of control strategies for a polymerization process assisted by an atmospheric pressure single electrode plasma jet.

The core of this dissertation is divided in two main sections, each dedicated to a specific control strategy. In the first one, a study of the validity of the Yasuda parameter (W/FM) as controlling parameter in the polymerization process assisted by the plasma jet and an aerosolized fluorinated silane precursor is proposed. The chemical and physical properties of thin films deposited under different W/FM values are characterized by means of attenuated total reflectance – Fourier transform infrared (ATR-FTIR) spectroscopy, X-ray photoelectron spectroscopy, water contact angle measurements, and scanning electron microscopy. The results of the surface characterization techniques reveal the presence of two deposition domains very well known in literature (the energy-deficient domain and the monomer-deficient domain), thus suggesting the validity of W/FM as controlling parameter. In addition, the key role of the Yasuda parameter in the process is further demonstrated since coatings deposited under the same W/FM exhibit similar properties, regardless of how W/FM is obtained.

In the second section, the development of a methodology for measuring the energy of reactions in the polymerization process assisted by the plasma jet and the vaporized precursor hexamethyldisiloxane is presented. The values of energy per precursor molecule are calculated through the identification and resolution of a proper equivalent electrical circuit, which also models the presence of parasitic effects. To validate the methodology, these energy values are correlated to the bond energies in the precursor molecule and to the properties of deposited thin films (assessed by means of ATR-FTIR spectroscopy and profilometry). It is shown that the precursor fragmentation in the discharge and the coating characteristics can be successfully explained according to the obtained values of energy per molecule. Comparing the energy per molecule values obtained with the methodology with those from the Lissajous method, it is demonstrated that a proper modeling of the parasitic effects in the circuit is crucial to achieve physically meaningful results.

Through the presentation of the obtained results and a detailed discussion of the limits and the potentialities of both the control strategies, this thesis provides useful insights into the control of polymerization processes assisted by APPJs. These insights can be valuable to support the advancing of the understanding of these unique processes, promote their implementation at industrial level, and further stimulating the research in this field.

Abbreviations

AP: atmospheric pressure

APPJ: atmospheric pressure plasma jet

ATR-FTIR: attenuated total reflectance Fourier transform infrared (spectroscopy)

DBD: dielectric barrier discharge

DR: deposition rate

HMDSO: hexamethyldisiloxane

LP: low pressure

PDMS: polydimethylsiloxane

PP: plasma polymerization

PE: polyethylene

SEM: scanning electron microscopy

TEOS: tetraethoxysilane

WCA: water contact angle

XPS: X-ray photoelectron spectroscopy.

Chapter 1

Plasma polymerization: an overview

1.1 Introduction

Plasma polymerization (PP) is a versatile technique to produce thin films with a wide range of properties on various substrates. [1]–[4] Nowadays, this technique is increasingly attractive since in many cases can constitute a great alternative to address issues encountered by conventional polymerization. [5] Indeed, PP offers unique advantages: it involves low process temperatures and reduced treatment times, can be used for monomers that do not polymerize under normal conditions, and is environmentally friendly due to the absence of solvents in the process. [3], [6], [7] Moreover, PP allows to tailor the chemical and physical properties of the deposited coatings by a judicious manipulation of the process parameters. [8] In addition, plasma polymerized thin films exhibit extremely interesting characteristics compared to the conventionally polymerized ones, such as a higher degree of cross-linking, insolubility, thermal stability, and good adhesion to most substrates. [3], [9]–[12]

Thanks to the attractive aspects mentioned above, PP has found over the years fruitful application in numerous industrial sectors, including optics, microelectronics, food packaging, and medicine [13]–[16]. For example, PP of silica barrier coatings represents a well-known strategy to decrease the gas permeation through polymeric packaging substrates by several orders of magnitude, ensuring a longer shelf-life of the packaged food. [17]

Nonetheless, PP is a highly complex process which involves various physical and chemical interaction mechanisms, some of them have yet to be fully understood. [18] For this reason, finding proper control strategies to obtain coatings with properties suitable for the target application is far from trivial and represents nowadays one of the most relevant challenges in this field.

To better understand these concepts, an overview of the PP process will be provided in this chapter.

1.2 Working principle

The fundamental actors in the production of thin films by PP are a plasma discharge and a precursor in gaseous, vaporized, or aerosolized state. [19], [20]

Plasma, also known as the fourth state of matter, is a quasi-neutral ionized gas composed of electrons, positive and negative ions, photons, and reactive species. [21] “Quasi-neutral” means that there is a balance of charges between electrons and ions, while “ionized” refers to the presence of at least one electron which is not bound to an atom or molecule, converting atoms or molecules into positively charged ions. Thanks to the existence of free electric charges (electrons and ions), plasma is also electrically conductive, internally interactive, and strongly responsive to magnetic fields. As in any gas, temperature in plasma is determined by the average energies of the plasma particles (neutral and charged) and their relevant degrees of freedom (translational, rotational, vibrational, and those related to electronic excitation). Therefore, as multi-component systems, plasmas exhibit multiple temperatures. [22]

Despite being massively present in nature (more than 99% of the visible Universe is in the plasma state), plasma discharges can also artificially be created by applying to a neutral gas an electric field sufficiently strong to provoke the *electric breakdown*, namely the process of transformation of a non-conducting material into a conductor. [23], [24]

The nature of the created plasma is defined by the temperature difference between electrons (T_e) and heavy particles (T_0), that is strictly determined by the energy exchanges between these species. Indeed, electrons, which are the lightest species in the system, first accumulate energy from the applied electric field along their mean free path and, subsequently, transfer it to heavy particles through elastic and inelastic collisions (Joule heating). When, because of these collisions, electrons and heavy particles equilibrate their temperatures ($T_e \approx T_0$), plasmas are classified as *equilibrium plasmas* (or thermal plasmas) and are characterized by macroscopic temperatures typically higher than 10000 K. When the equilibrium conditions cannot be reached because time or energy are not sufficient or there is a cooling mechanism preventing the heating of the entire gas, the temperature of the electrons is typically so much higher than the one of the heavy particles ($T_e >> T_0$) and plasmas are termed as *non-equilibrium plasmas* (or non-thermal plasmas). However, as the density of the electrons in the plasma discharge is very low compared to the density of the heavy particles, the macroscopic temperature is almost equivalent to T_0. When T_0 is close to the room temperature, these non-equilibrium plasmas are called *cold plasmas*. [22]

Plasmas involved in the thin film polymerization process are typically cold plasmas because, differently from thermal plasmas, they can interact with the substrates to be coated without inducing thermal damages. [19] This particular aspect allows to apply the PP process on a wide variety of substrates, including thermosensitive ones (e.g. polymers). [25] Moreover, cold plasmas provide highly energetic electrons, which help to produce films in a more energy-efficient manner than with other conventional techniques. [8], [18]

To reach the production of a thin film by a PP process, monomer molecules need to be introduced in the cold plasma discharge in gaseous, vaporized, or aerosolized state. Despite the interaction mechanisms between the discharge and the precursor will be described later in this text, the general explanation of the working principle of the PP process will be provided in this section.

PP consists of a set of gas phase and surface reactions guided by the plasma discharge which transform a monomer into a solid thin film. Once introduced in the discharge (typically sustained in argon or helium), the monomer is converted into reactive fragments which recombine or in gas phase (*gas phase polymerization*) or at the surface (*surface polymerization*), thus leading to the formation of the solid thin film. Contextually to these processes, etching of the already-formed coating may occur due to the ion bombardment, defining a competitive process called *ablation*. [8], [19], [26] The relative importance of these processes in the formation of the coatings depends on numerous factors, first the operating pressure.

Despite being frequently named “polymers”, plasma polymerized thin films present little resemblance to the conventional polymers since they are not characterized by the assembly of a repeating

unit but by a random network with a degree of cross-linking significatively higher than the one of conventional polymers (Figure 1.1). To easily distinguish the PP process from the conventional one, the term "precursor" would be preferable to the term "monomer" to indicate the starting material from which the coating is built. Nevertheless, both terms are currently used and accepted in the plasma community. [3], [27]

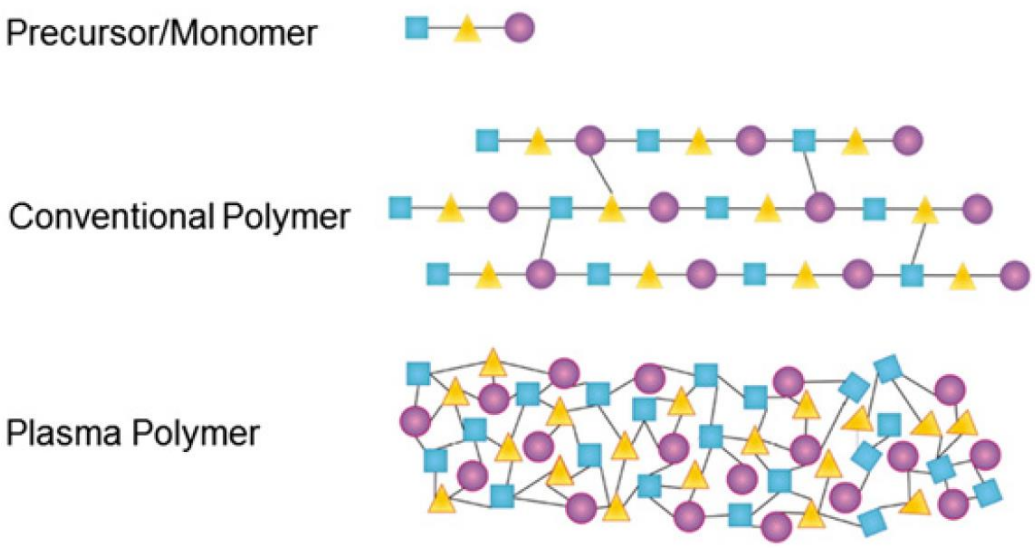

Figure 1.1: Schematic comparison of a plasma polymerized thin film and a conventional polymer obtained from the same precursor/monomer. [3]

The degree of fragmentation of the precursor in the discharge, strictly related to the degree of crosslinking of the final coating, depends on numerous factors which will be analyzed in the following.

1.3 Low pressure VS atmospheric pressure

PP was traditionally performed at low pressure (LP), around 10-100 Pa, but in recent years the interest of the research was mainly directed towards atmospheric pressure (AP) processes. [10] Both the operating pressures exhibit specific characteristics which deserve to be discussed in detail.

First, the choice of the operating pressure determines different equipment to be used for the polymerization process: at LP a closed and evacuated reactor chamber is needed, while at AP the process can be performed in open air. [28] This implies a less controlled environment in the case of AP and requires to consider possible effects due to the diffusion of the ambient air in the interpretation of the process. [29] On the other hand, the absence of expensive vacuum systems at AP represents a strong advantage from an industrial point of view since it allows to reduce the costs associated to the process, it well matches the constraints of in-line processing, and it poses no limits in the size of the substrates to be treated. [18], [27], [30]–[32]

In terms of physics of the discharge, the two operating pressures mainly differ for the mean free path of the reactive species, which is significatively shorter at AP (a few micrometers) than at LP (several millimeters). As a result, at AP the gas chemistry is more complex, and the control of the polymerization process is less straightforward. Indeed, the production of coatings with suitable characteristics for the specific application is easier at LP. [27], [33], [34] Furthermore, at LP the production of large homogeneous volumes of plasma is favored (while at AP the discharges typically exhibit a filamentary nature), with positive implications on the uniformity of the characteristics of the deposited coatings. [10], [27]

Another difference between the two operating pressures which is worthy to point out in this context is the presence of the intense ion bombardment at LP. To properly understand what ion bombardment means, a brief introduction to the concept of *sheaths* is needed. Sheaths are thin positively charged layers next to the wall surfaces which surround the plasma discharge. Since in these layers the ion density is higher than the one of the electrons, while in plasma they are almost equal (*quasi-neutrality condition*), the potential profile is positive within the plasma discharge and falls sharply to zero near the walls. In this way, the potential profile acts as a potential "hill" for ions: those ions from the plasma that enter the sheaths are accelerated into the walls. For this reason, the potential profile within the sheaths represents the key to control the ion energy and thus the intensity of the ion bombardment. [26], [34] In the initial stage of thin film growth, the presence of these high energy fluxes at LP can contribute to the cleaning and the activation of surface thus leading to improved properties of the deposited coatings, such as higher adhesion to the substrate and densification. [35], [36] Nonetheless, as specified in Section 1.2, the ion bombardment can enhance processes of etching of the deposited coating, thus having generally negative consequences on the characteristics of the deposited coatings. Since at AP the energetic ion bombardment cannot be used, due to the highly collisional nature of the sheaths, the produced coatings are typically less adherent to the substrate, the deposition rates are higher, and the ablation of deposited coatings is negligible. [27], [34]

The last difference between the two operating pressures which is mentioned in this context regards the management of the precursor in the discharge. First of all, at LP the precursor is introduced often undiluted in the discharge, while at AP the precursor is generally highly diluted (e.g. in the parts per thousand range) in a main gas which acts both as plasma gas and carrier flow. [37] Therefore, at LP the energy is mainly transferred by direct electron impact dissociation of the precursor molecules, whereas at AP a crucial role is also played by the ionization/carrier gas excited atoms which can transfer energy to the precursor molecules (Penning transfer). [38] Secondly, the precursor can be introduced in the discharge also in form of aerosols at AP, while this is not possible at LP. [18], [34] The use of aerosolized precursors determines a series of advantages which will be discussed later in this dissertation.

To conclude, AP plasma polymerization is receiving increasing attention due to the industrially relevant advantages with respect to LP. Nonetheless, obtaining coatings with characteristics suitable for

the target application is more challenging at AP because the control of the process is far from obvious, and the understanding of the mechanisms involved is less consolidated than at LP.

1.4 Factors involved in the process

Whatever the operating pressure, PP requires an optimal harmonization of numerous factors to result in thin films with tailored characteristics. The main factors involved in the process are plasma reactors, precursors, and process parameters.

1.4.1 Plasma reactors

The architecture of the plasma reactor plays a key role in determining the characteristics of the deposited thin films. Plasma reactors, home-made or commercially available, can work both at LP and AP with specific characteristics for one or the other case.

1.4.1.1 Low pressure reactors

At LP, the plasma deposition equipment typically consists of a reactor chamber, completed by the pumping system, a power supply, an electrical matching network, and the instrumentation for the control and the diagnostics of the process. [28] LP reactors can be classified based on the excitation frequency in two main categories: radiofrequency (RF) reactors and microwave (MW) reactors.

Figure 1.2 shows the schematics of two of the most used RF configurations: parallel plate plasma reactor (Figure 1.2a) and inductively coupled plasma reactor (Figure 1.2b). [28]

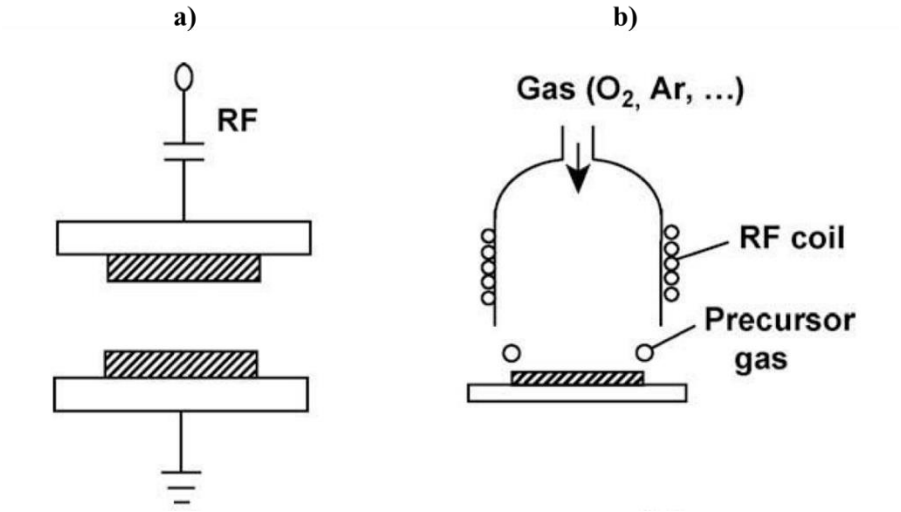

Figure 1.2: Schematics of an RF parallel plate reactor (a)) and an RF inductively coupled plasma reactor (b)). [28]

The RF system reported in Figure 1.2a recalls a typical system for plasma etching. Indeed, it exhibits the same main components: an RF-driven electrode, a grounded electrode, and a blocking

capacitor to couple the RF power supply to the system. [39] Likewise for reactive ion etching (RIE) systems, also in a parallel plates reactor the dimensions of the electrodes and their connections to RF power supply and ground can be properly selected to induce a bias voltage and strengthen the ion bombardment. While in RIE strengthening the ion bombardment serves to strongly increases the etch rate, in the case of parallel plate reactors this can contribute, for example, to the densification of the coating. [26], [35]

Figure 1.3 illustrates two examples of parallel plate reactors in which the introduction of the reaction gases and evacuation paths are different. [40]

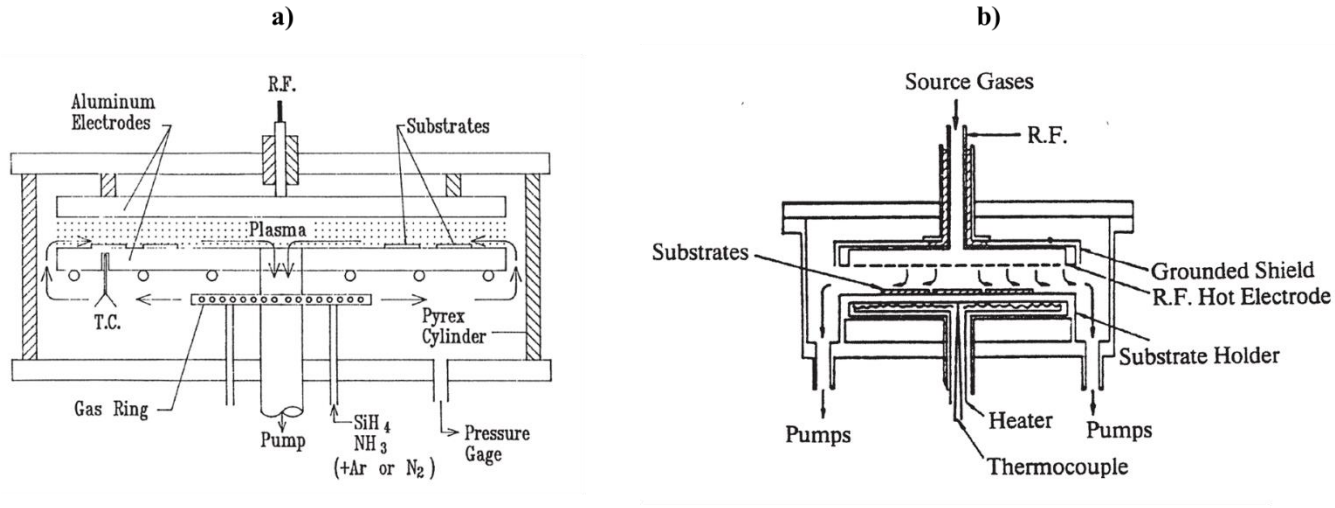

Figure 1.3: Two examples of parallel plate reactors: a) the reaction gas flows radially, b) the reaction gas is introduced by a shower. [40]

In the reactor reported in Figure 1.3a, the reaction gases are introduced through small holes drilled in a metal ring, which is situated beneath the substrate holder. Gas is passed over the substrates and is evacuated through a tube located in the centre of the substrate holder. The substrate holder plate can be rotated to improve the uniformity of the film in terms of thickness.

In the reactor presented in Figure 1.3b, the reaction gas is uniformly supplied to the substrates from many small holes in the RF electrode, like a shower. The chamber is evacuated downward through the space between the substrate holder and the chamber walls.

The main difference between an RF inductively coupled plasma reactor (Figure 1.2b) and a parallel plate one is the absence of metallic electrodes in the former case, which ensures a higher purity of the discharge. Indeed, in RF inductively coupled plasma reactors the plasma excitation is typically provided by a coil which is external to the insulating tube. [28] The insulating tube is usually realized in glass, quartz, or alumina and the working frequencies of the most commonly used power supplies range from 13.56 to 35 MHz. [39] Despite being easy to be assembled, the scale up for industrial applications of inductively coupled reactors is difficult. [40]

Figure 1.4 reports an example of an RF inductively coupled reactor, which includes a heater in the substrate holder. The purpose of this element is to increase the temperature of the substrates, thus

localizing the polymerization reactions on the substrates and favouring the densification of the deposited coatings. [40]

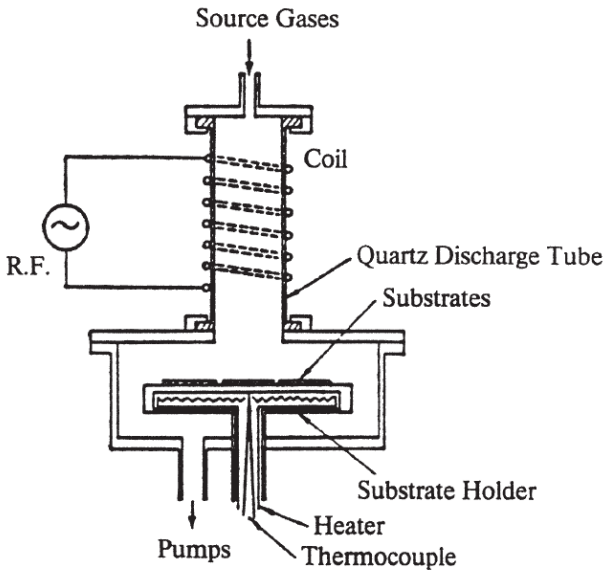

Figure 1.4: Example of an inductively coupled reactor. [40]

In MW reactors, the substrate is placed on a grounded or electrically floating substrate holder, facing a MW window (made of low water-content fused silica or alumina) through which the MW power (typically at a 2.45 GHz frequency) is supplied using different MW applicators. [28], [39] The schematics of different MW reactors are shown in Figure 1.5.

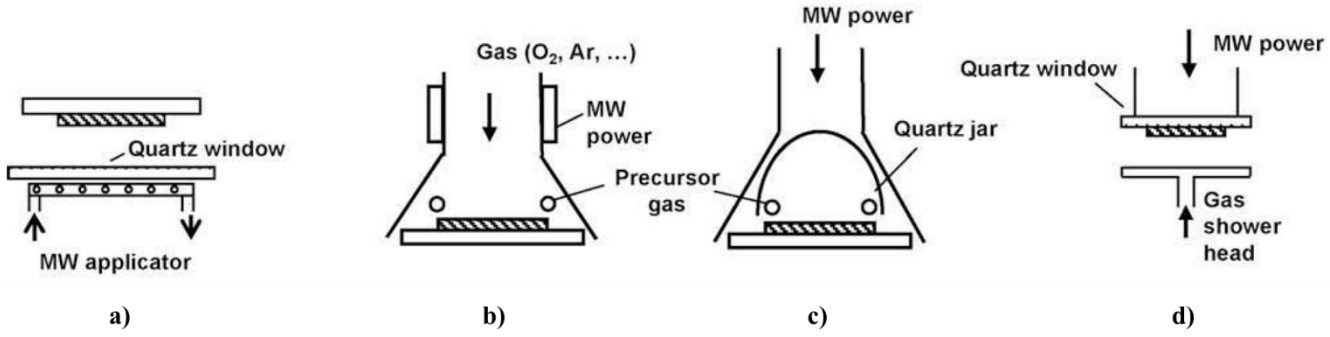

Figure 1.5: Schematics of different MW reactor configurations: a) linear applicator, b) remote MW excitation, c) horn antenna, d) plasma impulse CVD. [28]

As a general feature, MW discharges are characterized by higher electron densities which favour the precursor fragmentation and lead to substantially higher deposition rates than plasmas at lower excitation frequencies. [28], [35]

To combine the advantages of both MW and RF, a dual-mode MW/RF plasma reactor has been developed by Martinu et al. [41] As reported in the schematic in Figure 1.6, the substrates are placed on the RF-powered substrate holder facing the MW quartz window, through which the MW power is applied using a linear slow wave applicator. [42]

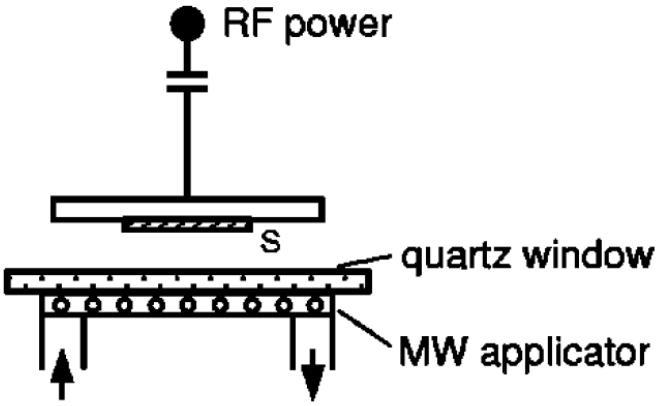

Figure 1.6: Schematic of a dual mode MW/RF reactor. [42]

1.4.1.2 Atmospheric pressure reactors

The most used configurations for PP at AP can be divided in two main categories: planar dielectric barrier discharges (DBDs) and jets. In DBDs plasma is generated between two planar electrodes and the substrate is confined within the generation zone, while in jets plasma is generated within a cylindrical body and then directed towards the substrate by means of a flow of gas. As an example, pictures of both the plasma sources are reported in Figure 1.7.

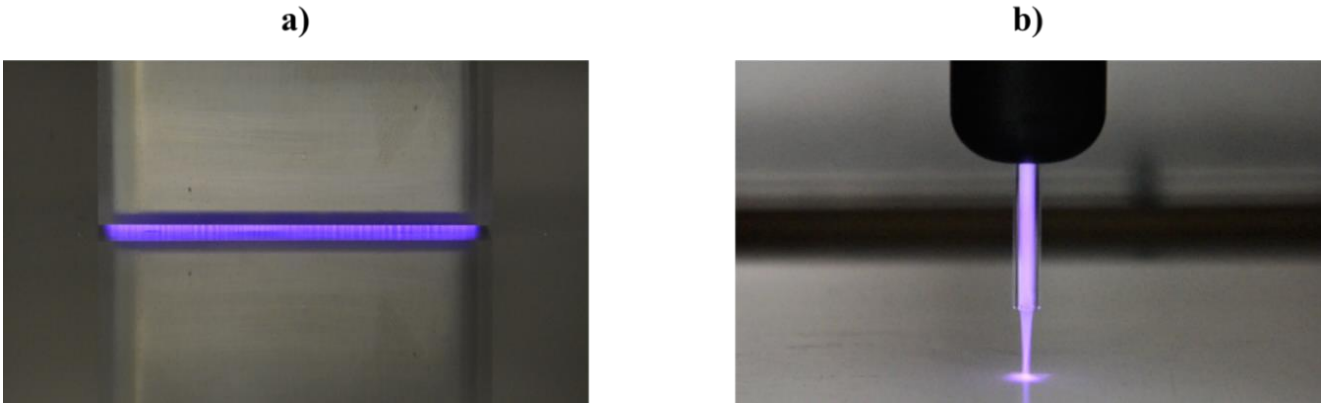

Figure 1.7: Pictures of atmospheric pressure plasma sources: a) DBD, b) jet. Both pictures were acquired in the Laboratories of the Research Group for Industrial Applications of Plasmas (University of Bologna, Italy).

A description of the characteristics of both the configurations will be provided in the following.

Planar DBDs

A typical DBD plasma source, whose schematic is shown in Figure 1.8, is composed of two planar electrodes (one connected to the high voltage generator and one grounded) and at least one dielectric barrier. [43] The dielectric barrier, generally made of an insulating material such as glass, quartz, or ceramics, prevents the transition to a thermal plasma discharge (*arc-like discharge*), which would otherwise occur between two uncovered metal electrodes. [44] The space between the electrode

and the dielectric (or between the two dielectrics), in which the plasma discharge takes place, is called *gas gap* and its amplitude is typically in the range of 0.1–10 mm. In most studies and applications, planar DBDs are operated with sinusoidal high voltages in the kHz range but in recent years their use have been extended also to pulsed or RF signals. [45]

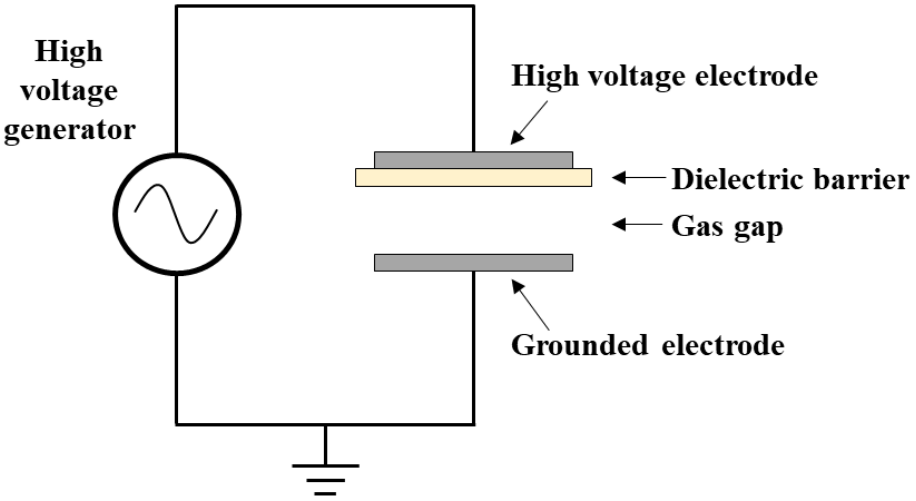

Figure 1.8: Schematic of a typical planar DBD.

To understand the working principle of a planar DBD, it is useful to analyze its equivalent circuit (Figure 1.9).

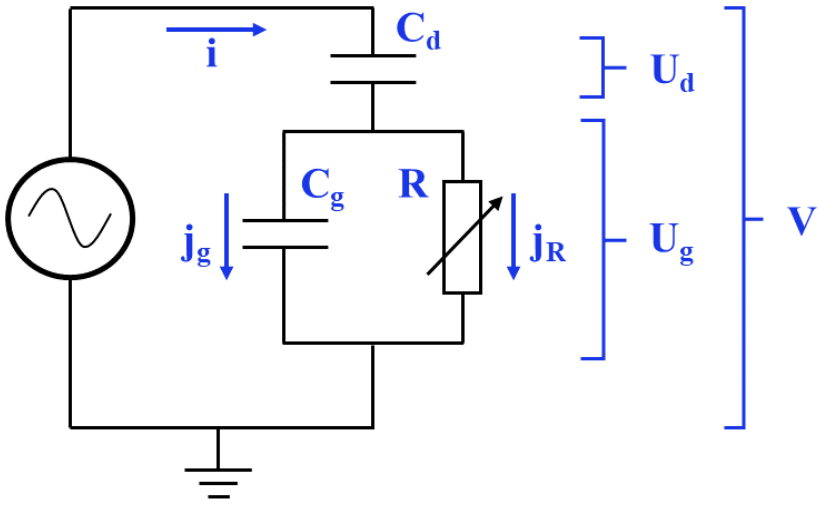

Figure 1.9: Equivalent circuit of a typical planar DBD.

In the equivalent circuit, the dielectric barrier is represented as a capacitor C_d, and the gas gap as a parallel connection of a gas gap capacitor C_g and a time-dependent current source or resistor R, which represents the discharge. $U_d(t)$ is the voltage across the dielectric barrier (defined as the ratio between

the charges accumulated at the dielectric Q(t) and C_d), while $U_g(t)$ is the gas gap voltage. V(t) and i(t) are the applied voltage and the total current, respectively; i(t) contains the current associated with charge transfer in the gas gap (the active current j_R) and the displacement current in the gas gap (j_g).

The working principle of a planar DBD is characterized by alternating active and passive phases. During the *passive phase*, the active current does not flow through R and the plasma source behaves as a capacitor C_{cell}, where C_{cell} is the result of the serial connection of C_d and C_g. During the *active phase*, the current flows through R, C_g is bypassed, and the plasma source behaves as a capacitor C_d.

The active phase starts when $U_g(t)$ overcomes the *breakdown voltage*, namely the voltage required to ignite a plasma discharge. The values of breakdown voltage for each gas can be derived by the Paschen curves (reported in Figure 1.10) which show the values of the breakdown voltage as function of the product of the operating pressure (p) and the distance between the electrodes (d). [22]

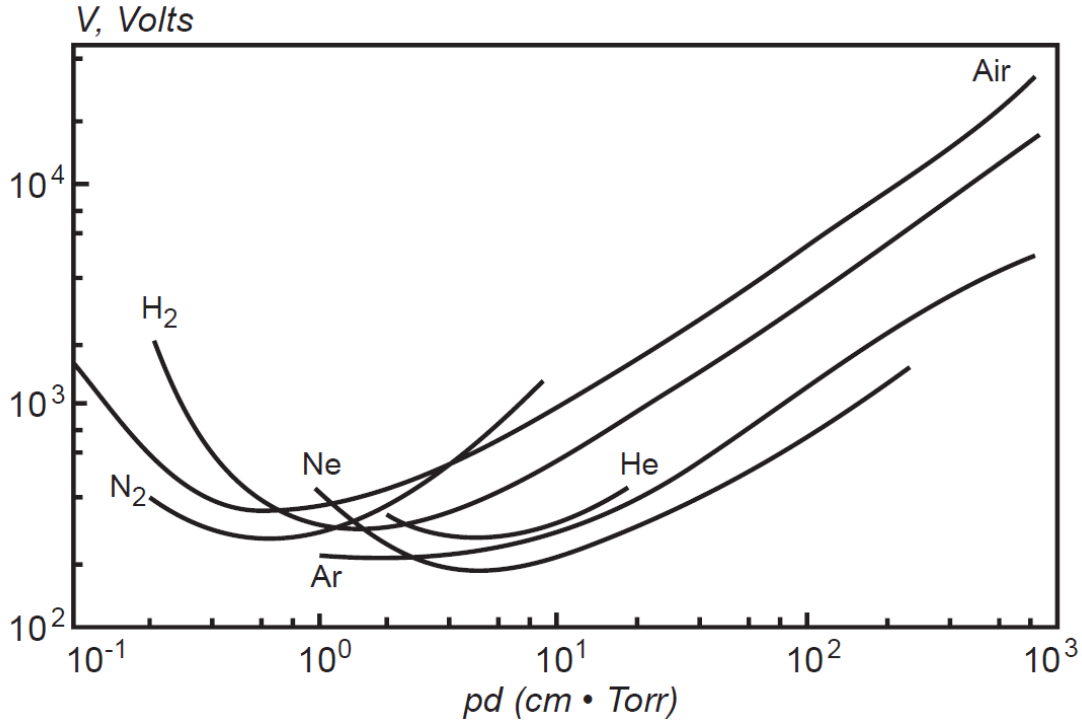

Figure 1.10: Paschen curves for different gases. [22]

When the breakdown voltage is reached, the charging of the dielectric surfaces occurs, thus inducing an electric field opposed to the applied electric field. When the increase of V(t) does not compensate the screening of the electric field by the charges deposited over the dielectric surfaces ($U_d(t)$), $U_g(t)$, which can be expressed as the difference between V(t) and $U_d(t)$, falls to the discharge extinguish voltage and the passive phase begins. For the next discharge ignition (active phase), the applied voltage must be increased further, or the polarity must be changed. This is the reason why planar DBDs are always driven by AC or pulsed voltage signals. [43], [45]

Since the working principle of planar DBDs has been clarified, the following will be focused on the relevant characteristics of these plasma sources in the context of PP.

One of the advantages of this configuration is the unprecedent flexibility with respect to geometrical configuration, working gas mixture composition, and operating parameters (e.g. power input, excitation frequency, and gas flow rates). [46] This feature allows to produce coatings with significatively different properties, thus strongly widening the spectrum of possible applications for these plasma sources. Moreover, as the area of the electrodes can be increased without compromising the characteristics of the discharge, planar DBDs are suitable for large-area treatments, easing the scale-up at industrial level of the polymerization processes optimized in laboratory. [30], [34], [47]

On the other hand, the narrow gaps (0.1-10 mm) typical of planar DBDs limit their use mainly to 2D substrates. Furthermore, planar DBDs at atmospheric pressure usually operate in the so-called *filamentary mode*, meaning that the breakdown is initiated in a large number of independent current filaments or microdischarges randomly distributed over the dielectric surfaces. [46], [47] In PP processes, a homogenous discharge, instead of a filamentary one is highly preferable since it allows to avoid inhomogeneities in the deposited coatings. [20] On this topic, it has been demonstrated that homogeneous (also called *glow*) discharges can be obtained with planar DBDs under special and restrictive conditions. [48]–[50]

In addition to these general aspects, some characteristics strictly related to the specific planar DBD configuration deserve to be discussed. Figure 1.11 shows three main categories of DBD designs classified through their gas injection system: lateral (1.11a), central (1.11b), and showerhead (1.11c). [51]

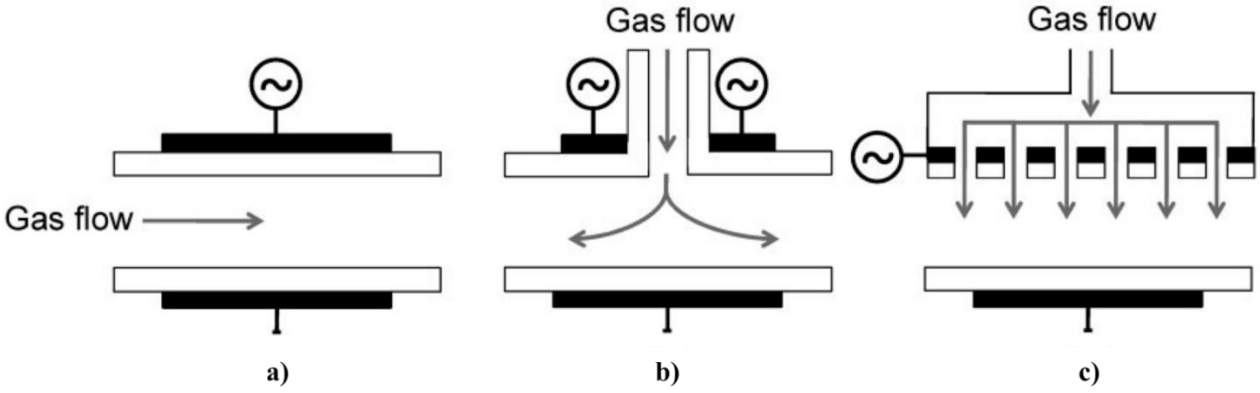

Figure 1.11: Examples of planar DBD configurations with different gas injection systems: a) lateral, b) central, c) showerhead. [51]

The lateral and central gas injection configurations (Figure 1.11a and 1.11b) are the most common ones. From a constructive point of view, the configuration with the central gas injection (Figure 1.11b) is the simplest one because the same elements constitute both electrodes and the gas injection system. In terms of operation, both the configurations require a proper movement of the substrate holder to obtain

uniform thin films on a large scale. For example, in the case of the gas lateral injection, the substrate holder must be moved parallel to the gas flow direction, which has the effect of ‘‘averaging’’ the film properties and guaranteeing uniform thicknesses on the whole surface.

The showerhead configuration (Figure 1.11c) consists of gas injection through one of the electrodes and uniformly directs the reactive species on the substrate to be treated. This configuration limits severe gradients in coating thickness due to lateral gas injection, but it makes more complicated to get homogeneous properties at the whole surface scale.

Jets

Various configurations of plasma jets have been reported in literature in PP literature, most of them working with noble gas, such as argon or helium. [34], [52] These plasma jet configurations can be classified into three main categories: dielectric-free electrode (DFE) jets, dielectric barrier discharge (DBD) jets, and single electrode (SE) jets. [52]

- **DFE jets**. A DFE jet, whose typical schematic is reported in Figure 1.12, consists of an inner electrode coupled to the plasma source and a grounded outer electrode. The noble gas is fed into the anular space between the two electrodes. Several characteristics of this configuration are presented in the following. If stable operation conditions are not met, arcing can occur in this configuration. Moreover, compared with DBD jets, the power delivered to the plasma is much higher in DFE jets, thus inducing higher gas temperature of the plasma discharge. Therefore, this kind of jet is suitable for PP on substrates which are not very sensitive to high temperatures.

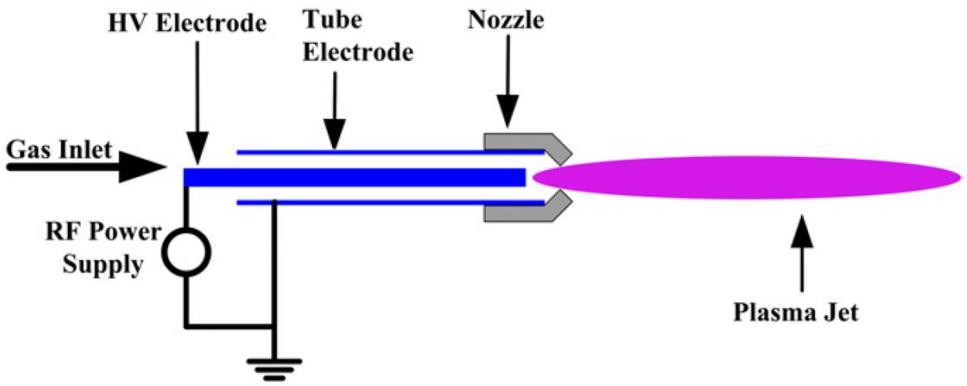

Figure 1.12: Schematic of a DFE jet. [52]

- **DBD jets**. The characteristic feature of DBD jet is the presence of a dielectric component. There are many different configurations of DBD jets, which differ for the assembly of the electrodes and the dielectric components. Figure 1.13 shows a schematic of one of these possible DBD jet configurations. This DBD jet consists of a dielectric tube with two metal ring electrodes on the outer side of the tube: one connected to the power supply, and one connected to the ground. When a working gas flows through the dielectric tube and a sufficiently high voltage is provided by the

power supply, the plasma discharge is ignited and propagates into the surrounding air. This configuration, as the others not presented in this context, can be operated, for example, by kHz AC power or by pulsed DC power and can reach length of the plasma jet of several centimetres. Its main advantage is the use of the dielectric component which avoids the risk of arcing and keeps the gas temperature of the plasma close to room temperature, thus enabling the plasma polymerization treatment on thermosensitive materials.

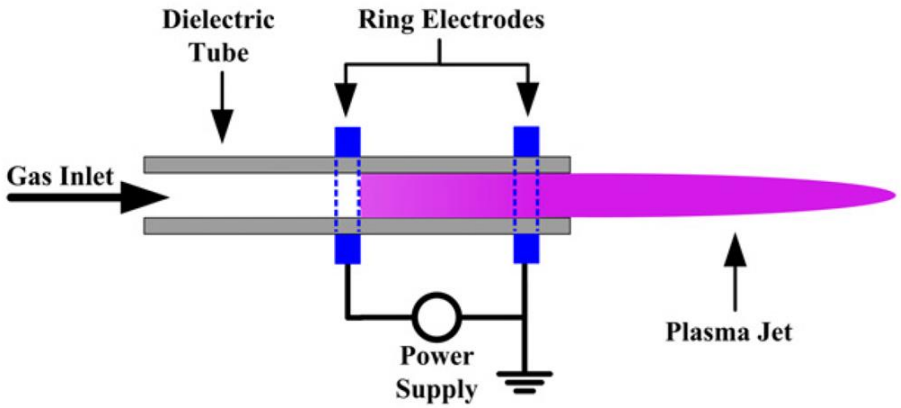

Figure 1.13: Schematic of a DBD jet. [52]

- **SE jets**. A SE jet is characterized by the presence of a single powered electrode. As an example, Figure 1.14 reports a schematic of this configuration. It consists of one rod or needle electrode located in the centre of the dielectric tube and connected to the power supply (e.g. kHz AC or pulsed and RF). Differently from the DBD jet configuration, the dielectric tube only plays the role of guiding the gas flow. In this configuration, the grounded electrode is not included in the body of the plasma source and it can be totally absent (in this case, due to the high potential in the powered electrode, the substrate itself is seen as the "ground plane") or physically placed outside (e.g. a grounded plane beneath the substrate to be treated). [53]

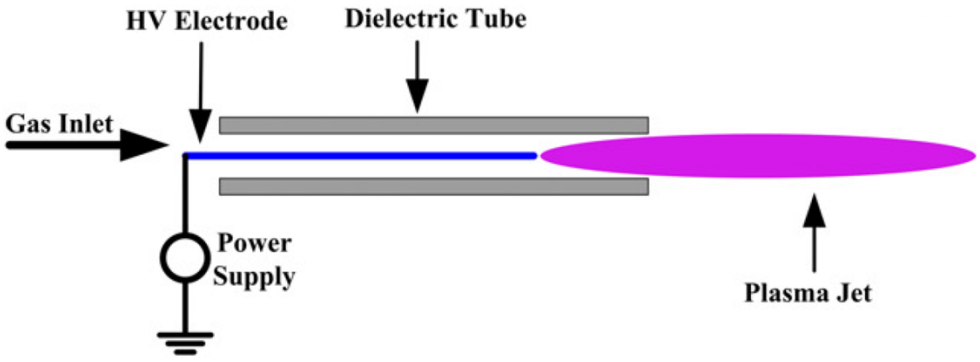

Figure 1.14: Schematic of a SE jet. [52]

Nowadays, plasma jets are increasingly attractive in the field of PP because of specific advantages with respect to planar DBDs. First, as the substrate is not confined between the electrodes, plasma jets can be used to coat complex 3D objects, without limitations in the size of the object to be treated. [52], [54] Furthermore, as the deposition spot can be scaled down to the submillimeter range and the plasma plume can reach length of several centimeters, plasma jets can be employed also for localized treatments on the inner surface of 3D objects, like trenches or cavities or capillary tubes. [34], [55]

On the contrary, the typical configuration of a plasma jet allows to perform exclusively single-spot deposition treatments, thus making complex their industrial applicability for the coating of large area surfaces. [51] It is necessary to specify that plasma jets can be properly moved to create patterns and cover larger areas, but this can lead to inhomogeneities in the final coating. Furthermore, for those plasma jets in which the powered electrode is located inside the plasma source, undesired PP can occur on the electrode and negatively affect the performance of the plasma source. [56]

1.4.2 Precursors

A PP process is accomplished by adding into the discharge a precursor which can be gaseous, vaporized, or aerosolized. [51] As the characteristics of the coating are mainly determined by the nature of the precursor, the choice of a proper precursor is crucial to obtain coatings suitable for the specific application. [57]

Since the number of precursors reported in PP literature is extremely large [3], [58], a single family of precursors will be presented as an example in this context: the organosilicons. Organosilicons provide a large variety of possible reactants for PP processes because numerous compounds of this family are sufficiently volatile near room temperature, characterized by low toxicity, non-flammable, cheap, and available from commercial sources. [20], [59] The main feature of these precursors, as the name suggests, is the presence of carbon and silicon atoms in the molecular structure. Due to their organic-inorganic character, organosilicons can lead to the deposition of organic coatings as well as inorganic coatings, thus resulting extremely appealing for numerous applications. [20]

Among the organosilicon precursors, hexamethyldisiloxane (HMDSO) is often preferred for PP (both at AP and LP) because it exhibits a rather high vapor pressure and is safe to handle. [36] The chemical structure of HMDSO, reported in Figure 1.15, shows a central core, composed of two silicon atoms and one oxygen atom, and six methyl groups.

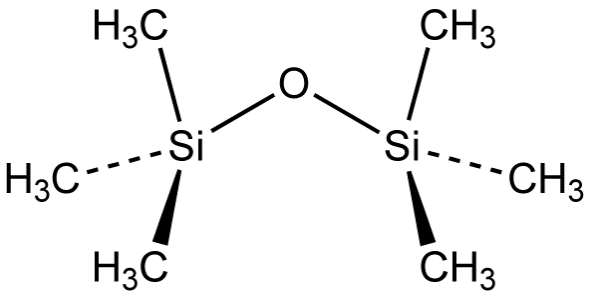

Figure 1.15: Chemical structure of HMDSO.

By properly varying the deposition conditions (i.e. following strategies which will be explained in detail in the next sections), HMDSO plasma-polymerized thin films can assume an organic chemical composition similar to polydimethylsiloxane (*PDMS-like* coatings) or an inorganic one similar to silicon dioxide, SiO_2 (*silica-like* coatings). As can be noticed from the chemical structures reported in Figure 1.16, the structure of PDMS resembles the pure repetition of the HMDSO starting unit, while silicon dioxide (silica) does not exhibit the functional groups typical of HMDSO, thus suggesting two different degrees of fragmentation of the precursor in the discharge to reach these chemical compositions.

a) **b)**

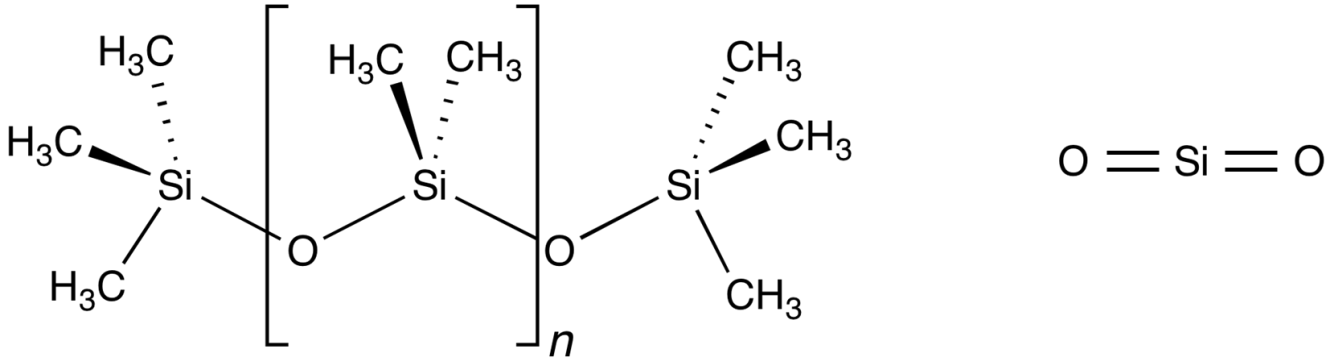

Figure 1.16: Chemical structures of a) PDMS and b) silica.

PDMS-like coatings are industrially attractive because their hydrophobic character plays an important role in diverse applications such as self-cleaning surfaces, microfluidics, and biomedical applications. [60] On the other hand, silica-like coatings have a great industrial potential as well since they can be used, for example, as gas barrier layers in the food packaging sector, or as layers resisting corrosion in the fabrication of photovoltaic solar cells, or as dielectric layers in the microelectronic field. [58], [61]

Regardless of the nature, also the physical state of the precursor plays a key role in the definition of the characteristics of the resulting coatings. As explained in Section 1.3, at LP the precursor can be added to the discharge exclusively in gaseous or vaporized state, while at AP it can be introduced also in aerosolized state.

Nowadays, aerosolized precursors are gaining increasing attention since they offer numerous advantages with respect to the vaporized ones. First, the use of aerosolized precursors leads to a considerable simplification of the PP experimental set-up. Indeed, as aerosols are usually generated by an atomizer, no heating systems, or special solutions to vaporize the liquid precursors are required. This aspect, combined with the possibility to have virtually no limits in the nature of the precursor (also non-volatile precursors can be aerosolized), greatly increases the potential of the technology at an industrial level. [51], [62] Moreover, aerosolized precursors appear particularly appealing for PP processes aimed to create biofunctional thin films. In fact, it has been proven that when a precursor solution containing biomolecules is atomized and introduced in the plasma discharge, the droplets protect biomolecules from the harsh plasma conditions and contribute to preserve their structure. [63]

Nonetheless, coupling an aerosol with a plasma induces several mechanisms which must be considered to reach a proper control and comprehension of the polymerization process. Since nowadays there is a significant lack of basic understanding concerning these mechanisms, a deep investigation in the field is highly required. [62], [64] The presence of liquid droplets may induce modifications of the plasma discharge. Indeed, the propagation of streamers can be significatively disturbed by the local modification of the electric field due to droplets polarization and charging, thus resulting in a variation of the local rate of ionization. The intensity of these effects depends on droplet characteristics (e.g. permittivity and particle size distribution). [65]–[67] Plasma discharge, in turn, may alter the characteristics of the liquid droplets entering the plasma region, by inducing charging, deformation, or evaporation. [68], [69] Hence, in the study of biphasic aerosol–plasmas the extremely transient and dynamic nature of aerosols should be carefully considered.

It is important to stress that the physical state of the precursor determines its interaction with the plasma discharge: in form of liquid droplets, the precursor structure is protected from the action of the energetic species in the plasma, while in form of molecules in vapor phase (or in gaseous phase), the precursor structure is directly exposed to the plasma discharge. This results in a minor fragmentation of the aerosolized precursor and in a consequent formation of thin films characterized by a higher retention degree of precursor molecular structure but a lower degree of crosslinking compared to those obtained starting from vaporized precursors. [51] A lower degree of crosslinking typically has a negative impact on the thin film stability upon immersion, which is a critical aspect for those polymerization processes aimed to produce coatings, for example, to be used in the biomedical field. Over the years, several strategies have been proven successfully to improve the degree of crosslinking of thin films deposited starting from aerosolized precursors. For example, it is known that the reduction in the size particle distribution increases the area exposed to plasma discharge thus favouring the precursor fragmentation. [53]

1.4.3 Process parameters

The chemical and physical properties of the deposited coating are strongly affected by the selected deposition parameters (e.g. excitation frequency, substrate temperature, and air content). [3] In this section an overview of the most investigated process parameters is presented.

Excitation frequency

The excitation frequency of a plasma source can be used to tailor the characteristics of the deposited coatings. An example on this subject is provided by da Silva Sobrinho et al. [35] who combined a MW-excited plasma (2.45 GHz) and a capacitively coupled RF plasma (13.56 MHz) to produce transparent barrier coatings on polyethylene terephthalate (PET). The dual-mode MW/RF reactor used in this work (whose schematic description was reported in Section 1.4.1.1) is shown in Figure 1.17a. The reactor can be operated also with a single excitation frequency (single-mode). SiO_2 films are grown from a mixture of HMDSO, Ar, and O_2 and are continuously deposited on PET substrate transported by a motor-driven roll-to-roll system.

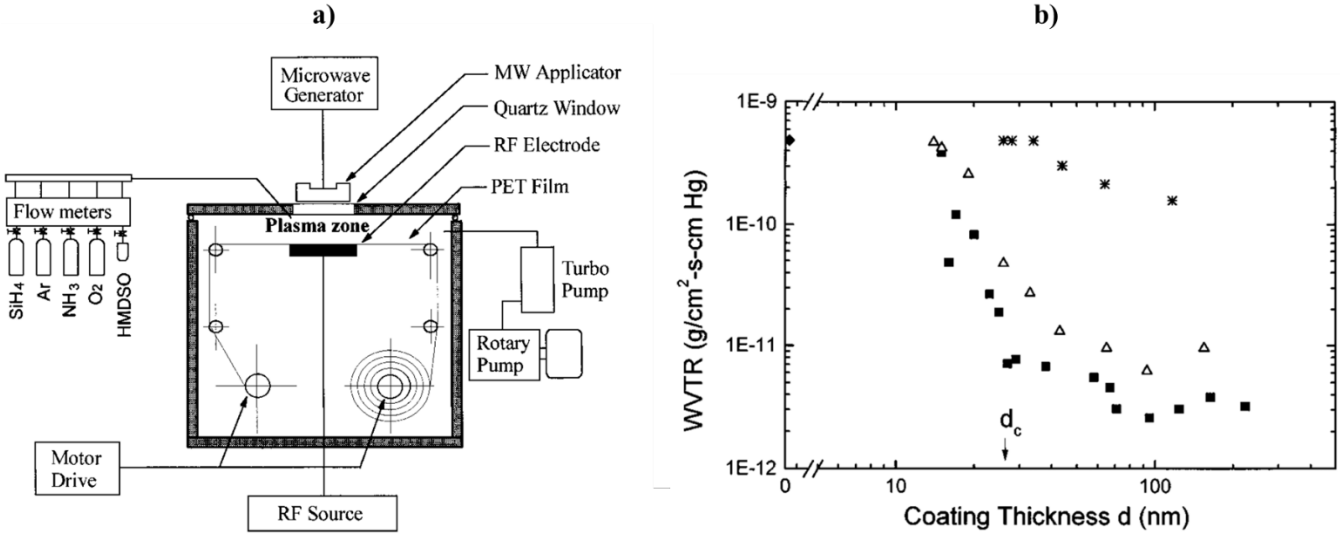

Figure 1.17: a) Schematic top view of the dual-frequency MW/RF reactor, b) WVTR as a function of coating thickness for SiO_2 coatings deposited on PET, using three different plasma modes: MW/RF (black squares), MW (stars), RF (white triangles). The black rhombus indicates the WVTR of the uncoated PET. [35]

As mentioned in Section 1.4.1,1, MW discharges are typically characterized by high electron densities which favour the monomer fragmentation and give rise to substantially higher deposition rates than plasmas at lower frequencies. On the other hand, RF plasmas offer the possibility to strengthen the ion bombardment (increasing the flow and the energy of the impinging ions), thus enabling the deposition of dense coatings. As can be seen from the graph in Figure 1.17b, the dual-mode MW/RF reactor clearly combines these advantages. The graph shows the water vapour transmission rate (WVTR) as a function of the coating thickness for coatings deposited in three different plasma modes: MW/RF (black squares), MW (stars), and RF (white triangles). In the case of MW/RF, a more pronounced drop in the WVTR can

be observed as the thickness increases, suggesting improved coating barrier properties thanks to the combination of the two frequencies. The coatings deposited by MW plasmas alone exhibit very poor moisture barrier characteristics because of their high porosity which favours the passage of water vapour molecules.

Substrate temperature

Besides ion bombardment, another possible strategy to obtain dense coatings is increasing the substrate temperature. On this topic, Babayan et al. [70] demonstrated the densification of silicon oxide coatings deposited on p-type silicon substrates by heating the substrate holder from 115 to 350 °C. The plasma source used in this work (Figure 1.18a) is an atmospheric pressure DFE-jet in which plasma is generated by applying RF power at 13.56 MHz to the centre electrode. Coatings are deposited on silicon wafer located at 1.7 cm from the plasma source using helium and oxygen as main gases and vaporized tetraethoxysilane (TEOS) as precursor.

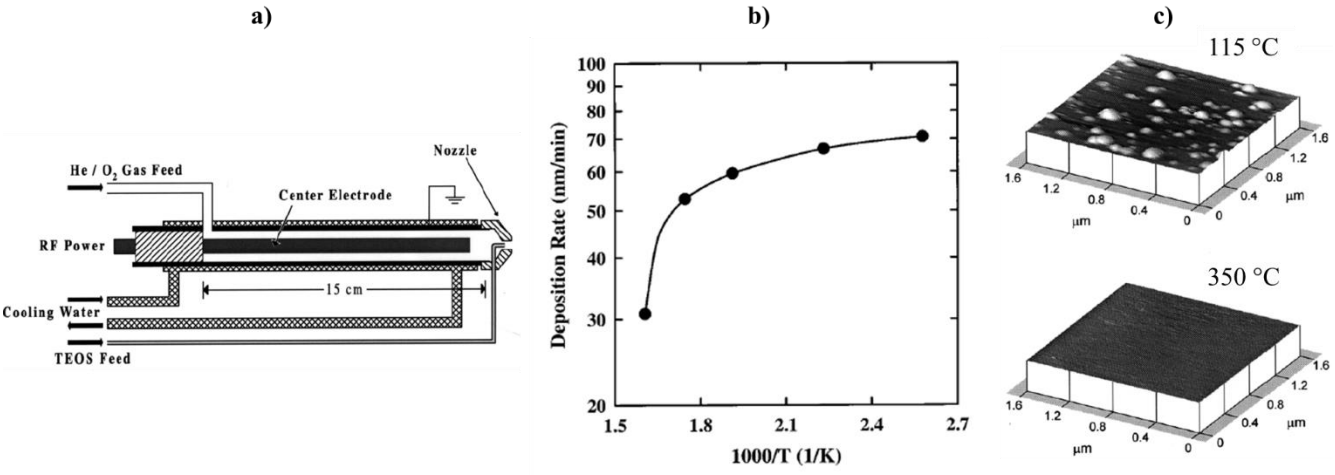

Figure 1.18: a) Schematic of the atmospheric pressure plasma jet; b) Deposition rate as a function of the substrate temperature; c) Atomic force micrographs of coatings grown at surface temperature of 115 and 350 °C. [70]

From the graph in Figure 1.18b, it can be clearly noticed that as the substrate temperature increases, the deposition rate (defined as the coating thickness divided per the deposition time) decreases, suggesting a progressively higher densification of the coatings. These results are also supported by atomic force micrographs of films grown at surface temperature of at 115 and 350 °C (Figure 1.18c) which show a much smoother face at higher temperatures. Indeed, at high temperature the hydroxyl incorporation is reduced, thus leading to a decreased porosity of the coating.

Nonetheless, it must be pointed out that heating of the substrates is a solution which is exclusively suitable for non-thermosensitive materials. In fact, thermosensitive ones (e.g. polymers) may be damaged by the high temperatures involved.

Air content

Over the years, many researchers focused their attention on studying of the influence of the air content in the feed mixture on the chemical and physical properties of the deposited coatings. Among these, Morent et al. showed how the air addition can be used to produce coatings from HMDSO with a SiO_2 chemical composition. [20] The setup employed in their work, reported in Figure 1.19a, includes an AP planar DBD operated at 50 kHz where the deposition is carried out with a fixed argon flow (3 slpm) and a variable air content (0-50 sccm). The concentration of vaporized HMDSO in the carrier gas is kept constant at 3 ppm and coatings are grown on PET films.

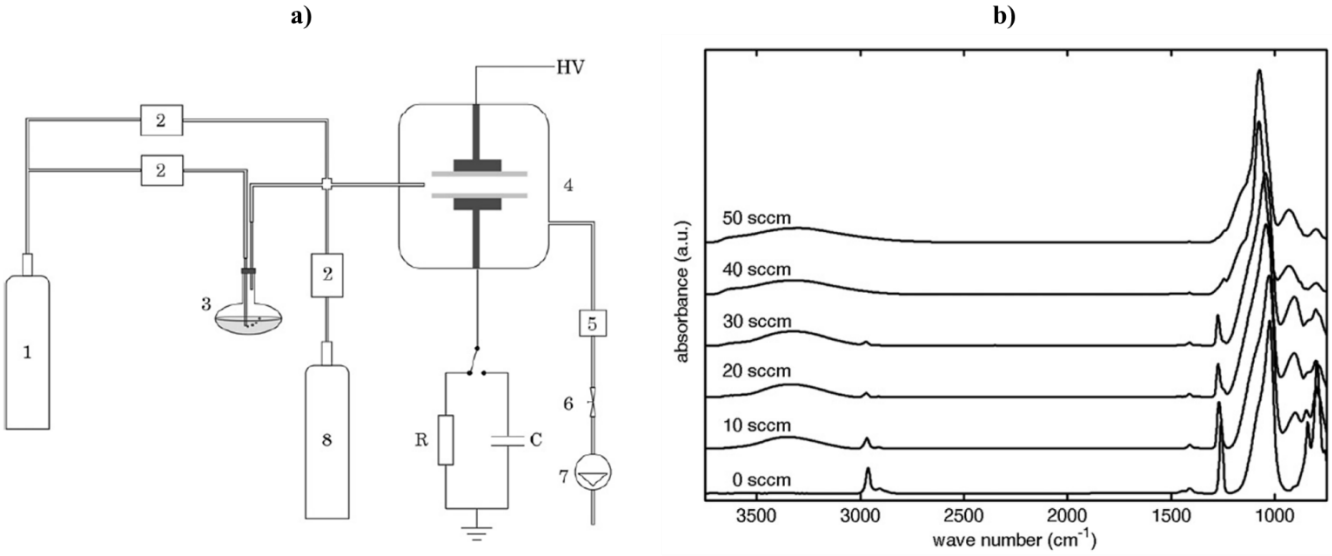

Figure 1.19: a) Schematic of the experimental setup; b) ATR-FTIR spectra of HMDSO plasma-polymerized coatings in pure argon and argon/air mixtures with various air flows. [20]

Figure 1.19b displays the ATR-FTIR (attenuated total reflectance – Fourier transform infrared) spectra of plasma-polymerized HMDSO films deposited with different air flow rates. When PP is performed in pure argon, coatings exhibit a chemical structure close to PDMS, characterized by a peak at 1020 cm^{-1} assigned to Si-O-Si stretching vibrations and numerous peaks associated to the functional groups of HMDSO (i.e. methyl groups), such as the CH_3 stretching at 2965 cm^{-1}, the CH_3 deformation vibrations at 1260 cm^{-1}, and the CH_3 rocking vibrations at 850 cm^{-1} and 800 cm^{-1}.

As the air content in the mixture is increased, peaks associated to methyl groups gradually decrease until they disappear and the Si-O-Si peak shifts towards higher wavenumbers (1050 cm^{-1}). Furthermore, spectra show new absorption bands at 3700-3100 cm^{-1} and 926 cm^{-1}, which correspond to Si-OH stretching and bending, respectively. This behavior highlights that the addition of increasing air in the mixture leads towards SiO_2 coatings.

Main gas flow rate

The flow rate of the main gas is a process parameter which strongly determines the fluid dynamics conditions in the discharge zone, thus influencing the polymerization process. Caquineau et al. gave evidence to this claim showing the effects of a variable flow rate on the characteristics of the deposited coatings. [71] The plasma source used in this work (Figure 1.20a) consists of a diffuser which injects the gas mixture perpendicularly to two pairs of metallized alumina plates onto which the silicon substrate is placed. The geometry of the plasma source forces the gas mixture to flow parallel to the substrate on both sides of the injection. When a sufficiently strong high voltage is applied, the simultaneous generation of two symmetric discharge zones on each side of the gas injection occurs. Thin films are deposited starting from a mixture of N_2 (main gas), silane (SiH_4) or HMDSO (precursors), and N_2O (oxidation agent).

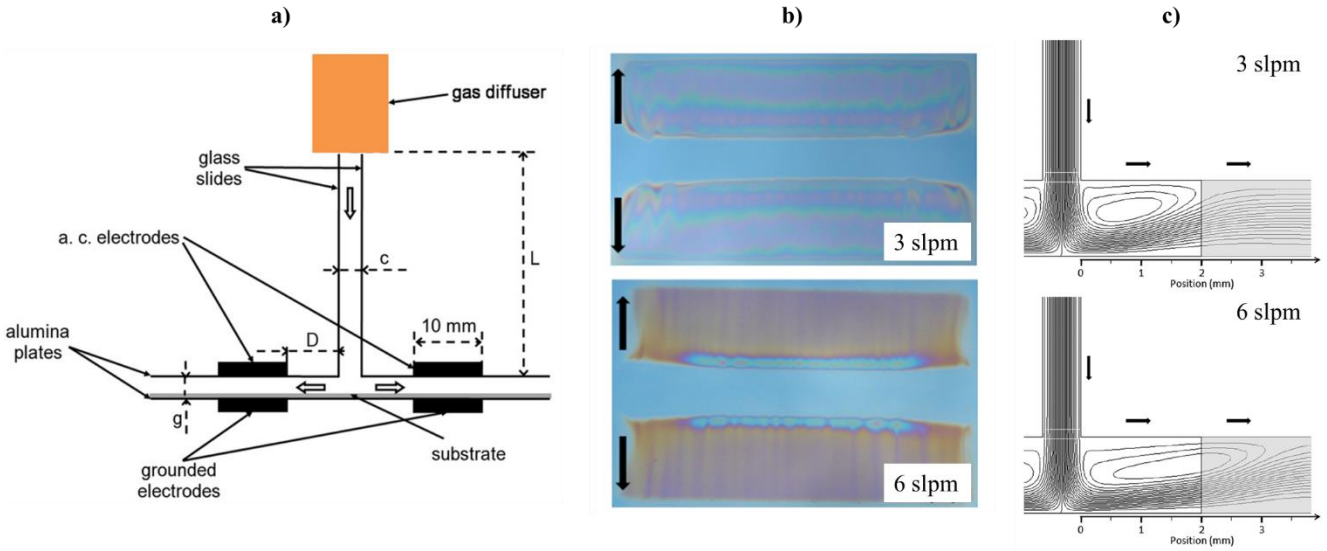

Figure 1.20: a) Schematic of the perpendicular injection discharge reactor; b) Photographs of coatings obtained from silane at 3 slm and 6 slpm of N_2 (black arrows indicate the gas flow direction); c) calculated flow streamlines at 3 slpm and 6 slpm of N_2. The discharge zone is shaded in grey. [71]

Photographs of coatings deposited from silane at 3 slpm and 6 slpm of N_2 are reported in Figure 1.20b, where the black arrows indicate the gas flow direction. At 6 slpm the layer is clearly less uniform along the width than at 3 slpm, with deposition spots (lighter zones characterized by higher deposition rates) located at the entrance of the discharge zones. To find the link between the increase in the flow rate and the appearance of deposit non-uniformities, the authors calculated the gas velocity by CFD simulations. The resulting streamlines are reported in Figure 1.20c (the discharge zone is shaded in grey). Despite for both the flow rates gas recirculation takes place just at the right angle defined by the vertical glass slides and the upper alumina plates, the higher flow rate leads to a larger recirculation zone and to a deeper penetration of the recirculation into the discharge zone. The recirculation induces a longer residence time of the gases in the discharge zone and negatively affects the quality of the deposited coatings.

Discharge power

The discharge power is strictly related to the precursor fragmentation in the discharge, thus representing an important process parameter to modify the properties of the deposited coating. On this subject, Morent et al. investigated the effects of varying the discharge power in a polymerization process from a mixture of argon and vaporized HMDSO. [13] Using the same experimental setup reported in Figure 1.19a, they performed tests at three different discharge power levels (5.8, 9.5 and 15.2 W) for a fixed HMDSO concentration (3.0 ppm).

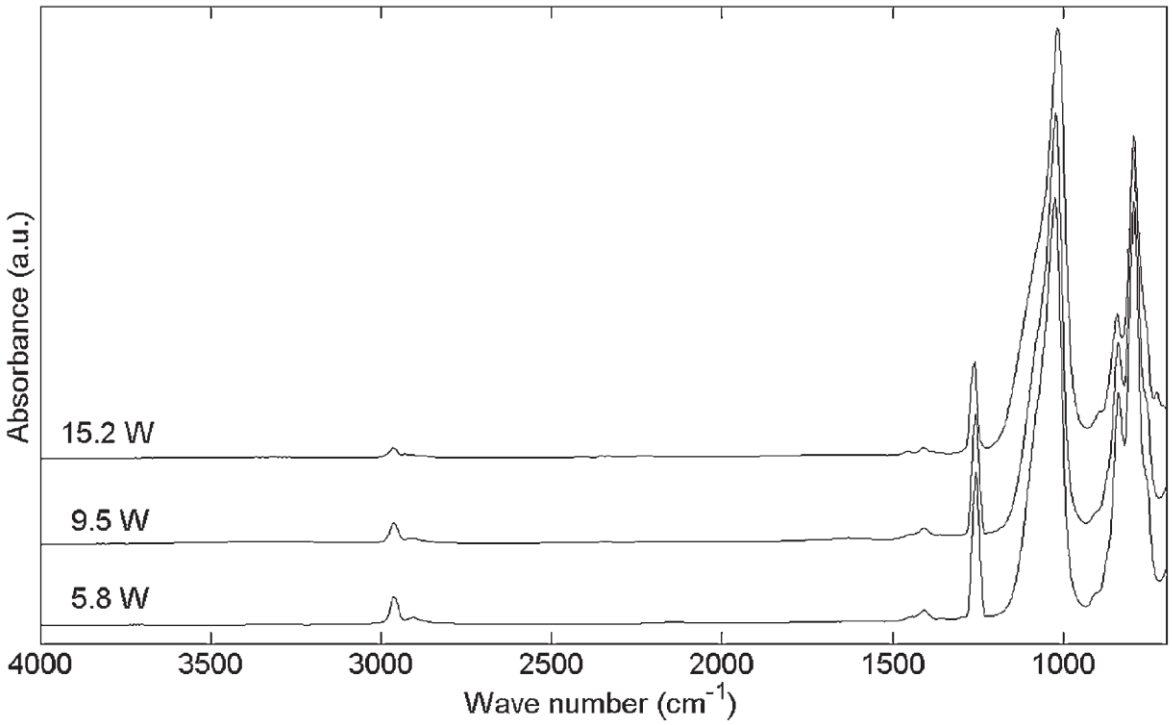

Figure 1.21: ATR-FTIR spectra of coatings deposited for different discharge powers. [13]

The work shows how higher discharge powers lead to more intense fragmentation processes in the discharge which result in coatings with lower retention of functional groups of the starting precursor. Indeed, from the ATR-FTIR spectra displayed in Figure 1.21 it can be noticed how the peaks related to CH_3 at 2965 cm^{-1}, at 1260 cm^{-1}, and at 850 cm^{-1} tend to become less pronounced as the discharge power increases.

Despite being an interesting strategy to produce coatings with little resemblance of the initial precursor, excessively increasing the discharge power may cause thermal stress and damaging of the substrate.

Precursor flow rate

The precursor flow rate is another process parameter which can have a significant effect on the characteristics of the deposited coating. In the same work mentioned above to discuss about the discharge power, Morent et al. investigated the properties of thin film when varying the HMDSO flow rate. [13] In this case, the plasma polymerization process was performed using three different monomer concentrations (1.3, 3.0, and 4.0 ppm) at a fixed discharge power of 9.5 W.

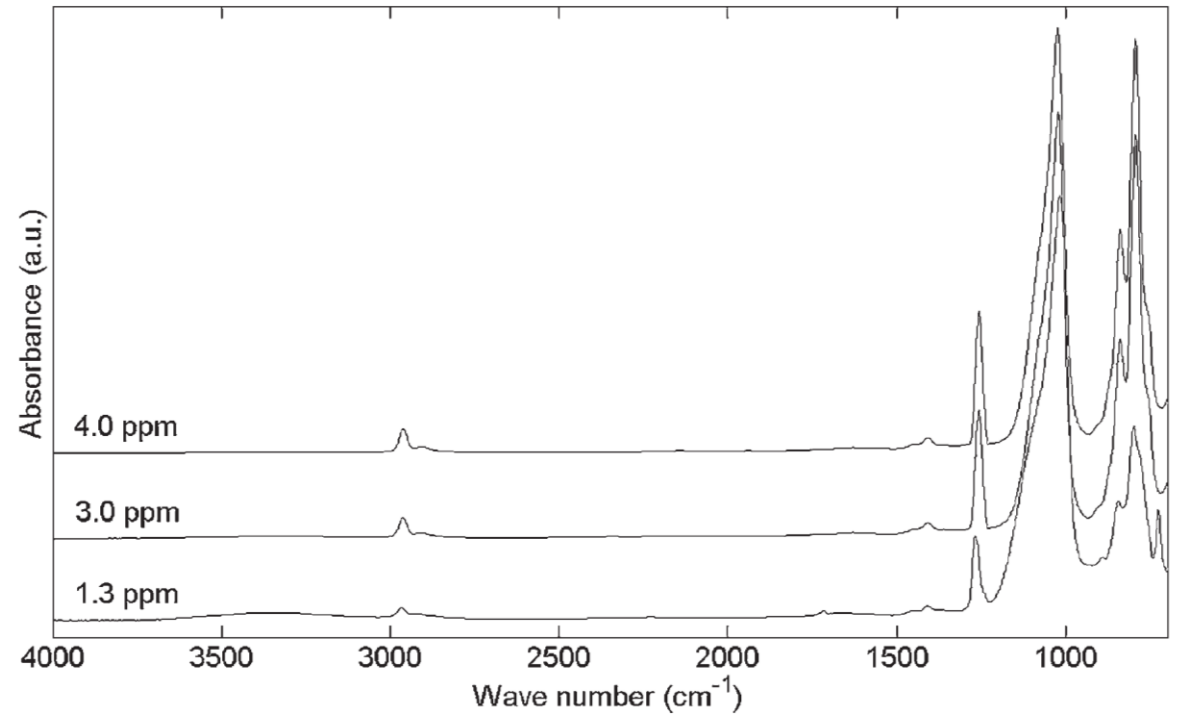

Figure 1.22: ATR-FTIR spectra of coatings deposited for different precursor flow rates. [13]

As the monomer concentration increases, an opposite trend with respect to the one observed for an increase of discharge power can be noticed in the ATR-FTIR spectra (Figure 1.22): higher monomer flow rates correspond to a higher conservation in the coating of the functional groups of the starting precursor. Indeed, methyl-related peaks at 2965 cm^{-1}, 1260 cm^{-1}, and 850 cm^{-1} become progressively more pronounced and the Si-O-Si asymmetric stretching shifts towards lower wavenumbers.

Besides the chemical composition, the precursor flow rate can also affect the morphological characteristics of the coatings. For example, it has been previously reported in literature of plasma polymerization of organosilicon precursors that high precursor flow rates can lead to the formation of particles in the coatings. [72], [73]

1.5 Control strategies for the process

Considering the PP mechanisms, the most important factor affecting the properties of a deposited coating is the energy applied per molecule, which governs the degree of precursor fragmentation in the discharge. [3] Therefore, all the PP control strategies proposed over the years in the scientific community are strongly related to this concept. This section offers a general description of the most relevant control strategies for PP processes.

1.5.1 The Yasuda parameter

In the context of LP plasma polymerization, Yasuda proposed the composite parameter W/(FM) (in J/kg), later named Yasuda parameter, which relates the discharge power (W, in J/s) to the product of the precursor molar flow rate (F, in mol/s) and the precursor molecular weight (M, in kg/mol). [74], [75]

As can be seen from the measurement unit, this parameter represents an energy input per unit mass of precursor, thus being strictly connected to the precursor fragmentation process: low W/FM values result in a reduced fragmentation of the precursor molecules and consequently in a higher retention of precursor functional groups in the deposited thin films, while higher values lead to an intense fragmentation of the precursor molecules and therefore to a loss of precursor functional groups in the films. The described behaviors correspond to different operating regions in PP which can be identified by plotting the thin film deposition rate (DR) as a function of W/FM, as shown by Figure 1.23. [76], [77]

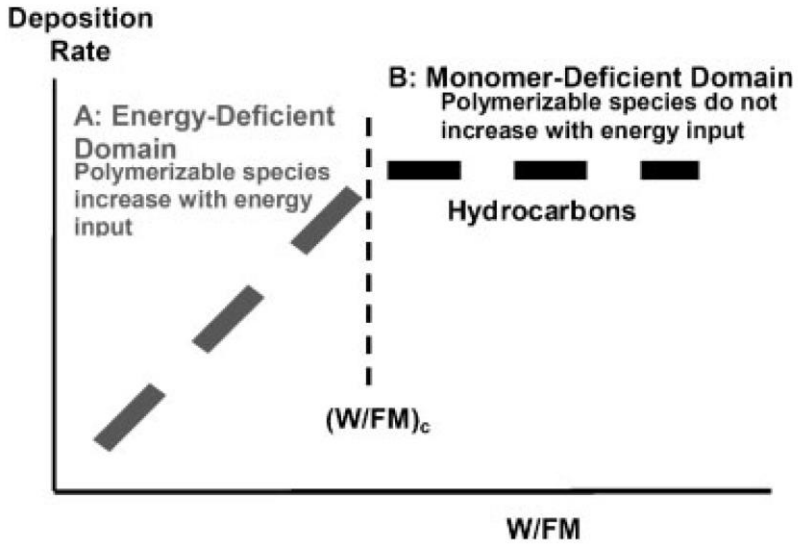

Figure 1.23: Deposition rate as a function of W/FM illustrating different deposition domains. [77]

At low W/FM, the DR evolves linearly with W/FM. In this region, the so-called “energy-deficient region”, ample monomer is available, and the supply of energy is the limiting factor for increasing the

DR. In this region, increasing the supply of energy in the discharge results in an increase in the concentration of film-forming species through collisional processes. Above a critical W/FM value $(W/FM)_c$, the DR becomes constant since the precursor fragmentation has attained its maximum. This region is called "monomer-deficient region", as sufficient energy is provided, but the precursor feed rate into the chamber is the limiting factor. [77] In addition, under high energy conditions, ion-induced reactions can be favored, thus leading to a decrease in the DR. [3]

The Yasuda parameter was extensively used in PP processes at LP but over the years several research groups attempted to extend its application also to the AP case. [1], [11], [13], [73], [78], [79] Nonetheless, the validity of W/FM as a control parameter at AP has been questioned because, differently from LP processes, 1) the precursor is usually highly diluted (typically in parts per thousand) in a ionization/carrier gas which takes part in the mechanisms of energy transfer to the precursor molecules and 2) it is not often possible to measure the discharge power with reasonable precision. [37], [80] Furthermore, some authors experimentally proved how, at AP, W/FM do not necessarily provide deposits of the same chemistry and morphology, unlike in LP processes. [73]

For these reasons, the validity of the Yasuda parameter as a process controlling parameter for polymerization processes at AP should be demonstrated on a case-by-case basis.

1.5.2 The macroscopic approach

The concept of Yasuda parameter was further developed by Hegemann et al. who offered a macroscopic description of PP which implies a unifying dependence of the deposition rate per unit of monomer flow (R_m/F) to W/F trough the quasi-Arrhenius expression:

$$\frac{R_m}{F} = G exp\left(-\frac{E_a}{\frac{W}{F}}\right), \tag{1.1}$$

where G is a reactor-depending geometrical factor related to the maximum conversion of the precursor into film growth and E_a the apparent activation energy required to initiate chemical reactions in the active zone. According to this approach, the plasma is divided into an active zone in which the activation takes place through collisional processes leading to the production of film forming species and a passive zone where the deposit is formed. [81]–[83]

Since a detailed explanation of this approach would require also complex mathematical and physical reasonings which are beyond the purpose of this general overview, the concise description of the approach given by Thiry et al. is proposed in the following. [3]

A typical example of an Arrhenius-type plot ($\ln(R_m/F)$ versus the inverse specific energy, $(W/F)^{-1}$), is shown in Figure 1.24 for the PP of methane. It can be noticed that $\ln(R_m/F)$ evolves linearly with $(W/F)^{-1}$ pointing to an Arrhenius-like behavior over the range of W/F investigated. In this regime, the film grows mainly through radical reactions and the kinetic limiting factor is the production rate of the film-forming species in the plasma.

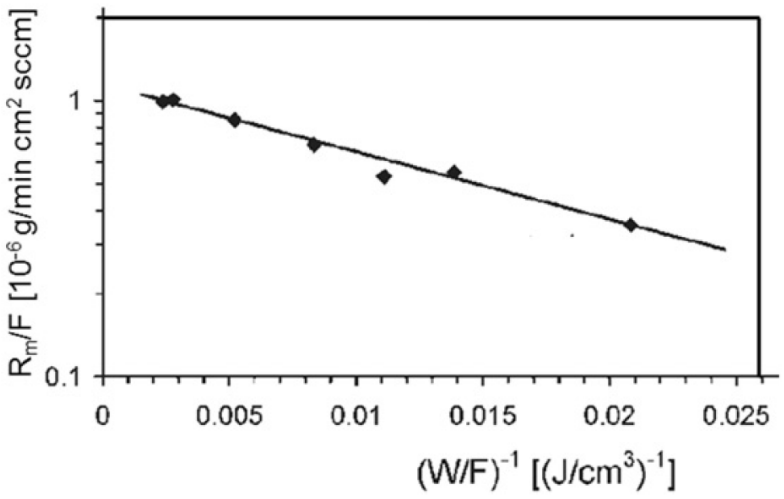

Figure 1.24: Arrhenius-like plot of the deposition rate versus the inverse energy input for a methane discharge. [3]

The above presented equation holds for many monomers and gas mixtures for a certain range of W/F. From the negative slope of the linear fit in Figure 1.24, the energy of activation, E_a, which is related to an ensemble of fragmentation reactions in the active zone, can be deduced. Its value is monomer specific and correlates with the bond dissociation energy of the precursor, thus allowing the interpretation of the precursor fragmentation mechanisms in the discharge. Compared to the Yasuda approach, the activation energy separates the PP into the energy and monomer deficient regime. When applied to several families of plasma polymerized thin films for a broad range of energy conditions, the macroscopic approach has revealed that more than the two deposition regimes presented above have to be considered depending on the PP system. This could be related to different growth mechanisms.

Although the macroscopic approach has shown its potential for describing the PP process, defining the plasma polymer formation mechanism based on the evolution of the R_m/F as a function of $(W/F)^{-1}$ in an Arrhenius-type plot is not straightforward and could lead to erroneous conclusions without additional data from, for example, plasma diagnostic measurements.

1.5.3 The *energy delta* methodology

In recent years, Nisol et al. proposed a methodology for measuring the energy absorbed per precursor molecule in AP plasma polymerization processes assisted by planar DBDs and argon as carrier gas. [37], [84]

Through the identification and resolution of a proper equivalent electrical circuit model (Figure 1.25), this methodology allows the calculation of the energy dissipated per cycle of applied sinusoidal voltage, E_g, according to the following formula:

$$E_g = \frac{\int V_{gap} I_d dt}{n}, \tag{1.2}$$

where V_{gap} is the effective voltage across the gas gap, I_d is the discharge current, and n is the number of complete cycles at the applied voltage frequency.

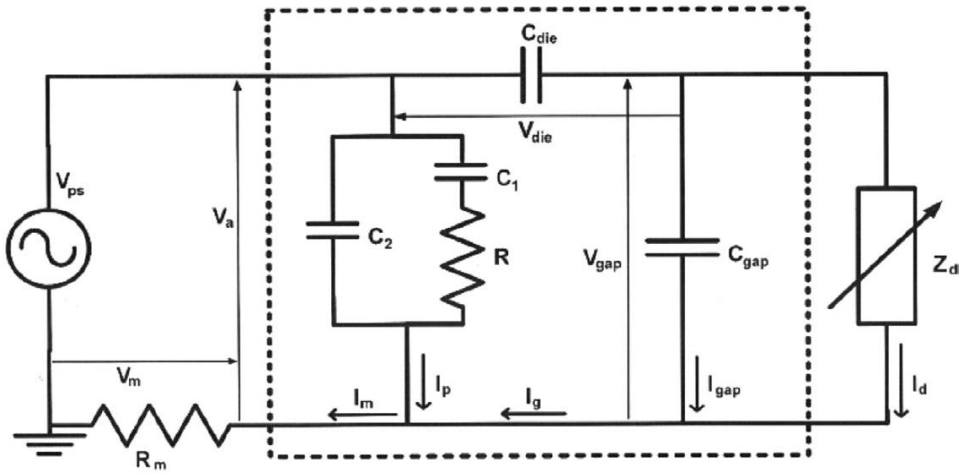

Figure 1.25: Equivalent electrical circuit (the portion in the dashed rectangle represents the DBD discharge cell). [37]

The main idea behind this methodology is that the *delta of energy*, ΔE_g, (calculated as the energy difference between energies in pure and doped Ar), represents the energy effectively provided to the precursor flow rate and can be used to derive the values of energy per molecule, E_m. The validation of this methodology has been performed by correlating the E_m values with the chemical and physical characteristics of coatings deposited from different families of gaseous and vaporized precursors. [85]–[91]

Considering these aspects, it appears clear that this methodology shows interesting potentialities in the field of AP plasma polymerization since it overcomes some limitations of the use of the Yasuda parameter such as the complexity of obtaining reliable discharge power values and distinguishing the amount of energy effectively provided to the precursor molecules.

Despite being validated for different families of precursors, this methodology is still limited to the context of planar DBDs and to gaseous and vaporized precursors. Nevertheless, as shown in Section 1.4.1.2, atmospheric pressure plasma jets (APPJs) are gaining interest in PP processes since they are suitable for the coating of complex three-dimensional geometries and for the possibility to scale down the dimension of the spot treatment to the submillimeter range. At the same time, as at AP the precursor can be injected into the discharge in liquid phase, aerosolized precursors are increasingly used because of the specific advantages with respect to the vaporized ones, such as the lower complexity of the experimental setup and the less intense fragmentation of the precursor molecules in the discharge (see Section 1.4.2).

1.6 References

[1] A. Kakaroglou, G. Scheltjens, B. Nisol, I. De Graeve, G. Van Assche, B. Van Mele, R. Willem, M. Biesemans, F. Reniers, and H. Terryn, "Deposition and characterisation of plasma polymerised allyl methacrylate based coatings," *Plasma Process. Polym.*, vol. 9, no. 8, pp. 799–807, 2012, doi: 10.1002/ppap.201100162.

[2] P. Cools, N. De Geyter, E. Vanderleyden, F. Barberis, P. Dubruel, and R. Morent, "Adhesion improvement at the PMMA bone cement-titanium implant interface using methyl methacrylate atmospheric pressure plasma polymerization," *Surf. Coatings Technol.*, vol. 294, pp. 201–209, 2016, doi: 10.1016/j.surfcoat.2016.03.054.

[3] D. Thiry, S. Konstantinidis, J. Cornil, and R. Snyders, "Plasma diagnostics for the low-pressure plasma polymerization process: A critical review," *Thin Solid Films*, vol. 606, pp. 19–44, 2016, doi: 10.1016/j.tsf.2016.02.058.

[4] S. Van Vrekhem, R. Morent, and N. De Geyter, "Deposition of a PMMA coating with an atmospheric pressure plasma jet," *J. Coatings Technol. Res.*, vol. 15, no. 4, pp. 679–690, 2018, doi: 10.1007/s11998-018-0049-4.

[5] J. Carneiro de Oliveira, M. de Meireles Brioude, A. Airoudj, F. Bally-Le Gall, and V. Roucoules, "Plasma polymerization in the design of new materials: looking through the lens of maleic anhydride plasma polymers," *Materials Today Chemistry*, vol. 23. Elsevier Ltd, Mar. 01, 2022, doi: 10.1016/j.mtchem.2021.100646.

[6] R. Jafari, S. Asadollahi, and M. Farzaneh, "Applications of plasma technology in development of superhydrophobic surfaces," *Plasma Chem. Plasma Process.*, vol. 33, no. 1, pp. 177–200, 2013, doi: 10.1007/s11090-012-9413-9.

[7] J. Carneiro de Oliveira, A. Airoudj, P. Kunemann, F. Bally-Le Gall, and V. Roucoules, "Mechanical properties of plasma polymer films: a review," *SN Appl. Sci.*, vol. 3, no. 6, 2021, doi: 10.1007/s42452-021-04655-9.

[8] M. Henini, *Handbook of Thin-Film Deposition Processes and Techniques*, vol. 31, no. 3. Noyes Publications, 2000.

[9] Y. Sawada, S. Ogawa, and M. Kogoma, "Synthesis of plasma-polymerized tetraethoxysilane and hexamethyldisiloxane films prepared by atmospheric pressure glow discharge," *J. Phys. D. Appl. Phys.*, vol. 28, no. 8, pp. 1661–1669, 1995, doi: 10.1088/0022-3727/28/8/015.

[10] N. De Geyter, R. Morent, S. Van Vlierberghe, P. Dubruel, C. Leys, L. Gengembrec, E. Schacht, and E. Payen, "Deposition of polymethyl methacrylate on polypropylene substrates using an atmospheric pressure dielectric barrier discharge," *Prog. Org. Coatings*, vol. 64, no. 2–3, pp. 230–237, 2009, doi: 10.1016/j.porgcoat.2008.07.029.

[11] M. Asandulesa, I. Topala, V. Pohoata, and N. Dumitrascu, "Influence of operational parameters on plasma polymerization process at atmospheric pressure," *J. Appl. Phys.*, vol. 108, no. 9, 2010, doi: 10.1063/1.3506528.

[12] J. Petersen, R. Bechara, J. Bardon, T. Fouquet, F. Ziarelli, L. Daheron, V. Ball, V. Toniazzo, M. Michel, A. Dinia, and D. Ruch, "Atmospheric plasma deposition process: A versatile tool for the design of tunable siloxanes-based plasma polymer films," *Plasma Process. Polym.*, vol. 8, no. 10,

pp. 895–903, 2011, doi: 10.1002/ppap.201100022.

[13] R. Morent, N. De Geyter, T. Jacobs, S. Van Vlierberghe, P. Dubruel, C. Leys, and E. Schacht, "Plasma-polymerization of HMDSO using an atmospheric pressure dielectric barrier discharge," *Plasma Process. Polym.*, vol. 6, no. SUPPL. 1, pp. 537–542, 2009, doi: 10.1002/ppap.200931101.

[14] P. E. C. Tan, C. L. S. Mahinay, I. B. Culaba, O. K. M. Streeter, and M. R. A. Hilario, "Plasma polymerization of styrene using an argon-fed atmospheric pressure plasma jet," *J. Vac. Sci. Technol. B*, vol. 36, no. 4, p. 04I102, 2018, doi: 10.1116/1.5030840.

[15] M. A. Gilliam, S. A. Farhat, G. E. Garner, B. P. Stubbs, and B. B. Peterson, "Characterization of the deposition behavior and changes in bonding structures of hexamethyldisiloxane and decamethylcyclopentasiloxane atmospheric plasma-deposited films," *Plasma Process. Polym.*, vol. 16, no. 7, 2019, doi: 10.1002/ppap.201900024.

[16] I. Muro-Fraguas, A. Sainz-García, R. Múgica-Vidal, E. Sainz-García, A. González-Marcos, and F. Alba-Elías, "Low-friction coatings on medical needles through atmospheric-pressure plasma-polymerization technology," *Plasma Process. Polym.*, 2022, doi: 10.1002/ppap.202200174.

[17] P. Scopece, A. J. Viaro, R. Sulcis, I. Kulyk, A. Patelli, and M. Guglielmi, "SiO_x-based gas barrier coatings for polymer substrates by atmospheric pressure plasma jet deposition," *Plasma Process. Polym.*, vol. 6, no. SUPPL. 1, pp. 705–710, 2009, doi: 10.1002/ppap.200931707.

[18] H. J. Jang, E. Y. Jung, T. Parsons, H. Tae, and C. Park, "A Review of Plasma Synthesis Methods for Polymer Films and Nanoparticles under Atmospheric Pressure Conditions," *Polymers (Basel).*, vol. 13, no. 2267, 2021, doi: https://doi.org/10.3390/polym13142267.

[19] T. Desmet, R. Morent, N. De Geyter, C. Leys, E. Schacht, and P. Dubruel, "Nonthermal Plasma Technology as a Versatile Strategy for Polymeric Biomaterials Surface Modification : A Review," vol. 10, no. 9, 2009, doi: 10.1021/bm900186s.

[20] R. Morent, N. De Geyter, S. Van Vlierberghe, P. Dubruel, C. Leys, and E. Schacht, "Organic-inorganic behaviour of HMDSO films plasma-polymerized at atmospheric pressure," *Surf. Coatings Technol.*, vol. 203, no. 10–11, pp. 1366–1372, 2009, doi: 10.1016/j.surfcoat.2008.11.008.

[21] I. Adamovich, "The 2022 Plasma Roadmap : low temperature plasma science and technology The 2022 Plasma Roadmap : low temperature plasma science and," *J. Phys. D. Appl. Phys.*, vol. 55, no. (37), 2022, doi: 10.1088/1361-6463/ac5e1c.

[22] A. Fridman, *Plasma Chemistry*. Cambridge University Press, 2008.

[23] Y. Raizer, *Gas Discharge Physics*. Springer Berlin, Heidelberg, 1991.

[24] A. Bogaerts and E. C. Neyts, "Plasma Technology: An Emerging Technology for Energy Storage," *ACS Energy Lett.*, vol. 3, no. 4, pp. 1013–1027, 2018, doi: 10.1021/acsenergylett.8b00184.

[25] A. Vesel and M. Mozetic, "New developments in surface functionalization of polymers using controlled plasma treatments," *J. Phys. D. Appl. Phys.*, vol. 50, no. 29, 2017, doi: 10.1088/1361-6463/aa748a.

[26] M. A. Lieberman and A. J. Lichtenberg, *Principles of plasma discharges and material processing*. Wiley, 2005.

[27] Y. Hamedani, “Plasma-enhanced chemical vapor deposition: where we are and the outlook for the future,” *Intech*, vol. 11, no. tourism, p. 13, 2016.

[28] L. Martinu, O. Zabeida, and J. E. Klemberg-Sapieha, *Plasma-Enhanced Chemical Vapor Deposition of Functional Coatings*, Third Edit. Elsevier Ltd., 2009.

[29] F. Barletta, C. Leys, V. Colombo, M. Gherardi, N. Britun, R. Snyders, and A. Nikiforov, “Insights into plasma - assisted polymerization at atmospheric pressure by spectroscopic diagnostics,” *Plasma Process. Polym.*, vol. 17, no. September, pp. 1–15, 2019, doi: 10.1002/ppap.201900174.

[30] S. Starostine, E. Aldea, H. de Vries, M. Creatore, and M. C. M. van de Sanden, “Atmospheric pressure barrier discharge deposition of silica-like films on polymeric substrates,” *Plasma Process. Polym.*, vol. 4, no. SUPPL.1, pp. 440–444, 2007, doi: 10.1002/ppap.200731203.

[31] J. Pulpytel, V. Kumar, P. Peng, V. Micheli, N. Laidani, and F. Arefi-Khonsari, “Deposition of organosilicon coatings by a non-equilibrium atmospheric pressure plasma jet: Design, analysis and macroscopic scaling law of the process,” *Plasma Process. Polym.*, vol. 8, no. 7, pp. 664–675, 2011, doi: 10.1002/ppap.201000121.

[32] K. N. Pandiyaraj, M.C. Ramkumara, A. Arun Kumara, D. Vasua, P.V.A. Padmanabhana, P. Saadat Esbah Tabaei, P. Cools, N. De Geyter, R. Morent, and S.K. Jaganathan, “Development of phosphor containing functional coatings via cold atmospheric pressure plasma jet - Study of various operating parameters,” *Appl. Surf. Sci.*, vol. 488, no. May, pp. 343–350, 2019, doi: 10.1016/j.apsusc.2019.05.089.

[33] Q. Chen, Q. Liu, A. Ozkana, B. Chattopadhyay, G. Wallaert, K. Baerte, H. Terryn, M.-P. Delplancke-Ogletree, Y. Geerts, and F. Reniers, “Atmospheric pressure dielectric barrier discharge synthesis of morphology-controllable TiO_2 films with enhanced photocatalytic activity,” *Thin Solid Films*, vol. 664, no. July, pp. 90–99, 2018, doi: 10.1016/j.tsf.2018.08.025.

[34] J.-P. Booth, M. Mozetic, A. Nikiforov, C. Oehr “Foundations of plasma surface functionalization of polymers for industrial and biological applications,” *Plasma Sources Sci. Technol.*, 2022.

[35] A. S. da Silva Sobrinho, M. Latrèche, G. Czeremuszkin, J. E. Klemberg-Sapieha, and M. R. Wertheimer, “Transparent barrier coatings on polyethylene terephthalate by single- and dual-frequency plasma-enhanced chemical vapor deposition,” *J. Vac. Sci. Technol. A Vacuum, Surfaces, Film.*, vol. 16, no. 6, pp. 3190–3198, 1998, doi: 10.1116/1.581519.

[36] D. Hegemann, B. Hanselmann, N. Blanchard, and M. Amberg, “Plasma-Substrate Interaction during Plasma Deposition on Polymers,” *Contrib. to Plasma Phys.*, vol. 54, no. 2, pp. 162–169, 2014, doi: 10.1002/ctpp.201310064.

[37] B. Nisol, H. Gagnon, S. Lerouge, and M. R. Wertheimer, “Energy of Reactions in Atmospheric-Pressure Plasma Polymerization with Inert Carrier Gas,” *Plasma Process. Polym.*, vol. 13, no. 3, pp. 366–374, 2016, doi: 10.1002/ppap.201500068.

[38] D. Hegemann, *Plasma Polymer Deposition and Coatings on Polymers*, vol. 4. Elsevier, 2014.

[39] F. F. Shi, “Recent advances in polymer thin films prepared by plasma polymerization Synthesis, structural characterization, properties and applications,” *Surf. Coatings Technol.*, vol. 82, no. 1–2, pp. 1–15, 1996, doi: 10.1016/0257-8972(95)02621-5.

[40] W. Steckelmacher, *Film deposition by plasma techniques*, vol. 44, no. 10. Springer-Verlag, 1993.

[41] L. Martinu, J. E. Klembergsapieha, and M. R. Wertheimer, , “Dual-mode microwave / radio frequency plasma deposition of dielectric thin films,” *Appl. Phys. Lett.*, 1989, doi: https://doi.org/10.1063/1.101566.

[42] L. Martinu and D. Poitras, “Plasma deposition of optical films and coatings: A review,” *J. Vac. Sci. Technol. A Vacuum, Surfaces, Film.*, vol. 18, no. 6, pp. 2619–2645, 2000, doi: 10.1116/1.1314395.

[43] A. V. Pipa and R. Brandenburg, “The equivalent circuit approach for the electrical diagnostics of dielectric barrier discharges: The classical theory and recent developments,” *Atoms*, vol. 7, no. 1, 2019, doi: 10.3390/atoms7010014.

[44] F. Peeters and T. Butterworth, “Electrical diagnostics of dielectric barrier discharges,” in *InTech*, no. Atmospheric Pressure Plasma - From Diagnostics to Applications Figure, 2018, p. 27.

[45] R. Brandenburg, “Corrigendum: Dielectric barrier discharges: progress on plasma sources and on the understanding of regimes and single filaments (Plasma Sources Science and Technology (2017) 26 (053001) DOI: 10.1088/1361-6595/aa6426),” *Plasma Sources Sci. Technol.*, vol. 27, no. 7, 2018, doi: 10.1088/1361-6595/aaced9.

[46] H. Wagner, R. Brandenburg, K. V Kozlov, A. Sonnenfeld, and P. Michel, “The barrier discharge : basic properties and applications to surface treatment,” vol. 71, pp. 417–436, 2003, doi: 10.1016/S0042-207X(02)00765-0.

[47] U. Kogelschatz, B. Eliasson, and W. Egli, “Dielectric-Barrier Discharges. Principle and Applications,” *J. Phys. IV*, vol. 7, no. 1 997, 1997.

[48] S. Okazaki, M. Kogoma, M. Uehara, and Y. Kimura, “Appearance of stable glow discharge in air, oxygen and nitrogen at atmospheric pressure using a 50 Hz source,” *J. Phys. D Appl. Phys.*, vol. 26, no. 5, pp. 889–892, 1993.

[49] D. Trunec, A. Brablec, and F. Stastny, “Experimental Study of Atmospheric Pressure Glow Discharge,” *Contrib. to Plasma Phys.*, vol. 38, no. 3, pp. 435–445, 1998.

[50] S. Kanazawa, M. Kogoma, T. Moriwaki, and S. Okazaki, “Stable glow plasma at atmospheric pressure,” *J. Phys. D. Appl. Phys.*, vol. 21, no. 5, pp. 838–840, 1988, doi: 10.1088/0022-3727/21/5/028.

[51] F. Massines, C. Sarra-Bournet, F. Fanelli, N. Naudé, and N. Gherardi, “Atmospheric pressure low temperature direct plasma technology: Status and challenges for thin film deposition,” *Plasma Process. Polym.*, vol. 9, no. 11–12, pp. 1041–1073, 2012, doi: 10.1002/ppap.201200029.

[52] X. Lu, M. Laroussi, and V. Puech, “On atmospheric-pressure non-equilibrium plasma jets and plasma bullets,” *Plasma Sources Sci. Technol.*, vol. 21, no. 3, 2012, doi: 10.1088/0963-0252/21/3/034005.

[53] P. A. F. Herbert, L. O’Neill, J. Jaroszyńska-Wolińska, C. P. Stallard, A. Ramamoorthy, and D. P. Dowling, “A comparison between gas and atomized liquid precursor states in the deposition of functional coatings by pin corona plasma,” *Plasma Process. Polym.*, vol. 8, no. 3, pp. 230–238, 2011, doi: 10.1002/ppap.201000119.

[54] H. Kakiuchi, H. Ohmi, and K. Yasutake, “Atmospheric-pressure low-temperature plasma processes for thin film deposition,” *J. Vac. Sci. Technol. A Vacuum, Surfaces, Film.*, vol. 32, no.

3, p. 030801, 2014, doi: 10.1116/1.4828369.

[55] S. Bornholdt, M. Wolter, and H. Kersten, “Characterization of an atmospheric pressure plasma jet for surface modification and thin film deposition,” *Eur. Phys. J. D*, vol. 60, no. 3, pp. 653–660, 2010, doi: 10.1140/epjd/e2010-00245-x.

[56] C. Huang, W.-T. Hsu, C.-H. Liu, S.-Y. Wu, S.-H. Yang, T.-H. Chen, and T.-C. Wei, “Low-temperature atmospheric-pressure-plasma jet for thin-film deposition,” *IEEE Trans. Plasma Sci.*, vol. 37, no. 7 SPEC. ISS. PART 1, pp. 1127–1128, 2009, doi: 10.1109/TPS.2008.2011636.

[57] G. Borcia and N. M. D. Brown, “Hydrophobic coatings on selected polymers in an atmospheric pressure dielectric barrier discharge,” *J. Phys. D. Appl. Phys.*, vol. 40, no. 7, pp. 1927–1936, 2007, doi: 10.1088/0022-3727/40/7/015.

[58] D. Merche, N. Vandencasteele, and F. Reniers, “Atmospheric plasmas for thin film deposition: A critical review,” *Thin Solid Films*, vol. 520, no. 13, pp. 4219–4236, 2012, doi: 10.1016/j.tsf.2012.01.026.

[59] V. S. Nguyen, J. Underhill, S. Fridmann, and P. Pan, “Plasma Organosilicon Polymers: Deposition, Characterization, and Application in Multilayer Resist,” *J. Electrochem. Soc.*, vol. 132, no. 8, pp. 1925–1932, 1985, doi: 10.1149/1.2114255.

[60] V. Jankauskaite, P. Narmontas, and A. Lazauskas, “Control of polydimethylsiloxane surface hydrophobicity by plasma polymerized hexamethyldisilazane deposition,” *Coatings*, vol. 9, no. 1, 2019, doi: 10.3390/coatings9010036.

[61] W. Guogang, L. Jing, Y. Haijiao, and C. Qiang, “Preparation Methods and Application of Silicon Oxide Films,” *Int. Conf. Mechatronics, Electron. Ind. Control Eng.*, no. Meic, pp. 479–483, 2014.

[62] F. Palumbo, C. Lo Porto, F. Fracassi, and P. Favia, “Recent Advancements in the Use of Aerosol-Assisted Atmospheric Pressure Plasma Deposition,” *Coatings*, vol. 10, p. 440, 2020, doi: 10.3390/ma13132931.

[63] P. Heyse, A. Van Hoeck, M. B. J. Roeffaers, J.-P. Raffin, A. Steinbuchel, T. Stoveken, J. Lammertyn, P. Verboven, P. A. Jacobs, J. Hofkens, S. Paulussen, and B. F. Sels, “Exploration of atmospheric pressure plasma nanofilm technology for straightforward bio-active coating deposition: Enzymes, plasmas and polymers, an elegant synergy,” *Plasma Process. Polym.*, vol. 8, no. 10, pp. 965–974, 2011, doi: 10.1002/ppap.201000170.

[64] A. Stancampiano, T. Gallingani, M. Gherardi, Z. Machala, P. Maguire, V. Colombo, J.-M. Pouvesle, and E. Robert, “Plasma and aerosols: Challenges, opportunities and perspectives,” *Appl. Sci.*, vol. 9, no. 18, 2019, doi: 10.3390/app9183861.

[65] P. Tardiveau and E. Marode, “Point-to-plane discharge dynamics in the presence of dielectric droplets,” *J. Phys. D. Appl. Phys.*, vol. 36, no. 10, pp. 1204–1211, 2003, doi: 10.1088/0022-3727/36/10/309.

[66] N. Y. Babaeva, A. N. Bhoj, and M. J. Kushner, “Streamer dynamics in gases containing dust particles,” *Plasma Sources Sci. Technol.*, vol. 15, no. 4, pp. 591–602, 2006, doi: 10.1088/0963-0252/15/4/001.

[67] E. D. Bennet, C. M. O. Mahony, H. E. Potts, P. Everest, D. Rutherford, S. Askari, D. A. McDowell, D. Mariotti, C. Kelsey, F. Perez-Martin, N. Hamilton, P. Maguire, and D. A. Diver, “Precision

charging of microparticles in plasma via the Rayleigh instability for evaporating charged liquid droplets," *J. Aerosol Sci.*, vol. 100, pp. 53–60, 2016, doi: 10.1016/j.jaerosci.2016.05.002.

[68] P. D. Maguire, C. M. O. Mahony, C. P. Kelsey, A. Bingham, E. P. Montgomery, E. D. Bennet, H. E. Potts, D. Rutherford, D. A. McDowell, D. A. Diver, and D. Mariotti, "Controlled microdroplet transport in an atmospheric pressure microplasma," *Appl. Phys. Lett.*, vol. 106, no. 22, 2015, doi: 10.1063/1.4922034.

[69] P. Ranieri, G. McGovern, H. Tse, A. Fulmer, M. Kovalenko, G. Nirenberg, V. Miller, A. Fridman, A. Rabinovich, and G. Fridman, "Microsecond-pulsed dielectric barrier discharge plasma-treated mist for inactivation of Escherichia coli in vitro," *IEEE Trans. Plasma Sci.*, vol. 47, no. 1, pp. 395–402, 2019, doi: 10.1109/TPS.2018.2878971.

[70] S. E. Babayan, J. Y. Jeong, A. Schutze, V. J. Tu, M. Moravej, G. S. Selwyn, and R. F. Hicks, "Deposition of silicon dioxide films with a non-equilibrium atmospheric-pressure plasma jet," *Plasma Sources Sci. Technol.*, vol. 10, no. 4, pp. 573–578, 2001, doi: 10.1088/0963-0252/10/4/305.

[71] H. Caquineau, I. Enache, N. Gherardi, N. Naudé, and F. Massines, "Influence of gas flow dynamics on discharge stability and on the uniformity of atmospheric pressure PECVD thin film," *J. Phys. D. Appl. Phys.*, vol. 42, no. 12, 2009, doi: 10.1088/0022-3727/42/12/125201.

[72] M. Rahman, R. Amsarani, D. A. Mooney, J. M. D. MacElroy, and D. P. Dowling, "Effect of process parameters on chemistry, growth rate and nano-sized particulate formation of atmospheric plasma deposited, nm thick siioxane coatings," *J. Nanosci. Nanotechnol.*, vol. 9, no. 6, pp. 3506–3513, 2009, doi: 10.1166/jnn.2009.NS24.

[73] A. Kakaroglou, G. Scheltjens, B. Nisol, I. De Graeve, G. Van Assche, B. Van Mele, R. Willem, M. Biesemans, F. Reniers, and H. Terryn, "Evaluation of the Yasuda parameter for the atmospheric plasma deposition of allyl methacrylate," *RSC Adv.*, vol. 5, no. 35, pp. 27449–27457, 2015, doi: 10.1039/c5ra02684a.

[74] H. Yasuda and T. Hirotsu, "Critical Evaluation of Conditions of Plasma Polymerization.," *J Polym Sci Polym Chem Ed*, vol. 16, no. 4, pp. 743–759, 1978, doi: 10.1002/pol.1978.170160403.

[75] H. Yasuda, "Glow Discharge Polymerization.," *J. Polym. Sci. Macromol. Rev.*, vol. 16, no. 198 1, pp. 199–293, 1981, doi: 10.1002/pol.1981.230160104.

[76] H. Yasuda, *Plasma Polymerization*. Academic Press, 1985.

[77] M. A. Gilliam, Q. Yu, and H. Yasuda, "Plasma polymerization behavior of fluorocarbon monomers in low-pressure AF and RF discharges," *Plasma Process. Polym.*, vol. 4, no. 2, pp. 165–172, 2007, doi: 10.1002/ppap.200600076.

[78] M. Bashir, J. M. Rees, and W. B. Zimmerman, "Plasma polymerization in a microcapillary using an atmospheric pressure dielectric barrier discharge," *Surf. Coatings Technol.*, vol. 234, pp. 82–91, 2013, doi: 10.1016/j.surfcoat.2013.01.041.

[79] J. Petersen, C. Becker, T. Fouquet, F. Addiego, V. Toniazzo, A. Dinia, and D. Rucha, "Nano-ordered thin films achieved by soft atmospheric plasma polymerization," *RSC Adv.*, vol. 3, no. 13, pp. 4416–4424, 2013, doi: 10.1039/c2ra21833j.

[80] G. Wulf, B. Mayer, and U. Lommatzsch, "Plasma Co-Polymerization of HMDSO and Limonene

with an Atmospheric Pressure Plasma Jet," *Plasma*, vol. 5, no. 1, pp. 44–59, 2022, doi: 10.3390/plasma5010004.

[81] D. Hegemann, M. M. Hossain, E. Körner, and D. J. Balazs, "Macroscopic description of plasma polymerization," *Plasma Process. Polym.*, vol. 4, no. 3, pp. 229–238, 2007, doi: 10.1002/ppap.200600169.

[82] D. Hegemann, E. Körner, and S. Guimond, "Plasma polymerization of acrylic acid revisited," *Plasma Process. Polym.*, vol. 6, no. 4, pp. 246–254, 2009, doi: 10.1002/ppap.200800089.

[83] D. Hegemann, "Macroscopic investigation of reaction rates yielding plasma polymer deposition," *J. Phys. D. Appl. Phys.*, vol. 46, no. 20, 2013, doi: 10.1088/0022-3727/46/20/205204.

[84] M. Archambault-Caron, H. Gagnon, B. Nisol, K. Piyakis, and M. R. Wertheimer, "Precise energy and temperature measurements in dielectric barrier discharges at atmospheric pressure," *Plasma Sources Sci. Technol.*, vol. 24, no. 4, 2015, doi: 10.1088/0963-0252/24/4/045004.

[85] B. Nisol, S. Watson, S. Lerouge, and M. R. Wertheimer, "Energetics of Reactions in a Dielectric Barrier Discharge with Argon Carrier Gas: II Mixtures with Different Molecules," *Plasma Process. Polym.*, vol. 13, no. 5, pp. 557–564, 2016, doi: 10.1002/ppap.201500161.

[86] B. Nisol, S. Watson, S. Lerouge, and M. R. Wertheimer, "Energetics of Reactions in a Dielectric Barrier Discharge with Argon Carrier Gas: III Esters," *Plasma Process. Polym.*, vol. 13, no. 9, pp. 900–907, 2016, doi: 10.1002/ppap.201600003.

[87] B. Nisol, S. Watson, S. Lerouge, and M. R. Wertheimer, "Energetics of reactions in a dielectric barrier discharge with argon carrier gas: IV ethyl lactate," *Plasma Process. Polym.*, vol. 13, no. 10, pp. 965–969, 2016, doi: 10.1002/ppap.201600099.

[88] B. Nisol, S. Watson, S. Lerouge, and M. R. Wertheimer, "Energetics of reactions in a dielectric barrier discharge with argon carrier gas: V hydrocarbons," *Plasma Process. Polym.*, vol. 14, no. 8, pp. 1–9, 2017, doi: 10.1002/ppap.201600191.

[89] B. Nisol, S. Watson, A. Meunier, D. Juncker, S. Lerouge, and M. R. Wertheimer, "Energetics of reactions in a dielectric barrier discharge with argon carrier gas: VI PEG-like coatings," *Plasma Process. Polym.*, vol. 15, no. 3, pp. 1–10, 2018, doi: 10.1002/ppap.201700132.

[90] J. Mertens, S. Watson, B. Nisol, M. R. Wertheimer, and F. Reniers, "Energetics of reactions in a dielectric barrier discharge with argon carrier gas: VII anhydrides," *Plasma Process. Polym.*, vol. 16, no. 5, pp. 1–7, 2019, doi: 10.1002/ppap.201800186.

[91] S. Watson, B. Nisol, and M. R. Wertheimer, "Energetics of reactions in a dielectric barrier discharge with argon carrier gas: VIII hydrofluoromethanes," *Plasma Process. Polym.*, vol. 17, no. 6, pp. 1–13, 2020, doi: 10.1002/ppap.201900125.

Chapter 2

This PhD thesis

2.1 Introduction

In recent years, polymerization processes assisted by atmospheric pressure plasma jets (APPJs) have received increasing attention in numerous industrially relevant sectors since they allow to coat complex 3D substrates without requiring expensive vacuum systems. Therefore, advancing the comprehension and the understanding of these processes has become a high priority topic of research. For this reason, my PhD thesis is focused on the study and the implementation of control strategies for a polymerization process assisted by an AP single electrode plasma jet. The contents reported in the following will cover 1) a detailed description of the mentioned plasma source, 2) the motivations behind the PhD project, and 3) the outline of this PhD thesis.

2.2 Atmospheric pressure single electrode plasma jet

The first prototype of the AP single electrode plasma jet investigated in this work (Figure 2.1) has been developed in the laboratories of the Research Group for Industrial Applications of Plasmas (IAP) of the University of Bologna (Italy) in 2014. In this prototype, the single electrode is a stainless steel sharpened metallic needle with a diameter of 0.3 mm driven by a commercial nano-pulsed DC power supply. The case in Delrin offers two gas inlets to introduce a primary gas sustaining the plasma (Ar, He, and air) and to separately inject a secondary flow (e.g. precursor carrier flow). The primary gas is injected through a 12-hole (0.3 mm diameter) diffuser aimed at ensuring a uniform and laminar distribution of the primary gas flow along the electrode, while the secondary gas is introduced through twelve 0.3 mm holes, tilted with respect to the plasma jet axis. The gas is ejected through a 1 mm orifice.

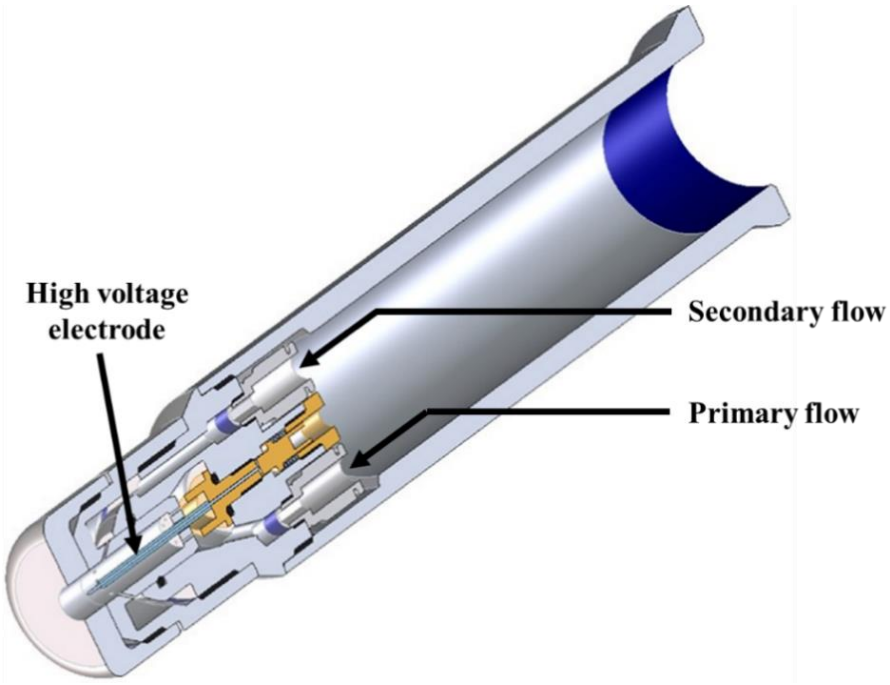

Figure 2.1: Schematic of the first prototype of the atmospheric pressure single electrode plasma jet. [1]

Between 2014 and 2016, the characteristics of the plasma discharge (i.e. fluid dynamic behaviour, characteristic temperature, and radiation emission) produced with this configuration in Ar and He mixtures were investigated by means of iCCD imaging, OES, and Schlieren high speed imaging. [1], [2] Furthermore, this plasma source was used for the PP of polyacrylic acid coatings (pPAA) and of nanocomposite coatings (pPAA + silver nanoparticles), which are appealing in the biomedical field since they can favour cells adhesion and exert antimicrobial action. [3], [4]

In 2018, the potentialities of the plasma source for the synthesis of copper-based nanostructures in different liquid mediums were also examined in detail. [5] In the same year, a novel version of the prototype was proposed and, apart from slight modifications over the years, it has been maintained to this day. The schematic of the final version is reported in Figure 2.2.

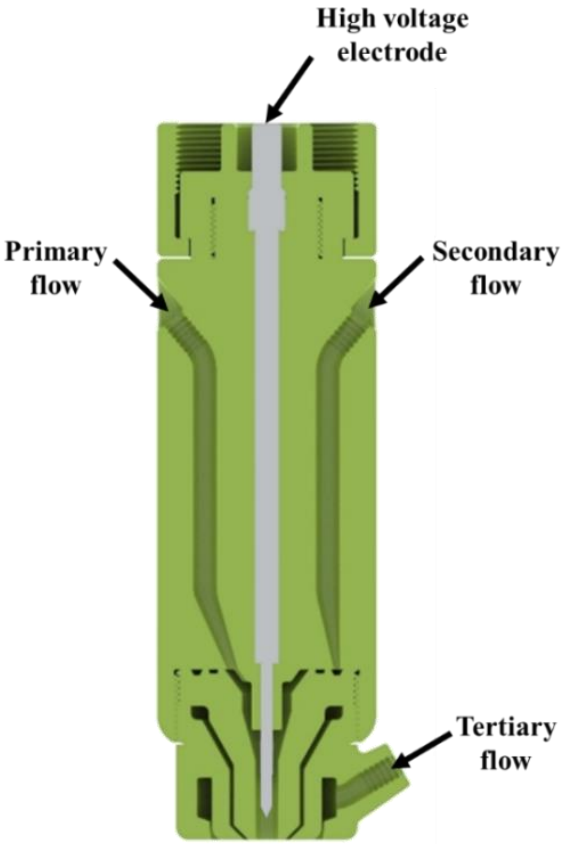

Figure 2.2: Schematic of the final version of the AP single electrode plasma jet.

As can be noticed from Figure 2.2, this version exhibits a stainless-steel high voltage electrode and two separate inlets, like the first prototype. Nonetheless, several differences must be pointed out. First, the electrode has a higher diameter (2 mm instead of 0.3 mm). Second, the possibility to introduce a third flow of gas is now enabled. The third flow can be used, for example, to increase the shielding of the plasma plume, thus limiting the contamination of the diffusing ambient air in the process. Third, the material of the case is no longer Delrin, but ABS-like to ensure a longer resistance of the plasma source

to the stress induced by the plasma discharge. Finally, the head of the plasma source is designed to be connected to a CNC system which permits the movement of the plasma source, thus facilitating the treatment of 3D complex substrates.

Contextually to the introduction of this plasma source, the IAP Research Group started to show interest for micro-pulsed power supplies (instead of nano-pulsed ones). For this reason, the activities carried out later with this source are typically associated to this type of power supply. Furthermore, the plasma source began to be mostly used in a "DBD-mode", where the high voltage single electrode is directly faced on the substrate, which is located on a grounded plate covered with a dielectric barrier. This configuration allows to perform an in-depth analysis of the electrical behavior of the plasma discharge (through the addition of electronic probes on the grounded line), but forces to consider the electrical properties of the substrate to be treated in the electrical circuit.

In more recent years, the plasma source was subject of several studies which aimed to explore the complex gas-phase mechanisms of fragmentation of the precursor TEOS in argon discharges by means of OES, Rayleigh scattering, and laser diagnostics. [6], [7] Moreover, this source was used to deposit PDMS/SiO_2-like surface gradients from HMDSO on polyethylene foils by varying the O_2 concentration in the discharge during the movement of the plasma source. Such surface gradients have great potential in the development of high-performance biosensing platforms. [8]

During my year as research fellow (before to start my PhD program), I had the opportunity to work with this plasma source in the frame of a research project aimed to develop SiO_2-like coatings to increase the gas barrier properties of complex 3D propylene substrates. In this context, I investigated the PP process in presence of two different vaporized organosilicon precursors, HMDSO ($Si_2C_6H_{18}O$) and TEOS ($SiC_8H_{20}O_4$), in order to identify the best one to provide SiO_2-like barrier coatings. It was demonstrated that, under equal deposition conditions (e.g. discharge power, precursor flow rate, and deposition time), the use of TEOS as precursor leads more easily to the production of SiO_2-like coatings. Indeed, as can be seen from Figure 2.3, the ATR-FTIR spectra of coatings from TEOS exhibit peaks of a typical pure inorganic coating (e.g. Si-O-Si asymmetric stretching at 1070 cm^{-1} and Si-OH bending at 930 cm^{-1}), while those from HMDSO highlight the presence of methyl-related groups (e.g. at 1265 cm^{-1}). Since the molecules of both precursors receive (at least in first approximation) the same amount of energy in the discharge, the described behavior might be explained considering the lower content of carbon and the higher content of oxygen in the starting molecules of TEOS, compared to those of HMDSO.

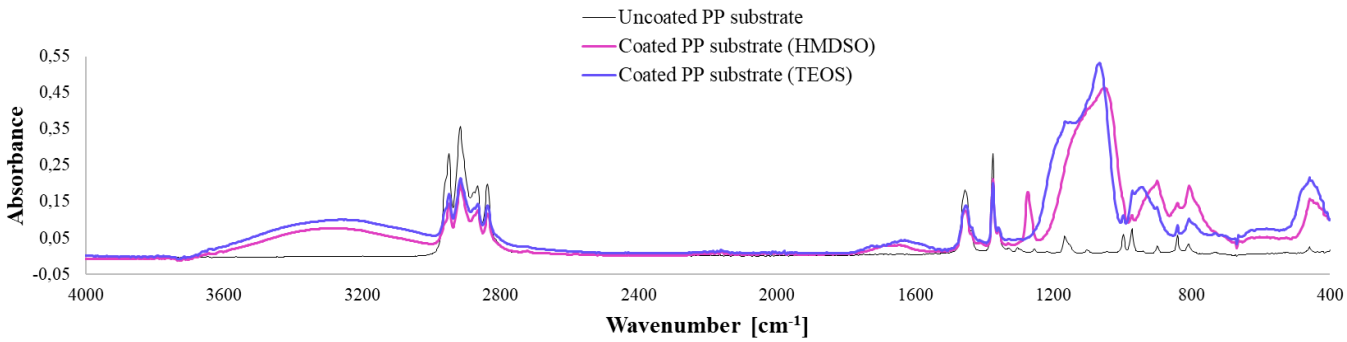

Figure 2.3: ATR-FTIR spectra of coatings deposited from vaporized HMDSO and TEOS on polypropylene substrates.

According to these results, TEOS appeared as the most suitable precursor to obtain SiO_2 coatings. Nonetheless, as depicted by the SEM images in Figure 2.4, its use was associated to the presence of large fractures (black lines in the picture), whose formation is probably ascribed to the large difference in the thermal dilatation coefficient of the SiO_2-like coatings and the polymeric substrate.

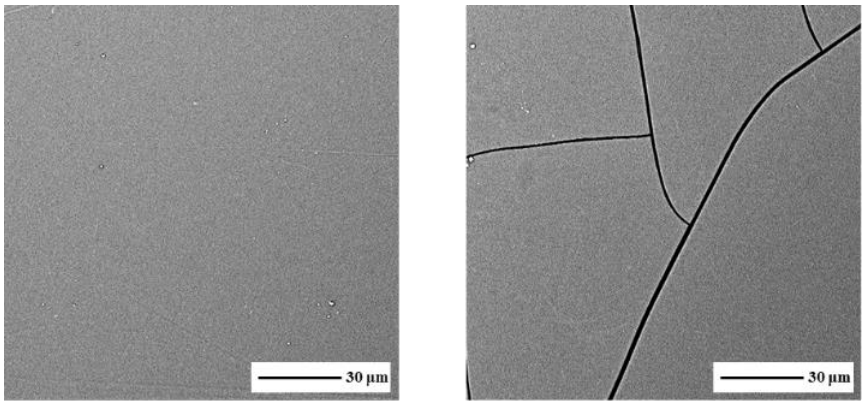

Figure 2.4: SEM images of coatings deposited from HMDSO (left) and TEOS (right).

These activities clearly highlighted how at AP obtaining the proper combination of chemical and morphological characteristics in a coating is far from trivial and requires in-depth analysis and control of the polymerization process.

2.3 Motivation

As explained in Section 2.2, the AP single electrode plasma jet has been widely used by the IAP Group over the years, for different purposes and deposition conditions. Despite the effects of numerous factors involved in the polymerization process have been investigated, the role of the control strategies in this process has never been object of an in-depth analysis. Considering the potentialities of this plasma source in the realization of thin films for a broad range of industrial applications, this PhD project aims

to advance the understanding of the polymerization process assisted by this plasma jet through the study and the implementation of control strategies.

2.4 Outline

With these premises, this dissertation is organized in two main sections, each focused on a particular control strategy for the polymerization process assisted by the AP single electrode plasma jet. In order to better contextualize the reasons behind the choice of deepening those control strategies, a short introduction is needed.

As shown in Chapter 1, the validity of the Yasuda parameter as controlling parameter at AP has been questioned because, differently from LP processes, the precursor is usually highly diluted in the carrier gas and the measurement of the adsorbed power is not straightforward. As a more accurate alternative, a methodology for measuring the energy absorbed per precursor molecule has been developed by Nisol et al. Despite being validated for different families of precursors, this methodology is limited to planar DBDs and to gaseous and vaporized precursors. Therefore, for AP plasma polymerization processes which involve other elements than the above described (such as, for example, plasma jets and aerosolized precursors), the Yasuda parameter may still be a useful controlling parameter whose validity should be demonstrated on a case-by-case basis.

According to this introduction:

- In **Chapter 3**, an investigation on the validity of the Yasuda parameter as controlling parameter in the PP process from an aerosolized fluorinated silane precursor is proposed.
- In **Chapter 4**, the development of a methodology for measuring the energy of reactions in polymerization processes assisted by APPJs is presented.
- In **Chapter 5**, the achievements reached in the two main sections are summarized and the future perspective are outlined.

2.5 References

[1] M. Boselli, V. Colombo, E. Ghedini, M. Gherardi, R. Laurita, A. Liguori, P. Sanibondi, A. Stancampiano, "Schlieren high-speed imaging of a nanosecond pulsed atmospheric pressure non-equilibrium plasma jet," *Plasma Chem. Plasma Process.*, vol. 34, no. 4, pp. 853–869, 2014, doi: 10.1007/s11090-014-9537-1.

[2] M. Boselli, V. Colombo, M. Gherardi, R. Laurita, A. Liguori, P. Sanibondi, E. Simoncelli, A. Stancampiano, "Characterization of a Cold Atmospheric Pressure Plasma Jet Device Driven by Nanosecond Voltage Pulses," *IEEE Trans. Plasma Sci.*, vol. 43, no. 3, pp. 713–725, 2015, doi: 10.1109/TPS.2014.2381854.

[3] A. Liguori, A. Pollicino, A. Stancampiano, F. Tarterini, M. L. Focarete, V. Colombo, M. Gherardi, "Deposition of Plasma-Polymerized Polyacrylic Acid Coatings by a Non-Equilibrium Atmospheric Pressure Nanopulsed Plasma Jet," *Plasma Process. Polym.*, vol. 13, no. 3, pp. 375–386, 2016, doi: 10.1002/ppap.201500080.

[4] A. Liguori, E. Traldi, E. Toccaceli, R. Laurita, A. Pollicino, M. L. Focarete, V. Colombo, M. Gherardi, "Co-Deposition of Plasma-Polymerized Polyacrylic Acid and Silver Nanoparticles for the Production of Nanocomposite Coatings Using a Non-Equilibrium Atmospheric Pressure Plasma Jet," *Plasma Process. Polym.*, vol. 13, no. 6, pp. 623–632, 2016, doi: 10.1002/ppap.201500143.

[5] A. Liguori, T. Gallingani, D. B. Padmanaban, R. Laurita, T. Velusamy, G. Jain, M. Macias-Montero, D. Mariotti, Matteo Gherardi, "Synthesis of Copper-Based Nanostructures in Liquid Environments by Means of a Non-equilibrium Atmospheric Pressure Nanopulsed Plasma Jet," *Plasma Chem. Plasma Process.*, vol. 38, no. 6, pp. 1209–1222, 2018, doi: 10.1007/s11090-018-9924-0.

[6] F. Barletta, C. Leys, V. Colombo, M. Gherardi, N. Britun, R. Snyders, A. Nikiforov, "Insights into plasma - assisted polymerization at atmospheric pressure by spectroscopic diagnostics," *Plasma Process. Polym.*, vol. 17, no. September, pp. 1–15, 2019, doi: 10.1002/ppap.201900174.

[7] F. Barletta, C. Leys, M. Gherardi, R. Snyders, and A. Nikiforov, "Studying the plasma - assisted polymerization at atmospheric pressure in Ar / TEOS by active laser diagnostics," no. August 2020, pp. 1–15, 2021, doi: 10.1002/ppap.202000149.

[8] H. Malekzad, T. Gallingani, F. Barletta, M. Gherardi, V. Colombo, and D. Duday, "Single - step deposition of hexamethyldisiloxane surface gradient coatings with a high amplitude of water contact angles over a polyethylene foil," *Plasma Process. Polym.*, vol. 18, no. August 2020, 2021, doi: 10.1002/ppap.202000044.

Chapter 3

Study of the validity of the Yasuda parameter as controlling parameter

3.1 Introduction

In this chapter, a study of the validity of the Yasuda parameter (W/FM) as controlling parameter for a polymerization process assisted by the AP single electrode plasma jet described in Chapter 2 and an aerosolized fluorinated silane precursor is proposed. The chemical and physical properties of thin films deposited under different W/FM values are characterized by means of attenuated total reflectance – Fourier transform infrared (ATR-FTIR) spectroscopy, X-ray photoelectron spectroscopy (XPS), water contact angle (WCA) measurements, and scanning electron microscopy (SEM). Considering the potentialities in the biomedical field of the PP process explored in this work, preliminary biological results of the antiadhesive activity of the deposited coatings against *P. aeruginosa* and *S. aureus* are presented.

3.1.1 Insights into the work

- A fluorinated silane precursor, trimethoxy(3,3,3-trifluoropropyl)silane, is selected for this work with the aim of depositing fluorine containing coatings suitable for antibacterial applications. In fact, it is known that these coatings can exhibit antiadhesive properties, thus representing a potential strategy to contain the onset of severe infections associated with the formation of biofilm of implantable medical devices (e.g. prostheses). [1], [2] These infections typically result in huge implications both for the patients and for the National Health Service and current treatments consist in prolonged and high-dose antibiotic therapies that are often ineffective, due to the antibiotic-resistant nature of biofilms [3]; consequently, prosthesis removal is thus necessary to prevent the infection from becoming systemic, with increased risks for patient health. In this perspective, the development of antiadhesive surfaces for implantable medical devices is a high priority topic of research. [4]–[8]
- According to a thorough literature research, the only study dedicated to PP of this precursor at AP is focused on the influence of several parameters (i.e. electrode-substrate gap distance, deposition time, and mode of deposition (static or dynamic)) on the overall deposition characteristics. [9] Hence, the role of W/FM as controlling parameter for processes involving this precursor is yet unexplored.
- The choice of using this liquid precursor in an aerosolized state, instead of in a vaporized one, is related to the less intense fragmentation of the precursor associated to this physical state, which should favour the preservation of fluorine moieties in the final coating. The introduction of the precursor in the secondary channel of the plasma source follows the same logic, as the residence time (and so the time available for fragmentation) of the precursor molecules in the plasma discharge is shorter than the one which results from an introduction in the primary channel.

3.1.2 Collaborations related to the work

The activities reported in this chapter were carried out in the context of a research collaboration which involved several academic and non-academic partners. In particular, the IAP Research Group, of which I am member, has received precious support from:

- IBM Tech s.r.l., in the definition of the aspects of the polymerization process strictly related to the target application (e.g. the precursor to be used);
- University of Catania, in the XPS analysis of the deposited coatings;
- University of Messina, in the testing of the antiadhesive activity of the deposited coatings.

The results of these activities led to a research article which is now published on Plasma Processes and Polymers: "***Control strategies for atmospheric pressure plasma polymerization of fluorinated silane thin films with antiadhesive properties***" – Giulia Laghi, Domenico Franco, Guglielmo Guido Condorelli, Riccardo Gallerani, Salvatore Guglielmino, Romolo Laurita, Dario Morganti, Francesco Traina, Sabrina Conoci, Matteo Gherardi.

3.2 Experimental section

3.2.1 Experimental setup

The experimental setup used in this work is schematically reported in Figure 3.1.

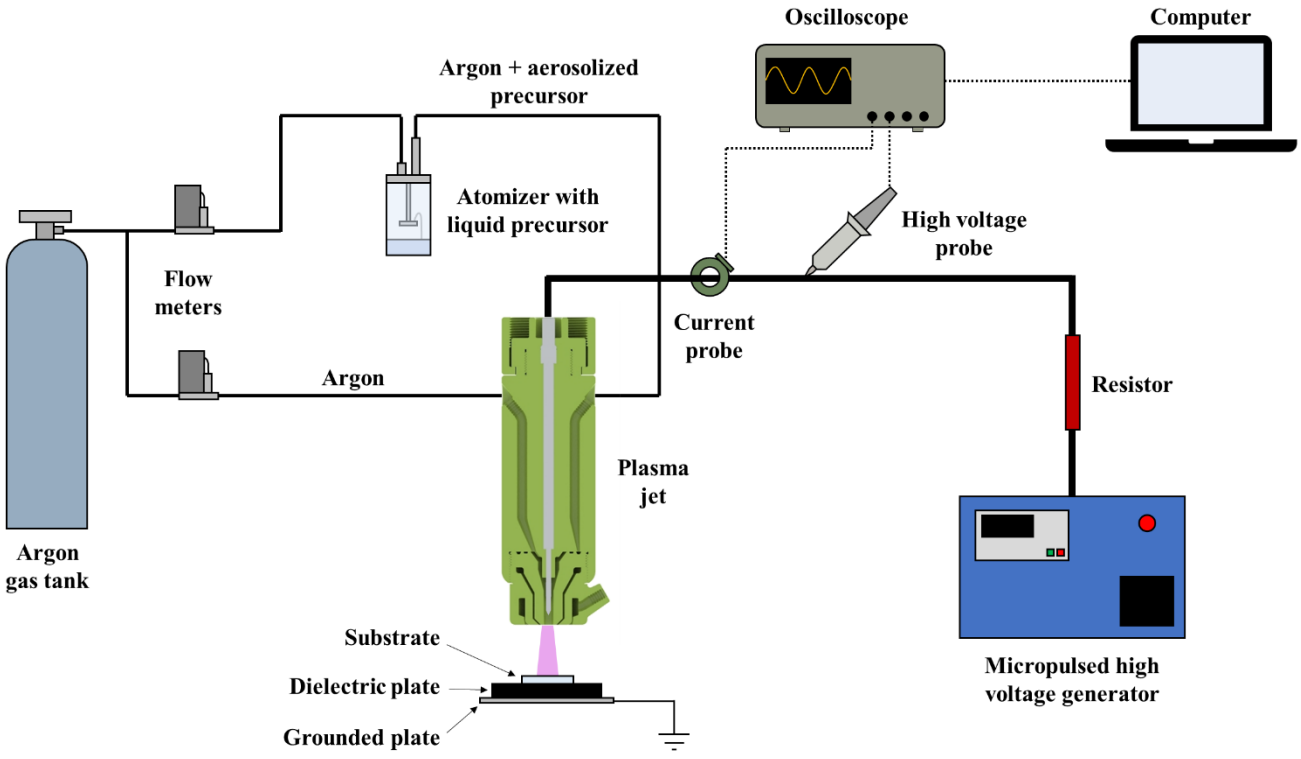

Figure 3.1: Schematical representation of the experimental setup.

The employed plasma source is the AP single electrode plasma jet descripted in Chapter 2. An argon flow rate of 3 slpm was injected in the discharge region through the primary channel, while, simultaneously, an aerosolized precursor flow rate was introduced through the secondary channel.

The liquid precursor used in this work is (3,3,3-trifluoropropyl)trimethoxysilane ($C_6H_{13}F_3O_3Si$, Sigma-Aldrich, ≥ 97.0%) and is characterized by three methoxy groups and a trifluoromethyl group, as shown in Figure 3.2.

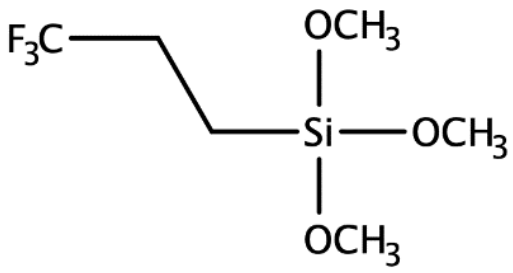

Figure 3.2: Precursor molecular structure.

A single-jet atomizer (BLAM, CH Technologies) fed with an argon flow was used to aerosolize the liquid precursor. To calculate the effective precursor feed rate, the quantity of liquid precursor consumed within a defined time interval (15 min) was measured. The argon flow rates were controlled by digital mass flow controllers (EL-FLOW, Bronkhorst).

The stainless-steel single electrode of the plasma source was connected to a micropulsed high voltage generator (AlmaPulse, AlmaPlasma s.r.l.), operated at a fixed frequency of 12 kHz and at a variable peak voltage; a ballast resistor of 70 kΩ was added along the high voltage cable between the generator and the plasma source. Bilayer films (area: 1 cm x 1 cm, thickness: 0.3 mm), composed of polyethylene (PE, approximately 0.15 mm thick) and polyvinyl chloride (PVC, approximately 0.15 mm thick) foils, were used as substrates, and were rinsed for 2 minutes with ethanol (Sigma Aldrich, ≥ 99.8%) to remove contaminants and dried in air prior to deposition. The deposition was performed onto the PE layer and the distance between the plasma source and the surface of the substrate was kept constant to 10 mm. The substrate was placed on a polyvinyl chloride (PVC) plate (thickness = 8 mm) positioned on a metallic plate connected to the ground. The deposition time was fixed to 60 s.

Despite coatings were deposited on PE substrates, in the future it might be interesting extending this polymerization process also to metallic substrates (similar, for example, to metallic implants). For this reason, and with a purpose of continuity in terms of experimental setup, the 70 kΩ resistor meant to avoid arc transition of the jet on conductive substrate was added along the high voltage line also in the process on plastic substrates.

Nine different combinations of peak voltage and precursor feed rate (covering the maximum operating range of the plasma jet source and the atomizer, respectively) were analyzed. Each combination, associated to a letter from A to I, is reported in Table 3.1 along with the corresponding

discharge power and W/FM value. Conditions from J to M, reported as well in Table 3.1, were investigated to study the properties of coatings deposited under similar W/FM values but obtained with different combinations of power discharge and precursor feed rate. The performed comparisons are the following: D-J, E-K, F-L, and H-M.

Deposition condition	Peak voltage [kV]	Precursor feed rate [g/h]	Discharge power [W]	W/FM [MJ/kg]
A	14	0.7	11.7 ± 0.6	60.2 ± 3.1
B	12	0.7	7.5 ± 0.4	38.6 ± 2.1
C	10	0.7	5.1 ± 0.3	26.2 ± 1.5
D	8	0.7	2.8 ± 0.4	14.4 ± 2.1
E	6	0.7	1.7 ± 0.2	8.7 ± 1.0
F	6	1.2	1.8 ± 0.1	5.4 ± 0.3
G	6	2.1	1.8 ± 0.1	3.1 ± 0.2
H	6	4.56	1.9 ± 0.2	1.5 ± 0.2
I	6	9.32	2.2 ± 0.1	0.8 ± 0.0
J	10	1.2	5.3 ± 0.4	15.9 ± 1.2
K	8	1.2	2.9 ± 0.1	8.7 ± 0.3
L	8	2.1	3.0 ± 0.2	5.1 ± 0.3
M	8	9.32	3.8 ± 0.2	1.5 ± 0.1

Table 3.1: Analyzed deposition conditions.

To calculate the discharge power, the voltage (V) and the current (i) were measured by means of a high voltage probe (Tektronix P6015A) and a current probe (Pearson 6585), both located on the high voltage cable between the resistor and the plasma source. The voltage and current waveforms were recorded using a digital oscilloscope (Tektronix DPO4034, 350 MHz, 2.5 GSa/s). As an example, Figure 3.3 shows voltage and current waveforms corresponding to a representative applied voltage period (deposition condition A).

The average discharge power (P) dissipated over the applied voltage period (T) was calculated directly from measured voltage and current using the following formula:

$$P = \frac{1}{T}\int_0^T V(t)\, i(t)\, dt \tag{3.1}$$

To monitor the discharge power evolution during the treatment, the electrical characterization was performed at 0 s, 20 s, 40 s, and 60 s from the plasma ignition. For all the investigated conditions, the

discharge power resulted constant in time, thus the representative discharge power value to be associated with the specific condition was calculated considering all the values obtained from the measurements performed during the treatment. Three replicates for each deposition condition were involved in the calculation (12 values in total), hence the results are shown as mean value ± standard deviation. The calculated discharge power was related to the precursor feed rate to calculate the corresponding W/FM values, which are presented as mean ± standard deviation as well.

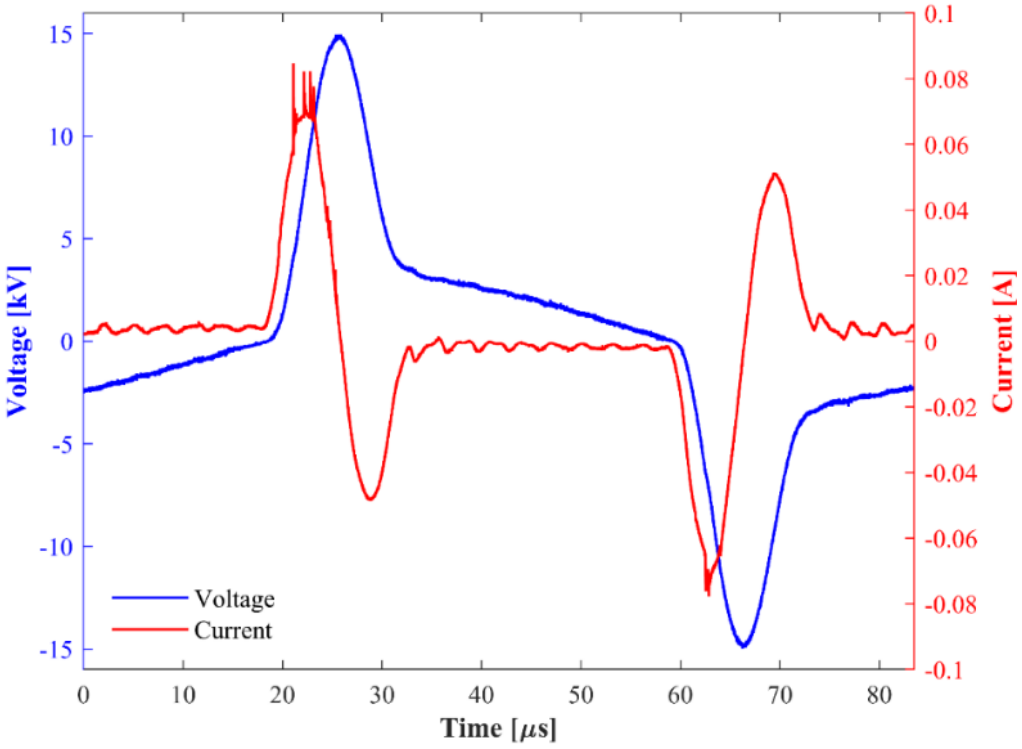

Figure 3.3: Voltage and current waveforms for deposition condition A.

3.2.2 Surface characterization of the deposited coatings

ATR-FTIR measurements were performed to gather information on the chemical structure of the flat PE substrates before and after the deposition of the fluorinated silane coatings. The Agilent Cary 660 FTIR spectrometer was equipped with an ATR sampling accessory, using a diamond crystal as internal reflection element and a beam set at 45°. Spectra were acquired in absorbance mode, from 4000 to 400 cm^{-1} with a resolution of 4 cm^{-1}; a total of 32 scans were recorded for each spectrum. The choice of PE as substrates facilitates the interpretation of ATR-FTIR coatings spectra since PE peaks appear in spectral regions other than those typically characteristic of silane coating peaks.

XPS was used to study the chemical composition of PE substrates and of the deposited fluorinated silane coatings. Spectra were recorded with a PHI 5000 Versa Probe Instrument equipped with a monochromatic Al Kα X-ray source excited with a micro-focused electron beam. Analyses were carried out at 15 W on 150 μm area with a photo-electron take-off angle of 45°. The XPS binding energy (BE)

scale was calibrated by centring the C 1s peak due to C-C, C-H hydrocarbon moieties of PE and "adventitious" carbon at 285.0 eV. [10]

WCA measurements were carried out to evaluate the wettability of the deposited coatings and to compare it with that of the uncoated substrates. For the WCA measurements a drop shape analyzer (DSA30, KRUSS) was employed, depositing distilled water droplets (2 μl) on the substrates, and using the Young–Laplace method. For each deposition condition, 3 replicates were analyzed, performing 5 measurements for each replicate. The results are presented as mean values ± standard deviations.

SEM was used to investigate the thickness of the deposited coatings. To facilitate the break in liquid nitrogen, polypropylene foils (thickness 0.5 mm and diameter 2 cm) were chosen as substrates (after verifying that the deposited coatings possess identical chemical characteristics to coatings deposited on PE/PVC foils) and a pre-cut was performed in the back of the samples prior to the deposition treatment. To carry out more accurate thickness measurements, the deposition time was set to 120 s. Top view analyses were conducted to analyze the morphology of the coatings deposited on polypropylene foils. All the observations were carried out using a scanning electron microscope (Phenom ProX, ThermoFisher Scientific) by applying an accelerating voltage of 10 kV. A sputter coater (SC7620, Quorum Technologies) was used to cover the coating surface with gold before SEM analysis.

3.2.3 Biological assay

For adhesion assay parameters, *P. aeruginosa* (ATCC 27853 strain, LGC Promochem, Milan, Italy) and *S. aureus* (ATCC2 9213 strain, LGC Promochem, Milan, Italy) were chosen as representative gram-negative and gram-positive bacterial strains. *P. aeruginosa* and *S. aureus* were cultured in Bertani Broth (LB, Sigma-Aldrich, Milan, Italy) and Tryptone Soya Broth (TSB, Sigma-Aldrich, Milan, Italy), respectively, and maintained in the respective medium added with 20% glycerol at -80 °C until they were used.

Adhesion activity tests were conducted according to the procedure described by Satriano et al. [11] with some modifications. Specifically, for each strain, an overnight culture was inoculated in fresh medium (dilution ratio 1:100) and incubated for 5 h at 37 °C under shaking at 150 rpm until an optical density. Bacteria, in the semi-exponential phase of growth, were washed twice in phosphate-buffered saline (PBS), then resuspended in PBS to obtain a turbidity equivalent (McFarland standard) of 0.5, corresponding about to 2×10^8 bacteria/mL. Then bacterial solution was stained with SYTO9 green fluorescent nucleic acid stain (3.34 mM; Molecular Probes) for 15 minutes in the dark at 37 °C. 100 μL of stained bacterial suspension were put on the different treated surfaces and incubated in the humidified room for 2h.

Bacterial concentration (approximatively 2×10^8 bacteria/mL) and incubation times (2h) were chosen as the most suitable condition based on previous experiences [12] and allowed to evidence the early stages of the adhesion process. In addition, since cell adhesion was evaluated in absence of nutrient

to avoid any influence of the results by the components of the culture medium or cell proliferation during the incubation period, viability of both bacterial strains at different incubation times was preliminary monitored in PBS at room temperature, indicating a negligible reduction of viable counts after 2 hours (data not shown).

After the incubation, each sample was gently rinsed twice with sterile PBS and visualized under fluorescence microscopy by using Leica DMRE epifluorescence microscope (Leica Microsystems, Heerbrugg, Switzerland). From each sample, several fields of observation were captured and a quantitative evaluation of cells adhering onto the surface was performed using the Scion Image software (Windows version of NIH Image software) in the automated counting (single colour) image mode in terms of integrate density (IntDen), allowing to evaluate the cell coverage by the following equation:

$$IntDen = N \times (M - B) \tag{3.2}$$

where N is the number of pixels in the selection, M is the average grey value of the pixels, and B is the most common pixel value.

3.3 Results

3.3.1 Surface characterization results

3.3.1.1 ATR-FTIR results

The ATR-FTIR spectra of PE substrates before and after the deposition under different W/FM values are shown in Figure 3.4.

The spectrum of uncoated PE exhibits two large absorption peaks at 2920 and 2852 cm^{-1} due to C-H asymmetric and symmetric stretching vibrations in CH_2, respectively. Furthermore, two smaller peaks can be observed at 1466 cm^{-1} and 723 cm^{-1}: the first corresponds to C-H deformation vibrations in $-(CH_2)_n-$, while the second one to C-C rocking vibrations in $-(CH_2)_n-$. [13], [14] The described peaks can be still detected in all the spectra related to coatings deposited under different W/FM values, suggesting that in no case the coating thickness exceeds the penetration depth of the infrared beam (approximatively 550 nm in region 3000-2800 cm^{-1} and 1.1-2.3 μm in region 1500-700 cm^{-1}).

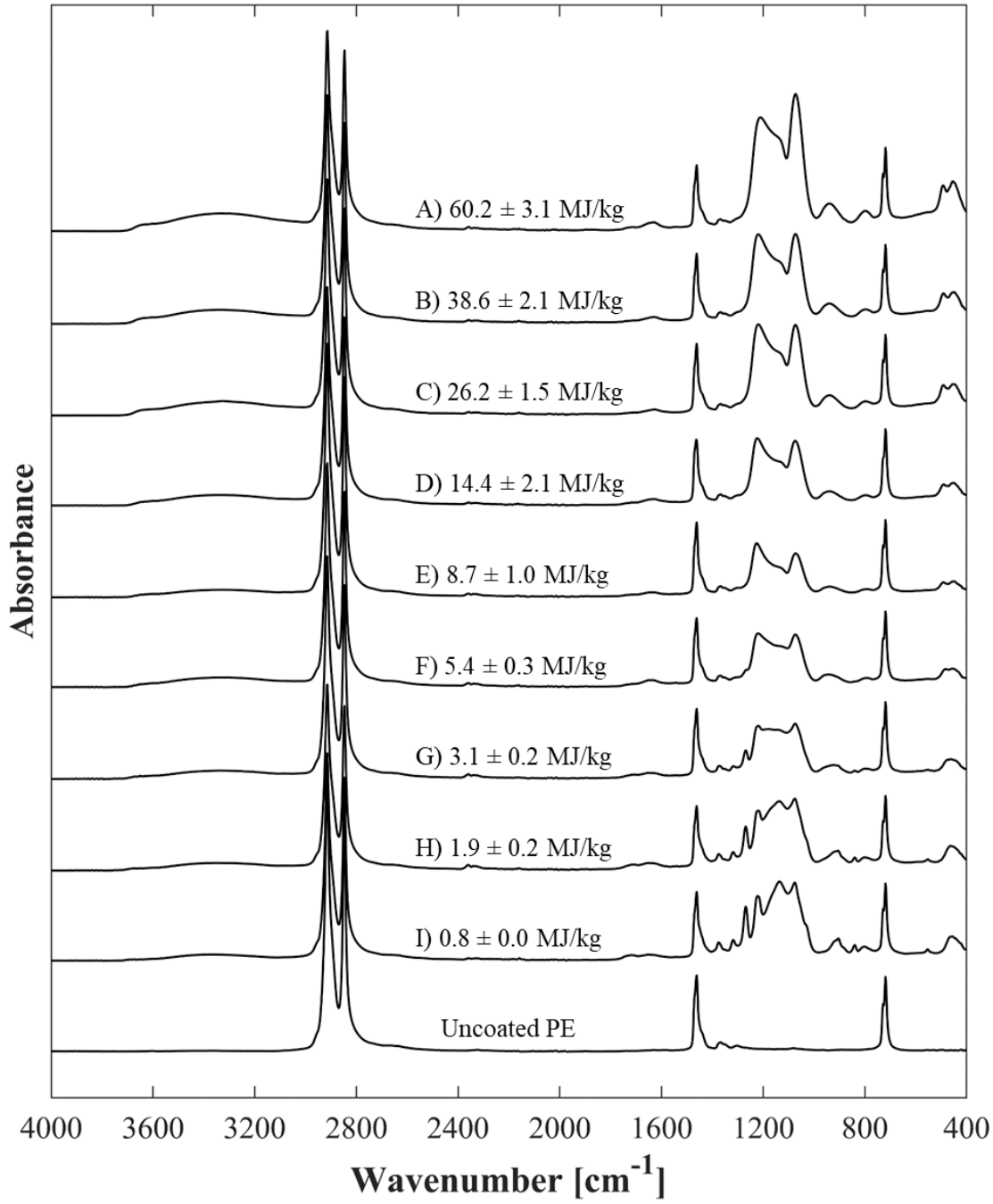

Figure 3.4: ATR-FTIR spectra of uncoated and coated PE substrates.

For all the deposition conditions, bands corresponding to OH stretching vibrations at 3700-2800 cm^{-1} [15], [16] and C=C and C-O stretching vibrations at 1850-1650 cm^{-1} [17], [18] can be recognized. The main differences among coatings deposited under different W/FM values can be observed in the region 400-1400 cm^{-1}. A list of possible assignments of the peaks in this region is reported in Table 3.2.

Wavenumbers [cm^{-1}]	Possible assignment	References
1375	CH_3 deformation	[19], [20]
	CF_2 symmetric stretching	[21]
	CF stretching	[9]
1317	CF stretching	[9]
	CF_3 asymmetric stretching	[22]
1270	CF, CF_2, CF_3 stretching	[22]–[24]
	CH_3 deformation in Si-CH_3	[25], [26]
1220	CF_2 asymmetric stretching	[27]–[30]
1190	Si-O-Si asymmetric stretching (transverse optical, LO)	[31], [32]
1141	CF_2 asymmetric stretching	[21], [33]
1075	Si-O-Si asymmetric stretching (longitudinal optical, TO)	[34]–[36]
1040	C-O stretching	[37]
1029	CF or CF_3 stretching	[22], [23], [30]
930	Si-OH stretching	[36], [38], [39]
906	CH_2 rocking	[40]
880	Si-C stretching	[41]
840	CH rocking	[20]
	$Si(CH_3)_3$ stretching	[38]
800	Si-O-Si bending	[42], [43], [38]
	Si-O-Si stretching	[25], [34]
	Si-C stretching	[9]
	Si-$(CH_3)_2$ stretching	[43]
	CH_3 rocking	[25]
553	CF_2 bending	[21], [30]
495	CF_2 deformation	[44]
450	Si-O rocking	[45]

Table 3.2: Assignment of the peaks in the region 1400-4000 cm^{-1}.

As W/FM decreases from condition A to condition E, no relevant differences in terms of peaks can be observed. All the spectra exhibit several peaks associated to silicon presence in the coating, such

as the Si-O rocking at 450 cm^{-1}, the Si-O-Si bending or stretching at 800 cm^{-1}, the Si-O stretching at 900 cm^{-1}, the Si-OH stretching at 930 cm^{-1}, and the Si-O-Si asymmetric stretching at 1075 cm^{-1} (transverse optical, TO). Furthermore, peaks corresponding to CF_2 deformation at 495 cm^{-1} and to CF_2 asymmetric stretching at 1220 cm^{-1} can be recognized in all the spectra. Additional peaks, like the CF_2 asymmetric stretching at 1141 cm^{-1} and the Si-O-Si asymmetric stretching (longitudinal optical, LO) at 1190 cm^{-1}, can be clearly appreciated only by a proper deconvolution of the spectra. As an example, the deconvoluted spectrum (for wavenumbers comprised between 1000 and 1350 cm^{-1}) of coatings deposited in conditions A is reported in Figure 3.5a.

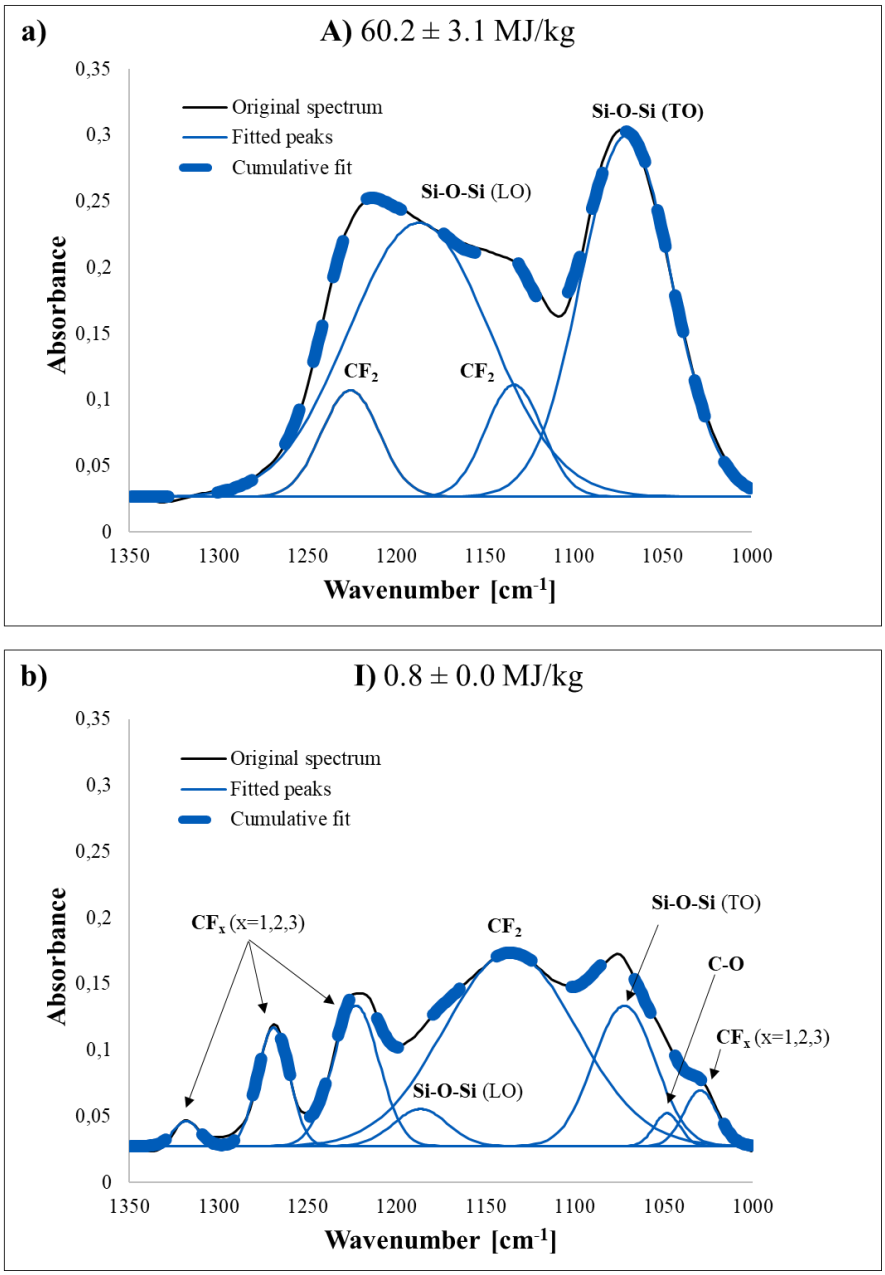

Figure 3.5: Deconvoluted spectra in conditions A (a) and I (b).

A different behavior can be observed in spectra from condition E to condition I, since a progressively higher fluorine and carbon content in the coatings can be detected as W/FM decreases. Fluorine-related peaks observed also in conditions A-E, like the one at 1141 cm^{-1}, become more pronounced, and the appearance of new peaks is registered at 553 cm^{-1}, 1030 cm^{-1}, 1270 cm^{-1}, 1316 cm^{-1} and 1370 cm^{-1} mainly attributed to CF_x (x=1,2,3), at 840 cm^{-1} and 906 cm^{-1} associated to CH_x (x=1,2,3) vibrations, at 880 cm^{-1} associated to Si-C stretching, and at 1040 cm^{-1} related to C-O stretching. The described behavior occurs along with a reduction of the contribution of the Si-O-Si related peaks at 450, 1075 and 1190 cm^{-1}. Figure 3.5b shows the deconvoluted spectrum of coatings deposited in condition I.

Since the deconvoluted spectra can provide quantitative information about the chemical composition of the coatings, the areas of two characteristic peaks present in all the investigated conditions, one related to the asymmetric stretching (LO) of Si-O-Si at 1190 cm^{-1} and one to CF_2 at 1141 cm^{-1}, were normalized with respect to the total integrated area and plotted as a function of W/FM (Figure 3.6) to analyze the chemical behavior of the coatings while varying W/FM. The ratio of the peaks and the total area remains almost constant for coatings deposited in conditions from A to E, while drastically changes between conditions E to I. More precisely, as W/FM decreases from E to I, the presence of the CF_2 asymmetric stretching increases at expenses of the Si-O-Si asymmetric stretching.

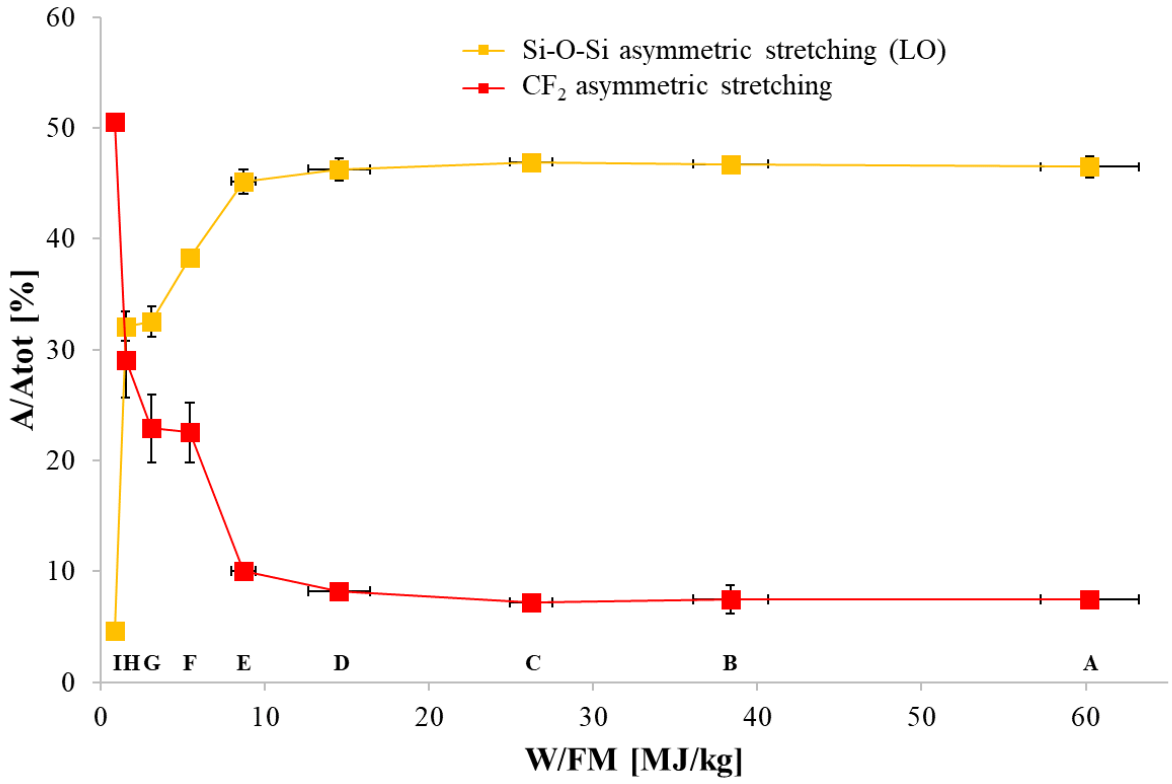

Figure 3.6: Ratio of the area of the peaks related to Si-O-Si asymmetric stretching (LO) and CF_2 asymmetric stretching and the total area as a function of W/FM.

3.3.1.2 XPS results

C 1s, F 1s, O 1s and Si 2p XPS spectral regions of coatings obtained under different W/FM values are reported in Figure 7. In particular, only coatings deposited in conditions E (8.7 ± 1.0 MJ/kg), G (3.1 ± 0.2 MJ/kg), and I (0.8 ± 0.0 MJ/kg) were analyzed through XPS because no significant differences were observed in the ATR-FTIR spectra of samples obtained for W/FM values ranging from 60.2 to 8.7 MJ/kg (A-E conditions). The spectra of an uncoated PE substrate are added as references.

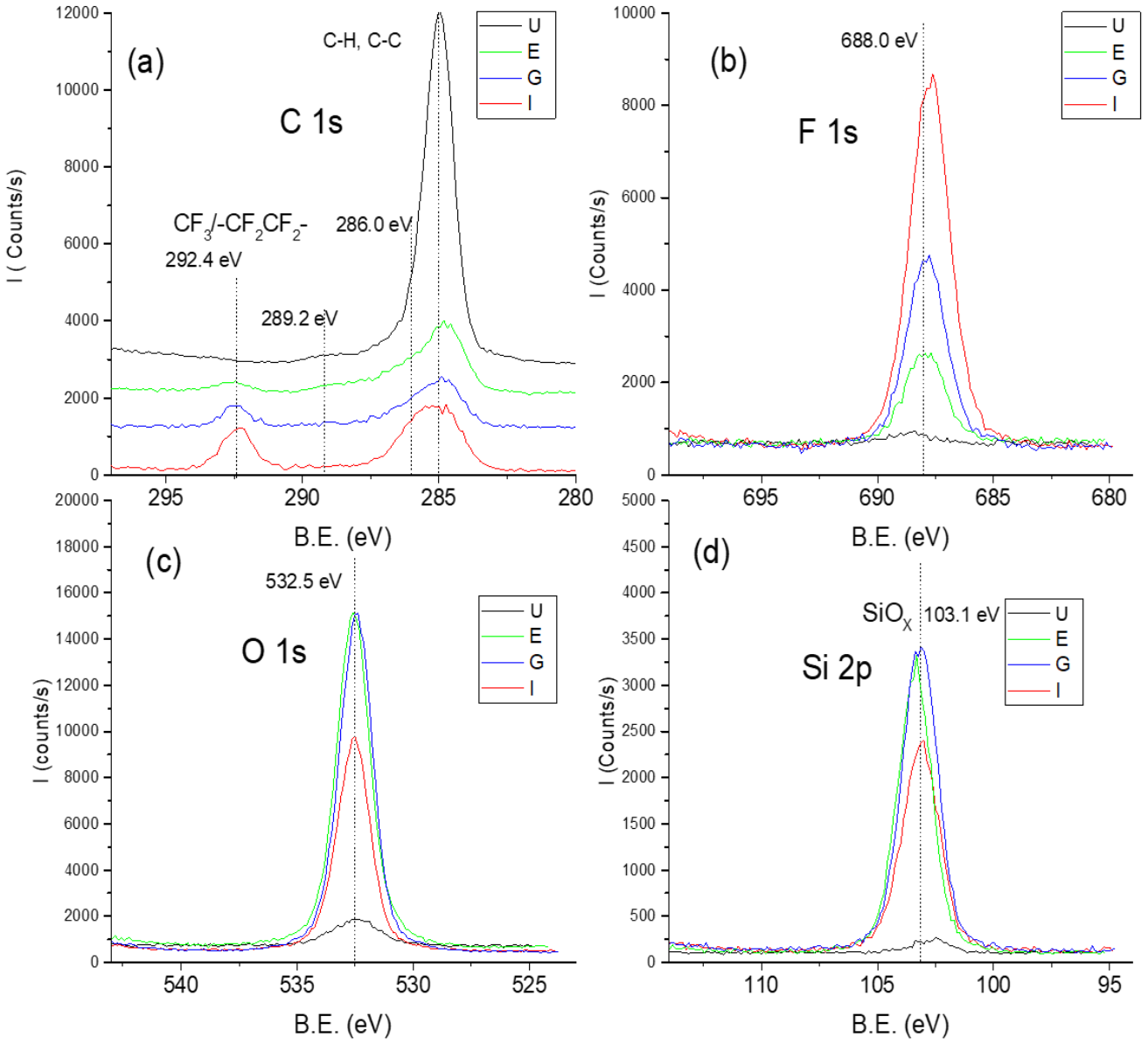

Figure 3.7: C 1s (a), F 1s (b), O 1s (c) and Si 2p (d) XPS spectral regions of the uncoated PE substrate (U) and of the coatings deposited in conditions E, G and I. C 1s spectra of the various samples are vertically translated for a better evaluation of the low intensity features.

C 1s spectrum (Figure 3.7a) of uncoated PE shows a main component at the Binding Energy (B.E.) of 285.0 eV due to -CH_2- . [10], [46] The small band at about 289.2 eV due to carbon atoms of carboxylic groups [10], [47] is indication of a slight surface oxidation. After the coating deposition on the substrate, a new band at 292.4 eV whose intensity increases by decreasing the W/FM value can be observed. Band position is consistent with the presence of both CF_3 groups [46]–[48] and -CF_2-CF_2- chains [46], [48]. Besides the band at 292.4 eV, coatings show a low band at 289.2 eV, which decreases by decreasing W/FM until it is no longer observable for coatings obtained in condition I, and a shoulder at about 286.0 eV, which instead increases by decreasing W/FM. These two components can be due to a small amount of oxidized carbons (carboxylic and C-O groups, respectively), but contributions due to monofluorinated carbons (usually around 289-288 eV [48]) and hydrocarbon atoms (CH_x) close to CF_x groups (usually around 286 eV [48]) cannot be excluded. The increasing presence of fluorinated groups by decreasing the W/FM ratio from E to I conditions is also confirmed by the atomic composition of the coatings obtained from XPS elemental analysis (Table 3.3) as well as by the spectrum of F 1s region (Figure 3.7b). Table 3.3 shows an evident increase of fluorine content by decreasing the W/FM ratio, which mirrors the increase of CF_3/-CF_2CF_2- groups. F 1s band consists of a single peak whose intensity increases moving from conditions E to I. The B.E is 688.0 eV for coatings deposited in condition E and decreases to 687.8 eV and 687.7 eV for conditions G and I, respectively. This B.E. shift suggests a progressive increase of CF_3 groups compared to CF_2 groups since F 1s B.E. is expected to be for CF_2 about 1.8 eV higher than CF_3 [48]. XPS elemental analysis (Table 3.3) shows that O and Si are also present in the coatings. Their concentrations slightly decrease reducing the W/FM ratio from E to G and strongly decrease for condition I. The B.E. positions of O 1s (532.5 eV) and Si 2p (103.1 eV) peaks (Figures 3.7c and 3.7d) are consistent with the presence of SiO_x moieties [46], [49] whose amount is reduced for W/FM ratio below 3.1 MJ/kg.

Deposition condition	**C_{tot}**	**(CF_x)**	**O**	**F**	**Si**
Uncoated PE	88.7	(0)	8.4	1.4	1.5
E	19.9	(1.4)	54.2	4.8	21.1
G	16.4	(3.4)	51.1	11.6	20.9
I	27.2	(7.2)	32.8	24.9	15.1

Table 3.3: XPS atomic concentration of uncoated PE substrates and coatings obtained under conditions E, G, and I.

3.3.1.3 WCA measurements

Water contact angles of thin films deposited under different W/FM values are reported in Figure 3.8. As W/FM decreases from condition A (60.2 ± 3.1 MJ/kg) to condition E (8.7 ± 1.0 MJ/kg), the contact angle remains constant around 58° degrees. At lower W/FM values, the contact angle gradually

increases, reaching a maximum value of about 83°. The uncoated PE substrate exhibits a contact angle of 93.3° ± 4.8°, which is higher than all the measured angles for the deposited coating.

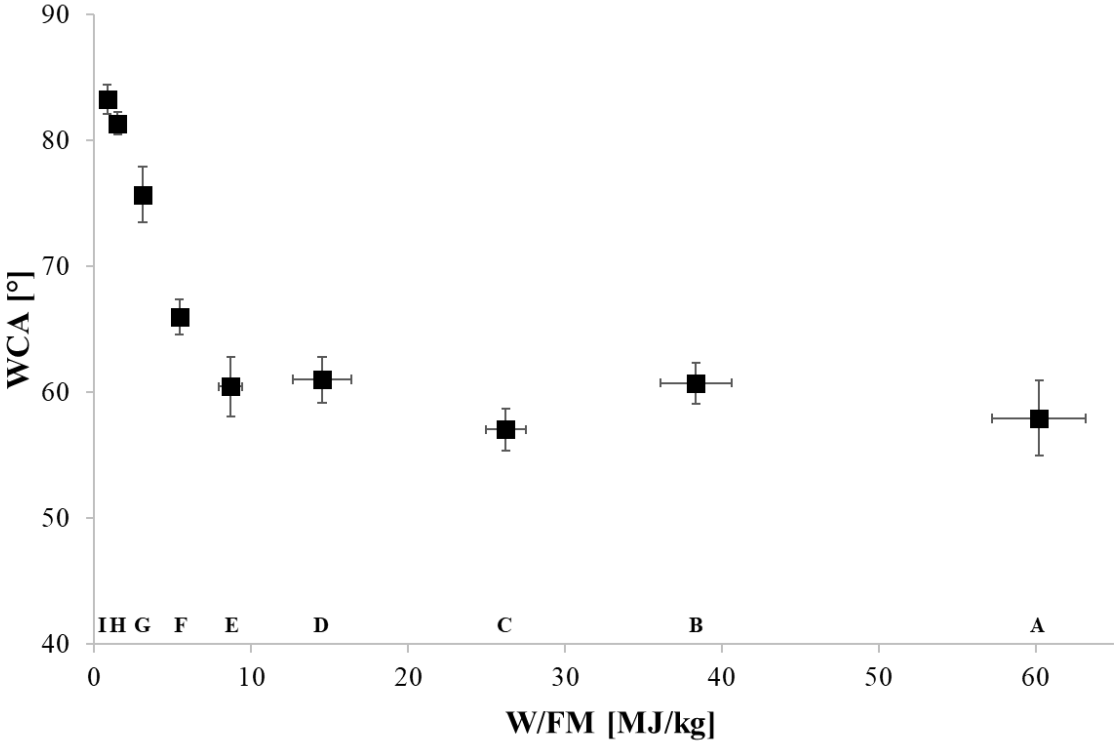

Figure 3.8: Water contact angles of thin films deposited under different W/FM values.

3.3.1.4 SEM results

Thickness analysis

The deposition rate (DR) of coatings deposited under different W/FM values was calculated from SEM images by measuring the thickness of the cross section of samples broken in liquid nitrogen (Figure 3.9) and dividing it for the deposition time (2 minutes). The DR, reported in Figure 3.10, is observed to decrease following a quasi-linear behaviour as W/FM decreases. Cross section images also highlight that, independently from the W/FM value, the structure of the coatings appears compact and non-porous.

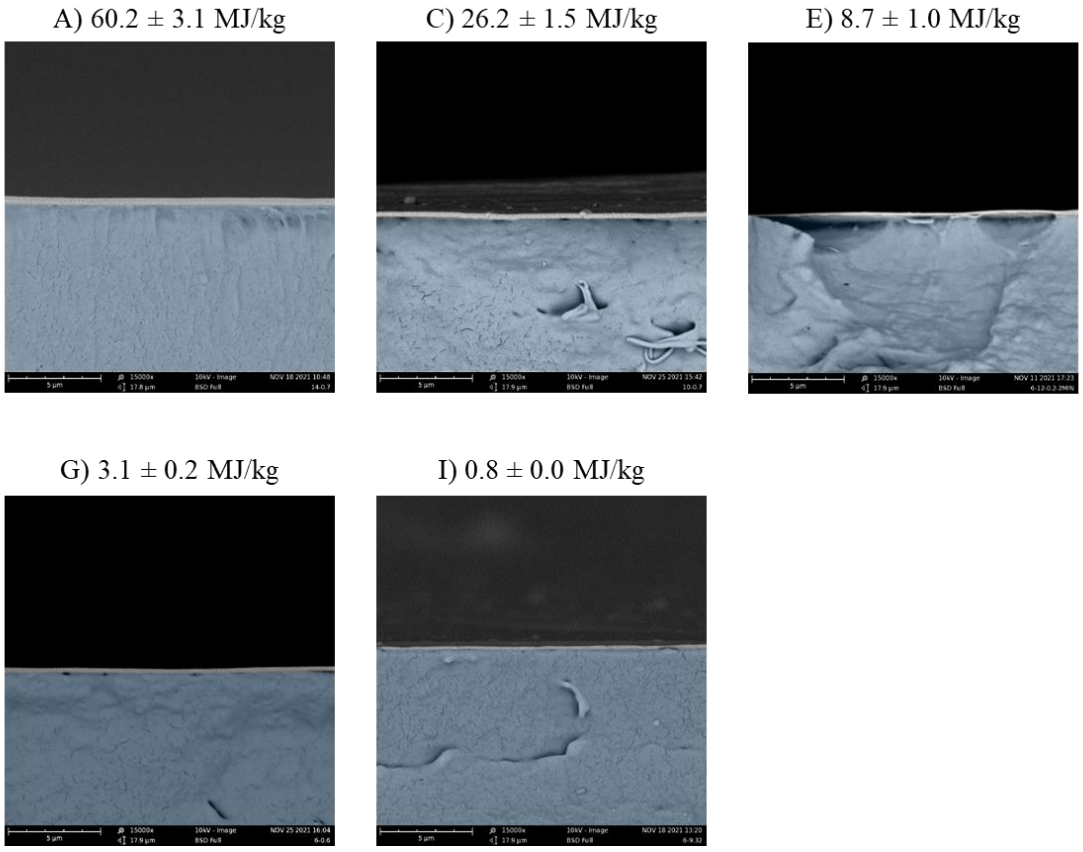

Figure 3.9: SEM images of cross-sections of thin films deposited under different W/FM values. To easily recognize the coating, the substrate is highlighted in light blue.

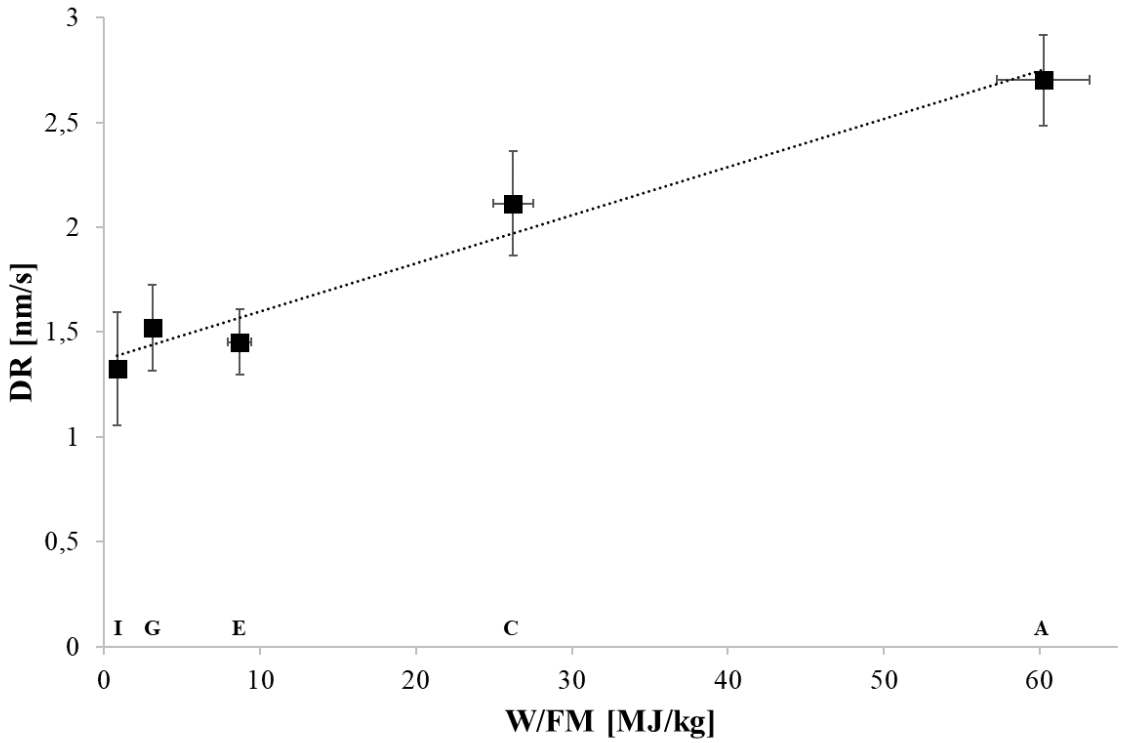

Figure 3.10: DR as a function of W/FM.

Morphological analysis

According to the SEM images reported in Figure 3.11, the surface of the uncoated PE substrate appears flat and smooth, while in coatings deposited in conditions A and C (conditions with the highest W/FM values), the presence of numerous fractures (black lines in the images) can be observed. As W/FM decreases, the fractures in the coating disappear, but the number of granular structures on the surface of the film progressively increases.

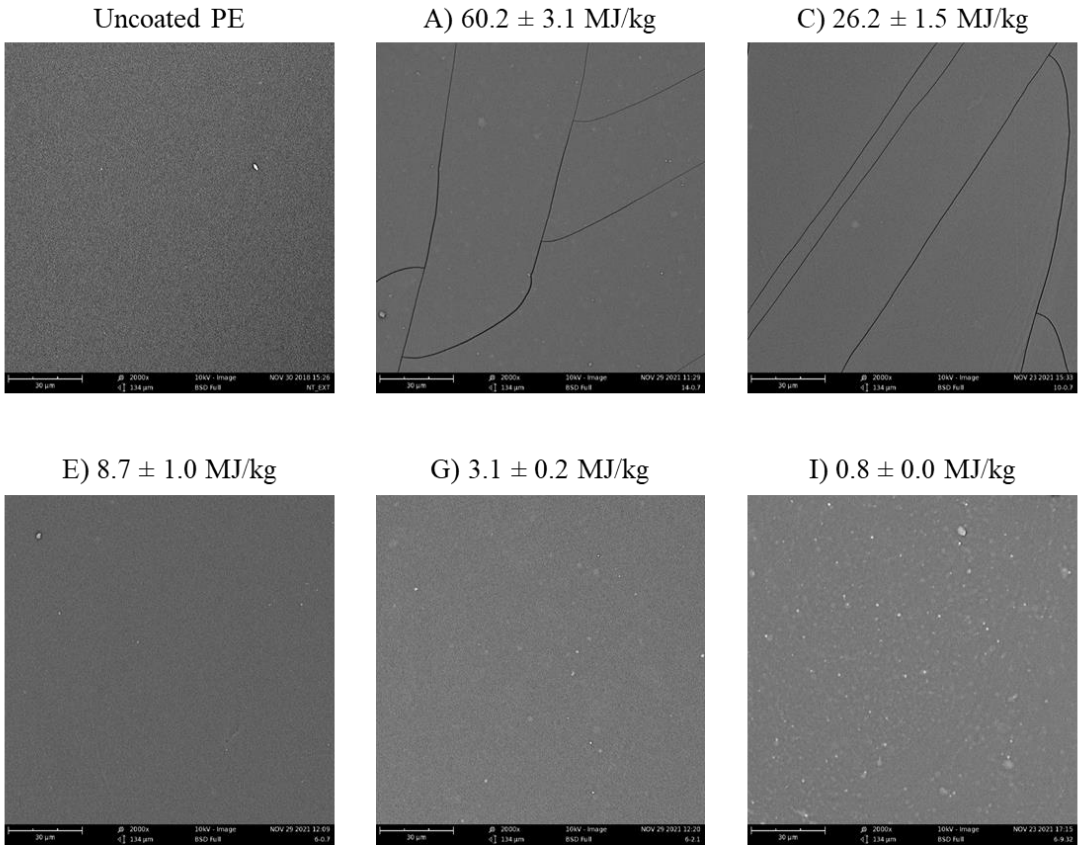

Figura 3.11: SEM images of uncoated and coated substrates.

3.3.2 Antiadhesive properties

The antibacterial activity of coatings deposited in condition E (8.7 ± 1.0 MJ/kg, representative of conditions ranging from A to E), G (3.1 ± 0.2 MJ/kg) and I (0.8 ± 0.0 MJ/kg) was assessed against *P. aeruginosa* and *S. aureus*. Adhesion patterns of both bacteria onto the uncoated PE and the coated surfaces are displayed in Figure 3.12. To easily associate the deposition condition to the investigated microorganism, subscripts P or S are added (e.g. E_P), representing *P. aeruginosa* and *S. aureus*, respectively.

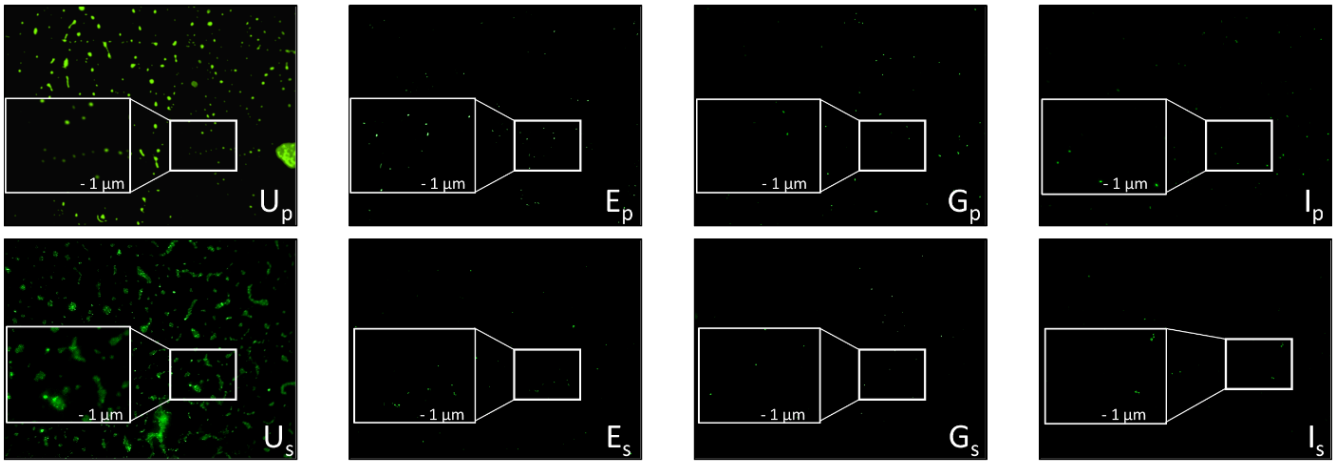

Figure 3.12: Fluorescent images of cells adhering on uncoated surface (U_P) and on surfaces coated in different deposition conditions: *P. aeruginosa* (first row) and *S. aureus* (second row). The inserts are magnifications of traced areas.

A visible reduction in the number of adhered bacteria can be observed on all the coated samples (Figures 3.12E_P-I_P and 3.12E_S-Is) on the account of the antiadhesive properties of the deposited coatings. The quantitative evaluation of the cell adhesion, estimated by Scion Image Software, and the related percentages of covered area (% A) are shown in Table 3.4.

Deposition condition	***P. aeruginosa***		***S. aureus***	
	IntDen mean	% A	IntDen mean	% A
Uncoated PE	4009.7	2.95	6257.4	4.6
E	134.6	0.099	124.9	0.092
G	29.1	0.02	14.4	0.011
I	57.1	0.04	38.4	0.028

Table 3.4: Adhesion of *P. aeruginosa* and *S. aureus* cells on the uncoated and coated surfaces in terms of integrate density (IntDen) and related percentages of covered area (% A).

IntDen values of 4009.7 and 6257.4 can be deduced in uncoated samples for *P. aeruginosa* and for *S. aureus*, corresponding to covered areas (% A) of about 2.95% and 4.6%, respectively. When a coating deposited in condition E is present, IntDen values are significantly reduced: *P. aeruginosa* exhibits an IntDen value of 134.6, corresponding to 0.099% A, and *S. aureus* exhibits a 124.9 IntDen value, corresponding to 0.092% A. A further improvement in the antiadhesive properties can be observed decreasing the W/FM to condition G, showing IntDen 29.1 and 0.02% A for *P. aeruginosa* and IntDen 14.4 and 0.011% A for *S. aureus.* Finally, for coatings deposited in condition I (corresponding to the minimum W/FM value), the percentage of cell surface coverage appears slightly increased, showing IntDen 57.1 and 0.04% A for *P. aeruginosa* and IntDen 38.4 and 0.028 % A for *S. aureus*.

By comparing the obtained percentages with those of the uncoated samples, a significant reduction (significance level of 99.9%, p-value < 0.001) is indicated by t-test for all the coated samples.

P. aeruginosa adhesion rate is reduced by about 96.6% for E_P, 99.3% for G_P and 99.6% for I_P (Figure 3.13A), while *S. aureus* adhesion rate is reduced by 98% for G_s, 99.8% for G_S and 99.4% for I_S (Figure 3.13B). In addition, only coatings deposited in condition G result in a significant increase in the antiadhesive properties compared to the coatings deposited in condition E (significance level of 95%, with p-value of 0.0236 and 0.0369 for *P. aeruginosa* and *S. aureus*, respectively).

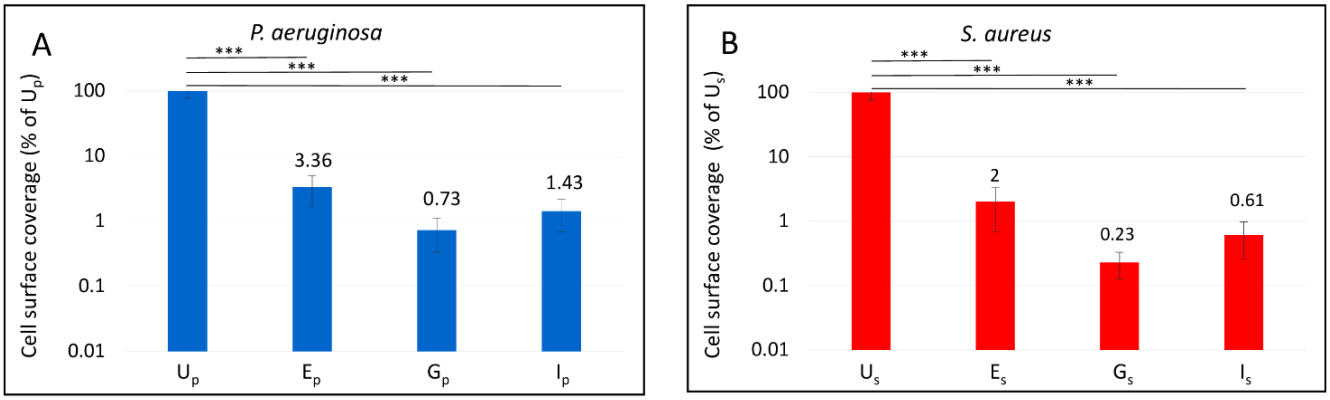

Figure 3.13: Percentage of cell surface coverage of coated samples vs uncoated samples for *P. aeruginosa* (A) and *S. aeurus* (B). Significance levels of 95% (*), 99% (**), 99.9% (***) are attributed for p-values lower than 0.05, 0.01 and 0.001 respectively. If not indicated, the deposition conditions do not show significant differences.

3.4 Discussion

According to the results obtained with several surface characterization techniques, W/FM appears as a suitable controlling parameter for the process since its variation allows to work in two distinguished deposition regimes which lead to coatings with different chemical and physical characteristics. Indeed, ATR-FTIR spectra show the presence of two deposition regimes when varying W/FM: the regime associated to conditions from A (60.2 ± 3.1 MJ/kg) to E (8.7 ± 1.0 MJ/kg) and the one associated to conditions from E to I (0.8 ± 0.0 MJ/kg). Spectra of coatings deposited in the first regime do not change as a function of W/FM, exhibiting a predominant presence of peaks related to vibrations of the bonding Si-O-Si. Since the molecular structure of the starting precursor involves a central silicon atom surrounded by three oxygens and one carbon, the presence of bonding Si-O-Si suggests that the W/FM values in the first regime lead to an intense fragmentation of the precursor in the discharge. Nonetheless, even in these conditions of intense fragmentation, a minimum retention of precursor functional groups in the thin films is guaranteed, as confirmed by the presence of fluorine and carbon peaks. In the second regime, the chemical composition of the coatings drastically varies as W/FM decreases: new peaks associated to fluorine and carbon (in form of CF_x and CH_x, x = 1,2,3) appear at expenses of the vibrations of the bonding Si-O-Si. XPS analysis further supports these results, showing a progressive increase in the content of fluorine and carbon in the coatings as W/FM decreases. This behavior, observed also in other works in literature related to PP processes at AP [25], [50], can be explained considering the lower values

of W/FM in the second regime with respect to the ones in the first regime: as the energy per precursor unit is reduced, the fragmentation of the precursor in the discharge becomes less intense and an increased presence of the functional groups of the precursor can be observed in the coating.

The existence of two deposition regimes can be clearly appreciated also by analyzing the behavior of the ratios of the areas of peaks related to the asymmetric stretching (LO) of Si-O-Si at 1190 cm^{-1} and of the one associated to one to CF_2 at 1141 cm^{-1} with respect to the total integrated area (ATR-FTIR quantitative analysis) as a function of W/FM. As W/FM decreases from A to E, both the ratios stay constant, suggesting a similar chemical composition for the coatings deposited in those conditions, while they vary from E to I highlighting a major retention of characteristic functional groups in the coatings.

WCA analysis provides a further confirmation of the presence of the two deposition regimes hypothesized based on ATR-FTIR and XPS analyses. Indeed, the wettability of the coating remains constant as W/FM decreases from condition A to condition E and then gradually decreases from E to I as W/FM decreases. The progressive decrease in the wettability of the coating is in agreement with the progressively higher presence in the coating of carbon and fluorine in form of alkyl and fluoroalkyl groups (CH_x and CF_x, with x = 1, 2, 3), which are known to increase the hydrophobicity degree of a surface [51].

The presence of two domains is supported also by SEM cross section analysis where the normalized DR (obtained by dividing DR for the precursor feed rate FM) is considered (Figure 3.14).

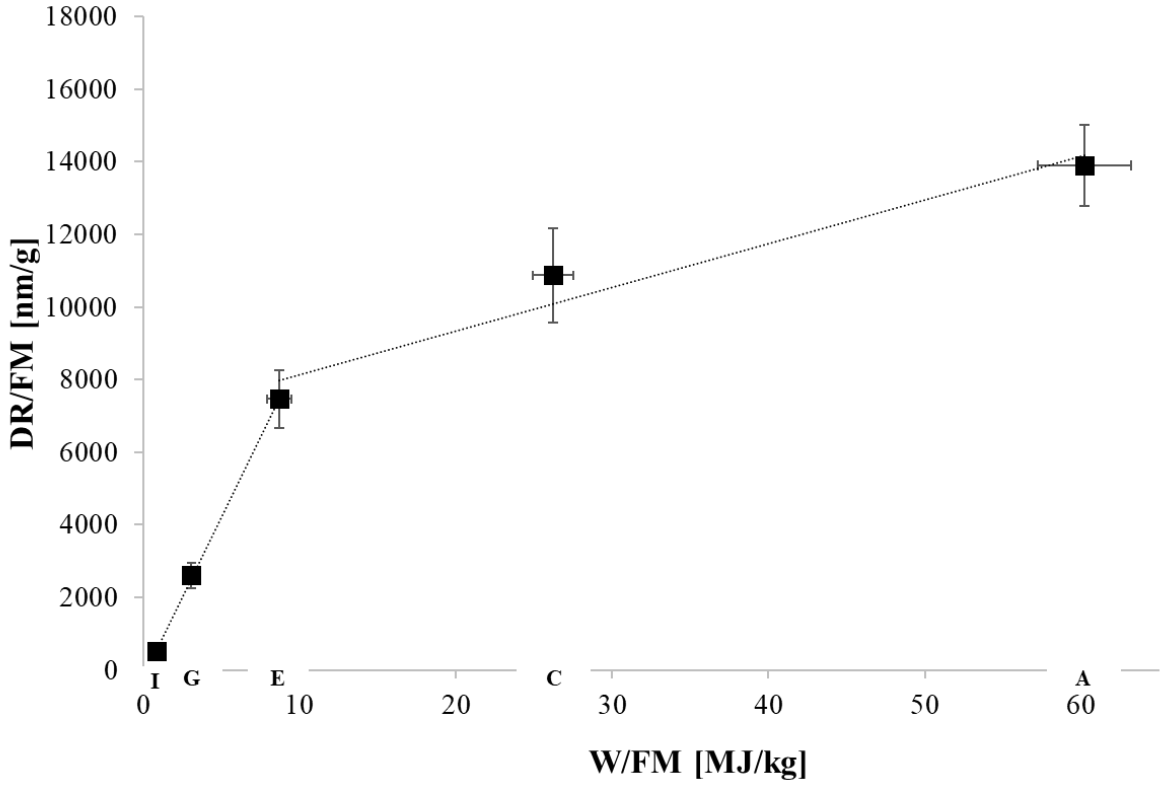

Figure 3.14: DR/FM as a function of W/F.

The behaviour of DR/FM as a function of W/FM has been discussed in detail in the work of Gilliam et al. [52], who investigated the PP of fluorocarbon monomers in LP audio-frequency and RF discharges. In that work, the normalized DR revealed two deposition domains for each monomer: the energy-deficient domain and the monomer-deficient domain. According to their discussion, the energy-deficient domain exists at low W/FM, in which the system contains excess of precursor, and the formation of depositing species is dependent on the energy input; in this domain, the normalized DR increases linearly with W/FM. When a critical value of the Yasuda parameter $(W/FC)_c$ is reached, a further increase of energy does not create more depositing species and the normalized deposition rate remains constant; this region is called the monomer-deficient region, in which the precursor is analogous to a limiting reactant. In this work, a similar behaviour to the one obtained by Gilliam at al. can be observed and condition E can be recognized as the critical value of W/FM which marks the distinction in two deposition domains: the energy-deficient domain from I to E, where the slope of DR/FM as a function of W/FM is 880.85 [nm/kJ], and the monomer-deficient domain from E to A, with a slope of 119.97 [nm/kJ]. Correlating these results with what observed by means of all the other characterization techniques, it emerges that in the energy-deficient domain the precursor undergoes to a limited fragmentation, resulting in high retention of fluorine and carbon content, while in the monomer-deficient region the energy excess results in intensive fragmentation and in a loss of characteristic functional groups.

According to the results presented and discussed so far, W/FM values from A to E lead to coatings with low retention of functional groups of the starting precursor and almost constant normalized deposition rate, while W/FM from E to I to coatings with higher retention of functional groups of the starting precursor (such as CF_x and CH_x, x=1,2,3), and decreasing normalized deposition rate. Nonetheless, it must be pointed out that conditions from A to E have been obtained using the same precursor feed rate and decreasing the discharge power, while conditions from E to I using the same discharge power and varying the precursor flow rate; in order to prove the controlling role of the Yasuda parameter itself in the process, coatings deposited under the same W/FM parameter but calculated with a different combination of discharge power and precursor feed rate were compared. Quantitative ATR-FTIR analysis (Figure 3.15) and WCA measurements (Figure 3.16) highlight almost identical chemical composition and wettability for coatings deposited under same W/FM values.

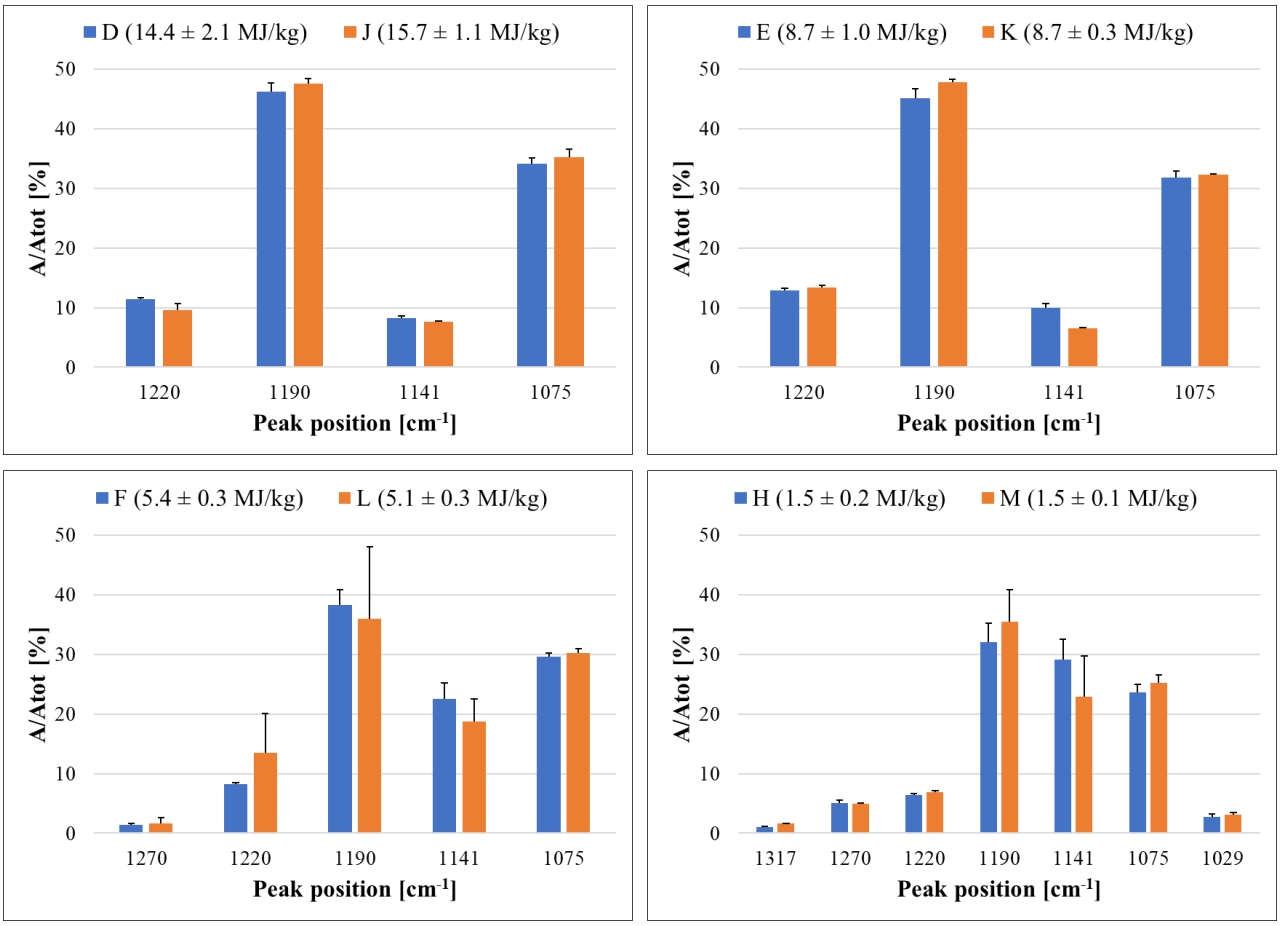

Figure 3.15: Ratio of the area and the total area for peaks related to coating deposited under same W/FM values.

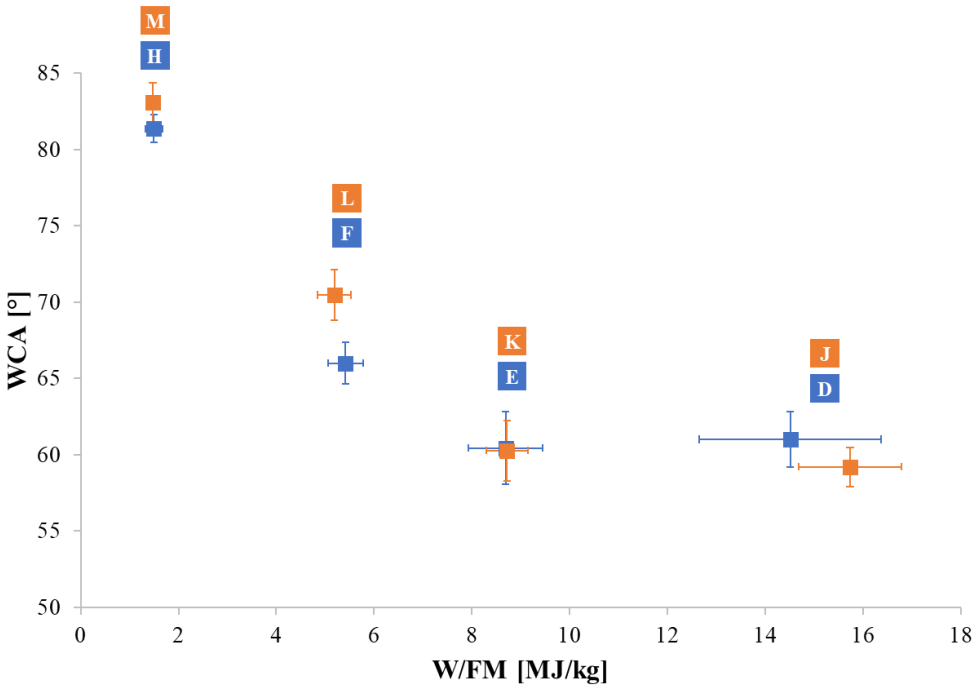

Figure 3.16: WCA of coatings deposited under same W/FM values.

The obtained results suggest that W/FM might be a proper parameter for the control of a polymerization process assisted by an AP single electrode plasma jet and an aerosolized fluorinated silane precursor.

Prior to adhesion activity tests, morphological characteristics of coatings deposited under different W/FM values were analyzed using SEM (Figure 3.11 and further discussion in the Section 3.6). Considering the presence of fractures in conditions A and C, exclusively coatings deposited in condition E (characterized by same chemical composition of A and C), G and I were investigated in terms of antiadhesive properties.

Uncoated samples show a high number of adhered bacteria for both bacteria strains, mainly characterized by an adhesion pattern with island-like multi-layered cell aggregates and empty areas (Figures 3.12U_P and 3.12U_S). According to the results, the surface covered by bacteria is higher for the case of *S. aureus,* as confirmed by IntDen values (4009.7 and 6257.4 for *P. aeruginosa* and *S. aureus,* respectively) and % A (2.95 and 4.6 for *P. aeruginosa* and *S. aureus,* respectively). However, all coated surfaces exhibit a significant reduction of initial bacterial attachment (reduction of 96.6% and 98% for *P. aeruginosa* and *S. aureus,* respectively). These findings can be attributed to the increased levels of fluorine compared to uncoated samples, as highlighted by XPS results. In fact, it is known that fluorine compounds have potential efficacy as antibacterial and anti-biofilm coating materials [1]. In this context, the highest antiadhesive effect is obtained in condition G, while a slight worsening is observed by further decreasing the W/FM value, namely condition I, even if the fluorine content is the highest (around 25%). As the contribution of the granular structure in condition I (Figure 3.11) on the antiadhesive activity of the surfaces cannot be excluded, further studies will be carried out to clarify the mechanisms underlying the interaction occurring between bacteria and coatings deposited under different W/FM conditions.

3.5 Conclusions

In this chapter, a polymerization process assisted by the AP single electrode plasma jet and a fluorinated silane precursor is investigated. The aim of the work is to assess the validity of the Yasuda Parameter (W/FM) as a controlling parameter for the process since nowadays no alternative methodologies for the calculation of the energy absorbed by precursor molecules have been developed for plasma jets and aerosolized precursors. To reach this purpose, the characteristics of coatings deposited under different W/FM values are analyzed using ATR-FTIR analysis, XPS analysis, WCA measurements, and SEM analysis.

ATR-FTIR and XPS results show the presence of two deposition domains as varying W/FM: one leading to coatings with a chemical composition that does not vary with W/FM, the other leading to coatings with a higher retention of functional groups of the starting precursors (such as CH_x and CF_x, x = 1,2,3) as W/FM progressively decreases. These findings are further confirmed by WCA measurements, which highlight a region of W/FM values where the wettability remains constant and one where the

wettability decreases as W/FM decreases (probably due to the increased content of fluorine and carbon in the coating). The plot of DR/FM as a function of W/FM reveals that the two deposition domains observed with the other characterization techniques can be associated with two deposition domains very well known in literature: the energy-deficient and the monomer-deficient domains. In addition to this evidence, the key role of the Yasuda parameter in the process is further demonstrated since coatings deposited under the same W/FM exhibit similar properties, regardless of how W/FM is obtained.

As the interest to study this atmospheric pressure PP process is related to the objective to create antiadhesive surfaces which can prevent the formation of biofilm on implantable medical devices, the antiadhesive activity of coatings deposited under different W/FM values (conditions E, G, I) is investigated against *P. aeruginosa* and *S. aureus*. The biological assay shows that the presence of a coating significatively improves the antiadhesive activity of the substrate and this is probably due to the presence of fluorine in the coating. Further decreasing the W/FM values until condition G contributes to increase the antiadhesive activity. Nonetheless, no further improvement can be seen for coatings deposited in condition I, which is the one with the highest fluorine content, suggesting that also other factors are probably involved in determining the antiadhesive properties of the surface.

3.6 Appendix

The SEM images reported in Figure 3.11, acquired mainly to identify the proper conditions to be analyzed in terms of antiadhesive activity, exhibit interesting characteristics whose detailed explanation, despite being a sort of deviation from the logical flow related to the presence of two regimes while varying W/FM, deserves to be provided in this context. Therefore, this Appendix will be focused on the possible reasons behind the presence of fractures and particles in the coatings.

According to images in Figure 3.11, coatings deposited in conditions A and C show numerous fractures, which disappear decreasing the W/FM value. Despite few articles address this aspect of plasma deposition processes [53], [54], the possible mechanism proposed for the formation of fractures in Si-coatings on thermosensitive polymeric substrates is the different coefficient of thermal dilation between the substrate and the deposited coating. The deposition process, indeed, can induce a thermal stress on the polymeric substrate and consequently lead to its stretching: if the coating is sufficiently adherent to the substrate and has a different coefficient of thermal dilatation, fractures can be formed in the coating. According to ATR-FTIR and XPS analyses, the uncoated substrate exhibits a more "organic character" than the coatings deposited in conditions from A to E, suggesting that in case of heating induced by the process, the thermal stretching of the substrate will be higher than that of the coating and may lead to fractures formation. Considering that the chemical composition of coatings deposited from condition A to condition E should be similar, the reason why fractures cannot be observed in condition E is probably related to the lower heating that is induced in that condition with respect to condition A. The only aspect which makes different conditions A and E is the fact that in the first one a higher discharge power is used, and higher discharge powers usually lead to higher surface heating. To prove this hypothesis, the heating of the substrate during the deposition treatment was investigated. More in detail, the evolution of the substrate surface temperature during the deposition process was analyzed using the infrared sensor Optris CT. Five positions along the diameter of the propylene samples (2 cm long), at a distance of 0.25 mm from each other. The substrate temperature profiles along the diameter of the polymeric substrate for deposition processes in conditions A and E are reported in Figure 3.17.

The temperature measurements confirm the higher heating of the substrate in condition A with respect to condition E. Indeed, while the temperature remains slightly higher than the ambient temperature in condition E, the temperature reaches an average value of 65°C in condition A. The two conditions exhibit also a different profile along the diameter: in condition A the surface temperature seems to be higher in correspondence of the edge of the sample (±10 mm) with respect to the central zone (0 mm) thus generating a "donut shape" behaviour, while in condition E the temperature seems to remain stable along the entire central axis. This behaviour can be related to the more pronounced ambient air diffusion into the plasma discharge in condition A, which increases the gas temperature due to Penning ionization reactions between N_2 molecules and Ar metastable atoms [55] in the part where there is the maximum air penetration (at the edge of the samples). Nonetheless, a detailed discussion on the

trend of the substrate temperature as a function of the position along the central line is beyond the purpose of this thesis.

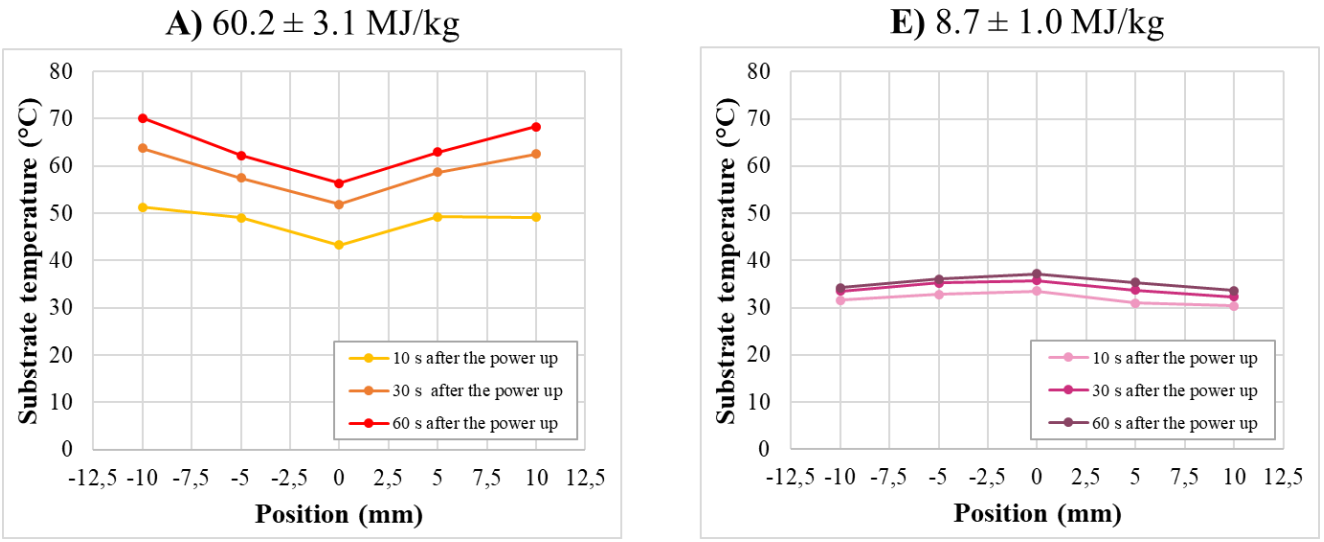

Figure 3.17: Substrate temperature profiles along the diameter of the sample in deposition conditions A and E.

As W/FM further decreases from E to I, the number of granular structures on the surface of the film progressively increases: if in condition E a reduced and almost negligible number of particles can be observed, in conditions G and I their presence is pronounced and proportional to the amount of precursor feed rate (E, G and I are indeed characterized by an increased precursor feed rate). The formation of these structures is due to plasma produced radicals originating from the initial monomer which are recombined in the volume of the discharge and then deposited in form of particles on the substrate. The formation of such particles and their increase with the precursor feed rate has been previously reported in the literature related to atmospheric pressure plasma polymerization of organosilicon precursors. [56], [57] This difference in the surface morphology of the coatings indicates a change in the formation mechanism of the plasma polymers and thus again suggests the presence of two deposition regimes.

3.7 References

[1] Q. Bao N. Nishimura, H. Kamata, K. Furue, Y. Ono, M. Hosomi, and A. Terada, "Antibacterial and anti-biofilm efficacy of fluoropolymer coating by a 2,3,5,6-tetrafluoro-p-phenylenedimethanol structure," *Colloids Surfaces B Biointerfaces*, vol. 151, pp. 363–371, 2017, doi: 10.1016/j.colsurfb.2016.12.020.

[2] S. Parsaei, J. Keeney, and J. Marschall, *Infections of Prosthetic Joints and Related Problems*, Fourth Edi. Elsevier Ltd, 2017.

[3] Z. Khatoon, C. D. McTiernan, E. J. Suuronen, T. F. Mah, and E. I. Alarcon, "Bacterial biofilm formation on implantable devices and approaches to its treatment and prevention," *Heliyon*, vol. 4, no. 12, p. e01067, 2018, doi: 10.1016/j.heliyon.2018.e01067.

[4] A. Trampuz and W. Zimmerli, "Prosthetic joint infections: Update in diagnosis and treatment," *Swiss Med. Wkly.*, vol. 135, no. 17–18, pp. 243–251, 2005, doi: 2005/17/smw-10934.

[5] R. D. Monds and G. A. O'Toole, "The developmental model of microbial biofilms: ten years of a paradigm up for review," *Trends Microbiol.*, vol. 17, no. 2, pp. 73–87, 2009, doi: 10.1016/j.tim.2008.11.001.

[6] J. Fu, Y. Zhang, S. Lin, W. Zhang, G. Shu, J. Lin, H. Li, F. Xu, H. Tang, G. Peng, L. Zhao, S. Chen, and H. Fu, "Strategies for Interfering With Bacterial Early Stage Biofilms," *Front. Microbiol.*, vol. 12, no. June, pp. 1–15, 2021, doi: 10.3389/fmicb.2021.675843.

[7] A. Ghimire and J. Song, "Anti-Periprosthetic Infection Strategies: From Implant Surface Topographical Engineering to Smart Drug-Releasing Coatings," *ACS Appl. Mater. Interfaces*, vol. 13, no. 18, pp. 20921–20937, 2021, doi: 10.1021/acsami.1c01389.

[8] B. R. Coad, P. Favia, K. Vasilev, and H. J. Griesser, "Plasma polymerization for biomedical applications: A review," *Plasma Process. Polym.*, 2022, doi: 10.1002/ppap.202200121.

[9] J. H. Yim, V. Rodriguez-santiago, A. A. Williams, T. Gougousi, D. D. Pappas, and J. K. Hirvonen, "Atmospheric pressure plasma enhanced chemical vapor deposition of hydrophobic coatings using fl uorine-based liquid precursors," *Surf. Coat. Technol.*, vol. 234, pp. 21–32, 2013, doi: 10.1016/j.surfcoat.2013.03.028.

[10] D. Briggs and G. Beamson, "Primary and Secondary Oxygen-Induced C1s Binding Energy Shifts in X-ray Photoelectron Spectroscopy of Polymers," *Anal. Chem.*, vol. 64, no. 15, pp. 1729–1736, 1992, doi: 10.1021/ac00039a018.

[11] C. Satriano, G. M. L. Messina, S. Carnazza, S. Guglielmino, and G. Marletta, "Bacterial adhesion onto nanopatterned polymer surfaces," *Mater. Sci. Eng. C*, vol. 26, no. 5–7, pp. 942–946, 2006, doi: 10.1016/j.msec.2005.09.096.

[12] S. Carnazza, G. Marletta, M. Frasca, L. Fortuna, and S. Guglielmino, "Spatial patterns of microbial retention on polymer surfaces," *J. Adhes. Sci. Technol.*, vol. 25, no. 17, pp. 2255–2280, 2011, doi: 10.1163/016942411X574943.

[13] L. S. Shi, L. Y. Wang, and Y. N. Wang, "The investigation of argon plasma surface modification to polyethylene: Quantitative ATR-FTIR spectroscopic analysis," *Eur. Polym. J.*, vol. 42, no. 7, pp. 1625–1633, 2006, doi: 10.1016/j.eurpolymj.2006.01.007.

[14] N. De Geyter, R. Morent, and C. Leys, “Surface characterization of plasma-modified polyethylene by contact angle experiments and ATR-FTIR spectroscopy,” *Surf. Interface Anal.*, vol. 40, no. 3–4, pp. 608–611, 2008, doi: 10.1002/sia.2611.

[15] R. Morent, N. De Geyter, S. Van Vlierberghe, P. Dubruel, C. Leys, and E. Schacht, “Organic-inorganic behaviour of HMDSO films plasma-polymerized at atmospheric pressure,” *Surf. Coatings Technol.*, vol. 203, no. 10–11, pp. 1366–1372, 2009, doi: 10.1016/j.surfcoat.2008.11.008.

[16] A. S. Meshkova, Y. Liu, F. M. Elam, S. A. Starostin, M. C. M. van de Sanden, and H. W. de Vries, “The role of the gradient film properties in silica moisture barriers synthesized in a roll-to-roll atmospheric pressure plasma enhanced CVD reactor,” *Plasma Process. Polym.*, vol. 15, no. 1, pp. 1–10, 2018, doi: 10.1002/ppap.201700093.

[17] G. Socrates, *Infrared and Raman Characteristic Group Frequencies: Tables and Charts*, vol. 5, no. 2. 1981.

[18] F. Fanelli, F. Fracassi, and R. d’Agostino, “Atmospheric pressure PECVD of fluorocarbon coatings from glow dielectric barrier discharges,” *Plasma Process. Polym.*, vol. 4, no. SUPPL.1, pp. 430–434, 2007, doi: 10.1002/ppap.200731201.

[19] N. M. Mackie, N. F. Dalleska, D. G. Castner, and E. R. Fisher, “Comparison of Pulsed and Continuous-Wave Deposition of Thin Films from Saturated Fluorocarbon/H_2 Inductively Coupled rf Plasmas,” *Chem. Mater.*, vol. 9, no. 1, pp. 349–362, 1997, doi: 10.1021/cm960388q.

[20] J. Fang, L. Zhang, D. Sutton, X. Wang, and T. Lin, “Needleless Melt-Electrospinning of Polypropylene Nanofibres,” 2012, doi: 10.1155/2012/382639.

[21] T. J. Lenk, V. M. Hallmark, C. L. Hoffmann, J. F. Rabolt, D. G. Castner, C. Erdelen, and H. Ringsdorf, “Structural Investigation of Molecular Organization in Self-Assembled Monolayers of a Semifluorinated Amidethiol,” *Langmuir*, vol. 10, no. 12, pp. 4610–4617, 1994, doi: 10.1021/la00024a037.

[22] R. M. Romano, J. Czarnowski, and C. O. Della Védova, “Preparation and conformational properties of the perfluoro diether $CF_3OCF_2OCF_2C(O)F$, a model molecule to study properties of perfluoro polyethers,” *Inorg. Chem.*, vol. 40, no. 13, pp. 3039–3047, 2001, doi: 10.1021/ic0008520.

[23] L. Martinu, H. Biederman, and J. Nedbal, “Dielectric properties of fluorocarbon and chlorofluorocarbon films plasma polymerized in an R.F. glow discharge,” *Thin Solid Films*, vol. 136, no. 1, pp. 11–19, 1986, doi: 10.1016/0040-6090(86)90103-3.

[24] V. Y. Osipov, N. M. Romanov, K. Kogane, H. Touhara, Y. Hattori, and K. Takai, “Intrinsic infrared absorption for carbon–fluorine bonding in fluorinated nanodiamond,” *Mendeleev Commun.*, vol. 30, no. 1, pp. 84–87, 2020, doi: 10.1016/j.mencom.2020.01.028.

[25] R. Morent, N. De Geyter, T. Jacobs, S. Van Vlierberghe, P. Dubruel, C. Leys, and E. Schacht, “Plasma-polymerization of HMDSO using an atmospheric pressure dielectric barrier discharge,” *Plasma Process. Polym.*, vol. 6, no. SUPPL. 1, pp. 537–542, 2009, doi: 10.1002/ppap.200931101.

[26] D. P. Dowling, C. E. Nwankire, M. Riihimäki, R. Keiski, and U. Nylén, “Evaluation of the anti-fouling properties of nm thick atmospheric plasma deposited coatings,” *Surf. Coatings Technol.*, vol. 205, no. 5, pp. 1544–1551, 2010, doi: 10.1016/j.surfcoat.2010.10.010.

[27] H. Giegengack and D. Hinze, “Investigations of the structure of thin fluorocarbon films by x-ray diffraction and infrared spectroscopy,” *Phys. Status Solidi*, vol. 8, no. 2, pp. 513–520, 1971, doi: 10.1002/pssa.2210080221.

[28] J. J. Senkevich and D. W. Sherrer, “Plasma enhanced chemical vapor deposition of fluorocarbon thin films via CF3H/H2 chemistries: Power, pressure, and feed stock composition studies,” *J. Vac. Sci. Technol. A Vacuum, Surfaces, Film.*, vol. 18, no. 2, pp. 377–384, 2000, doi: 10.1116/1.582196.

[29] K. K. S. Lau, J. A. Caulfield, and K. K. Gleason, “Structure and morphology of fluorocarbon films grown by hot filament chemical vapor desposition,” *Chem. Mater.*, vol. 12, no. 10, pp. 3032–3037, 2000, doi: 10.1021/cm000499w.

[30] K. P. Huang, P. Lin, and H. C. Shih, “Structures and properties of fluorinated amorphous carbon films,” *J. Appl. Phys.*, vol. 96, no. 1, pp. 354–360, 2004, doi: 10.1063/1.1755849.

[31] B. Karmakar, *Fundamentals of Glass and Glass Nanocomposites*. Elsevier Inc., 2016.

[32] L. Adumeau, C. Genevois, L. Roudier, C. Schatz, F. Couillaud, and S. Mornet, “Impact of surface grafting density of PEG macromolecules on dually fluorescent silica nanoparticles used for the in vivo imaging of subcutaneous tumors,” *Biochim. Biophys. Acta - Gen. Subj.*, vol. 1861, no. 6, pp. 1587–1596, 2017, doi: 10.1016/j.bbagen.2017.01.036.

[33] M. Inayoshi, M. Hori, T. Goto, M. Hiramatsu, M. Nawata, and S. Hattori, “ Formation of polytetrafluoroethylene thin films by using CO_2 laser evaporation and XeCl laser ablation ,” *J. Vac. Sci. Technol. A Vacuum, Surfaces, Film.*, vol. 14, no. 4, pp. 1981–1985, 1996, doi: 10.1116/1.580071.

[34] A. Fidalgo and L. M. Ilharco, “The defect structure of sol-gel-derived silica/polytetrahydrofuran hybrid films by FTIR,” *J. Non. Cryst. Solids*, vol. 283, no. 1–3, pp. 144–154, 2001, doi: 10.1016/S0022-3093(01)00418-5.

[35] H. Sanaeishoar, M. Sabbaghan, and F. Mohave, “Synthesis and characterization of micro-mesoporous MCM-41 using various ionic liquids as co-templates,” *Microporous Mesoporous Mater.*, vol. 217, pp. 219–224, 2015, doi: 10.1016/j.micromeso.2015.06.027.

[36] S. A. Starostin, M. Creatore, J. B. Bouwstra, M. C. M. Van De Sanden, and H. W. De Vries, “Towards roll-to-roll deposition of high quality moisture barrier films on polymers by atmospheric pressure plasma assisted process,” *Plasma Process. Polym.*, vol. 12, no. 6, pp. 545–554, 2015, doi: 10.1002/ppap.201400194.

[37] M. N. Chai and M. I. N. Isa, “The Oleic Acid Composition Effect on the Carboxymethyl Cellulose Based Biopolymer Electrolyte,” *J. Cryst. Process Technol.*, vol. 03, no. 01, pp. 1–4, 2013, doi: 10.4236/jcpt.2013.31001.

[38] X. Zhu, F. Arefi-khonsari, C. Petit-etienne, and M. Tatoulian, “Open Air Deposition of SiO 2 Films by an Atmospheric Pressure Line-Shaped Plasma,” pp. 407–413, 2005, doi: 10.1002/ppap.200400049.

[39] B. Shokri, M. A. Firouzjah, and S. I. Hosseini, “FTIR analysis of silicon dioxide thin film deposited by metal organic-based PECVD,” *Proc. 19th Int. Plasma Chem. Soc.*, pp. 1–4, 2009.

[40] A. M. Udrea, A. Dinache, J. M. Pagès, and R. A. Pirvulescu, “Quinazoline derivatives designed

as efflux pump inhibitors: Molecular modeling and spectroscopic studies," *Molecules*, vol. 26, no. 8, pp. 1–15, 2021, doi: 10.3390/molecules26082374.

[41] Y. Sawada, S. Ogawa, and M. Kogoma, "Synthesis of plasma-polymerized tetraethoxysilane and hexamethyldisiloxane films prepared by atmospheric pressure glow discharge," *J. Phys. D. Appl. Phys.*, vol. 28, no. 8, pp. 1661–1669, 1995, doi: 10.1088/0022-3727/28/8/015.

[42] M. T. Kim, "Deposition behavior of hexamethydisiloxane films based on the FTIR analysis of Si-O-Si and Si-CH_3 bonds," *Thin Solid Films*, vol. 311, no. 1–2, pp. 157–163, 1997, doi: 10.1016/S0040-6090(97)00683-4.

[43] F. Babonneau, K. Thorne, and J. D. Mackenzie, "Dimethyldiethoxysilane/Tetraethoxysilane Copolymers: Precursors for the Si-C-O System," no. 10, pp. 554–558, 1989.

[44] Y. Kawano and S. C. De Araujo, "Raman and infrared spectra of polychlorotrifluoroethylene," *Journal of the Brazilian Chemical Society*, vol. 7, no. 6. pp. 491–496, 1996, doi: 10.5935/0103-5053.19960088.

[45] E. Herth, R. Zeggari, J. Y. Rauch, F. Remy-Martin, and W. Boireau, "Investigation of amorphous SiOx layer on gold surface for Surface Plasmon Resonance measurements," *Microelectron. Eng.*, vol. 163, no. October 2017, pp. 43–48, 2016, doi: 10.1016/j.mee.2016.04.014.

[46] J. F. Moulder, W. F. Stickle, P. E. Sobol, and K. D. Bomben, *Handbook of X-ray Photoelectron Spectroscopy*. Perkin-Elmer Corporation, 1993.

[47] X. L. Zhu, S. B. Liu, B. Y. Man, C. Q. Xie, D. P. Chen, D. Q. Wang, T. C. Ye, and M. Liu, "Analysis by using X-ray photoelectron spectroscopy for polymethyl methacrylate and polytetrafluoroethylene etched by KrF excimer laser," *Appl. Surf. Sci.*, vol. 253, no. 6, pp. 3122–3126, 2007, doi: 10.1016/j.apsusc.2006.07.002.

[48] G. Nansé, E. Papirer, P. Fioux, F. Moguet, and A. Tressaud, "Fluorination of carbon blacks: An X-ray photoelectron spectroscopy study: I. A literature review of XPS studies of fluorinated carbons. XPS investigation of some reference compounds," *Carbon N. Y.*, vol. 35, no. 2, pp. 175–194, 1997, doi: 10.1016/S0008-6223(96)00095-4.

[49] C. Tudisco, G. T. Sfrazzetto, A. Pappalardo, A. Motta, G. A. Tomaselli, I. L. Fragalà, F. P. Ballistreri, and G. G. Condorelli, "Covalent functionalization of silicon surfaces with a cavitand-modified salen," *Eur. J. Inorg. Chem.*, no. 13, pp. 2124–2131, 2011, doi: 10.1002/ejic.201001239.

[50] M. A. Gilliam, S. A. Farhat, G. E. Garner, B. P. Stubbs, and B. B. Peterson, "Characterization of the deposition behavior and changes in bonding structures of hexamethyldisiloxane and decamethylcyclopentasiloxane atmospheric plasma-deposited films," *Plasma Process. Polym.*, vol. 16, no. 7, 2019, doi: 10.1002/ppap.201900024.

[51] C. R. Crick and I. P. Parkin, "Preparation and characterisation of super-hydrophobic surfaces," *Chem. - A Eur. J.*, vol. 16, no. 12, pp. 3568–3588, 2010, doi: 10.1002/chem.200903335.

[52] M. A. Gilliam, Q. Yu, and H. Yasuda, "Plasma polymerization behavior of fluorocarbon monomers in low-pressure AF and RF discharges," *Plasma Process. Polym.*, vol. 4, no. 2, pp. 165–172, 2007, doi: 10.1002/ppap.200600076.

[53] P. Scopece, A. J. Viaro, R. Sulcis, I. Kulyk, A. Patelli, and M. Guglielmi, "SiO_x-based gas barrier coatings for polymer substrates by atmospheric pressure plasma jet deposition," *Plasma Process.*

Polym., vol. 6, no. SUPPL. 1, pp. 705–710, 2009, doi: 10.1002/ppap.200931707.

[54] J. Petersen, J. Bardon, A. Dinia, D. Ruch, and N. Gherardi, "Organosilicon coatings deposited in atmospheric pressure townsend discharge for gas barrier purpose: Effect of substrate temperature on structure and properties," *ACS Appl. Mater. Interfaces*, vol. 4, no. 11, pp. 5872–5882, 2012, doi: 10.1021/am3015229.

[55] X. Lu, G. V. Naidis, M. Laroussi, and K. Ostrikov, "Guided ionization waves: Theory and experiments," *Phys. Rep.*, vol. 540, no. 3, pp. 123–166, 2014, doi: 10.1016/j.physrep.2014.02.006.

[56] M. Rahman, R. Amsarani, D. A. Mooney, J. M. D. MacElroy, and D. P. Dowling, "Effect of process parameters on chemistry, growth rate and nano-sized particulate formation of atmospheric plasma deposited, nm thick siloxane coatings," *J. Nanosci. Nanotechnol.*, vol. 9, no. 6, pp. 3506–3513, 2009, doi: 10.1166/jnn.2009.NS24.

[57] A. Kakaroglou, G. Scheltjens, B. Nisol, I. De Graeve, G. Van Assche, B. Van Mele, R. Willem, M. Biesemans, F. Reniers, and H. Terryn, "Evaluation of the Yasuda parameter for the atmospheric plasma deposition of allyl methacrylate," *RSC Adv.*, vol. 5, no. 35, pp. 27449–27457, 2015, doi: 10.1039/c5ra02684a.

Chapter 4

Development of a methodology for measuring the energy of reactions

4.1 Introduction

In this chapter, the development of a methodology for measuring the energy of reactions in a PP process assisted by the AP single electrode plasma jet described in Chapter 2 and an organosilicon vaporized precursor is presented. The values of energy per precursor molecule (E_m) are calculated through the identification and resolution of a proper equivalent electrical circuit model. To validate the methodology, these energy values are correlated to the chemical and physical properties of deposited thin films assessed by means of ATR-FTIR spectroscopy and profilometry.

4.1.1 Insights into the work

- Since this work represents the first attempt to develop a methodology for measuring the energy absorbed per precursor molecule in PP processes assisted by APPJs, a sinusoidal power supply is selected to simplify the signal processing.
- The organosilicon precursor HMDSO is chosen for this work because, being very well-known in AP plasma polymerization literature [1]–[4], it can facilitate the correlation between the calculated energy values and the characteristics of the deposited coatings.
- The choice of using HMDSO in vaporized state follows the same logic: it is frequently used in PP processes and its interaction mechanisms with the plasma discharge have been widely studied over the years. The introduction of the precursor in the primary channel of the plasma source is again a solution to ease the comprehension and schematization of the polymerization process since in this way the presence of precursor molecules is guaranteed along the entire plasma plume.

4.1.2 Collaborations related to the work

The activities presented in this chapter were carried out in the frame of a joint research project between the IAP Research Group of the University of Bologna (Italy), of which I am member, and the Plasma Research Group of the Polytechnique Montréal (Canada). In the context of this joint project (which is currently going on), I had the opportunity to spend 4 months abroad at the Polytechnique Montréal, under the supervision of Professors Michael Wertheimer and Stephan Reuter. During my stay abroad, I combined my competences on the electrical and functional characterization of APPJs for PP with the expertise of the Canadian Research group, which had already developed the methodology for measuring the energy of reactions in processes assisted by planar DBDs (driven by a sinusoidal power supply) and gaseous or vaporized precursors [5].

Since the topic of this joint research project can be strongly related to the possibility of control the polymerization process and produce thin films with characteristics suitable for antimicrobial

applications in medicine, the activities performed during my stay abroad were supported by a Grant provided by the PlasTHER COST Action 20114, which aims to promote the use of cold plasma for therapeutical applications.

The results of these activities led to a research article which will be submitted soon to Plasma Processes and Polymers: "***Energetics of reactions in an atmospheric pressure plasma jet with argon carrier gas and HMDSO reagent***" – Giulia Laghi, Sean Watson, Matteo Gherardi, Stephan Reuter, Michael Wertheimer.

4.2 Experimental section

4.2.1 Experimental setup

The experimental setup used in this work is schematically reported in Figure 4.1.

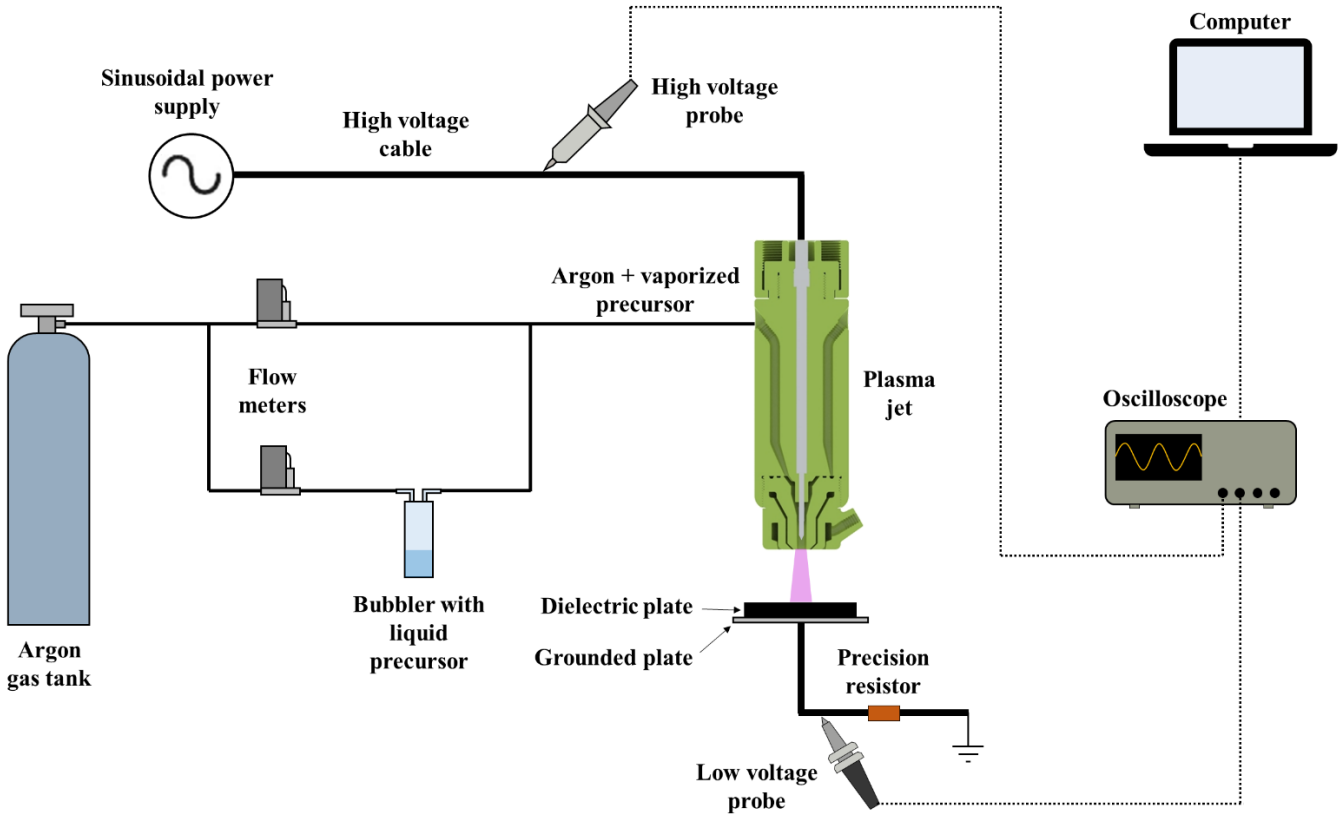

Figure 4.1: Schematical representation of the experimental setup.

The plasma source employed in this work is again the AP single electrode plasma jet described in Chapter 2. An argon (99.9+% purity, Air Liquide Canada, Ltd., Montréal) flow rate of 1.5 slpm was injected in the discharge region through the primary channel along with a variable flow rate of vaporized organosilicon precursor HMDSO ($Si_2OC_6H_{18}$, Sigma Aldrich ≥ 98%) ranging from 0.01 to 2 sccm. The

argon flow rate was controlled by a rotameter-type flowmeter (Matheson, model 7642H, tube 605). For vaporizing the HMDSO, a glass bubbler (diameter = 30 mm, height = 70 mm) containing several cm^3 of liquid precursor was fed with an argon flow rate controlled by an electronic mass flow meter (MKS, model 1259B) and a dedicated power supply (MKS, model 247B). To calculate the effective precursor flow rate (F_d), the quantity of liquid precursor consumed within a defined time interval for different argon flow rates was measured.

The source was placed at 10 mm (13 mm starting from the tip of the high voltage electrode) from a polyvinyl chloride (PVC) plate (thickness = 8 mm) positioned on a metallic plate connected to the ground via a 50 Ω precision resistor. The stainless-steel electrode was connected to a sinusoidal power supply, comprising a variable-frequency a.c. generator (1 Hz to > 50 kHz, Hewlett-Packard 3310A), a power amplifier (QSC Ltd., model RMX2450), an HV transformer (Enercon, model LM2727-03), and an impedance matching unit. The behaviour of the plasma source was examined for applied voltages ranging from 5.5 kV_{p-p} to 9.5 kV_{p-p} and frequencies ranging between 0.5 kHz and 40 kHz.

The voltage provided by the sinusoidal power supply was monitored by means of a high voltage probe (Tektronix, P6015A) located on the high voltage cable, while the current was evaluated measuring the voltage across the precision resistor located on the grounded cable by means of a low voltage probe (Tektronix, TPP0500B). This work aims to develop for the first time a valid methodology for the calculation of the energy of reactions in a polymerization process assisted by an APPJ. For this reason, it was chosen to measure the current on the grounded cable (and not on the high voltage one) to guarantee a measurement which was representative of the behavior in the plasma discharge.

Voltage and current signals were recorded using a digital storage oscilloscope (Instek GDS-2204A, 200 MHz) and transmitted and acquired in real time by USB link on a PC. The data were then post-processed by a MATLAB code designed to calculate the effective voltage across the gas gap and the discharge current, thus the energy dissipated per cycle. The calculations were performed in the frequency domain using Fast-Fourier Transform (FFT) and inverse FFT whenever appropriate. To limit numerical instabilities, the DC component and any frequency components greater than 25 times the applied voltage frequency were removed from all signals. The length of all recorded signals was truncated to the nearest number of complete cycles to limit FFT tapering effects. The typical number of complete cycles per frame varied from 2 to 5 depending on the frequency selected for data acquisition. Data frames were then accumulated over 60 s.

4.2.2 Equivalent electrical circuit model

Figure 4.2a shows the equivalent electrical circuit model originally proposed by Nisol et al. [5] for a planar DBD plasma source driven by a sinusoidal power supply. As the single electrode plasma jet employed in my PhD project exhibits the same components of the planar DBD (i.e. a high voltage

electrode, a ground electrode, and a dielectric layer), the aforementioned equivalent circuit can be reasonably applied also to this source (Figure 4.2b).

V_{ps} and V_m correspond to the voltage signals measured by the high- and low-voltage probes, respectively. R_m is the precision 50 Ω resistor, which serves to measure the discharge current pulse amplitude and shape. Z_d is a non-linear variable impedance whose value, although unknown with precision, tends toward zero during discharges and toward infinity between discharges. C_{die} and C_{gap} represent the characteristic capacitances of the plasma source: C_{gap} is the capacitance associated to the gas gap between the plasma tip and the dielectric plate, while C_{die} is the capacitance associated to the PVC dielectric plate. Between the discharges the circuit is characterized by the series of these capacitances, while during the discharges the main capacitance is C_{die}. To model the several parasitic effects present in the experimental setup, the equivalent circuit includes a parallel between a capacitor C_2 and the series of a capacitor C_1 and a resistor R.

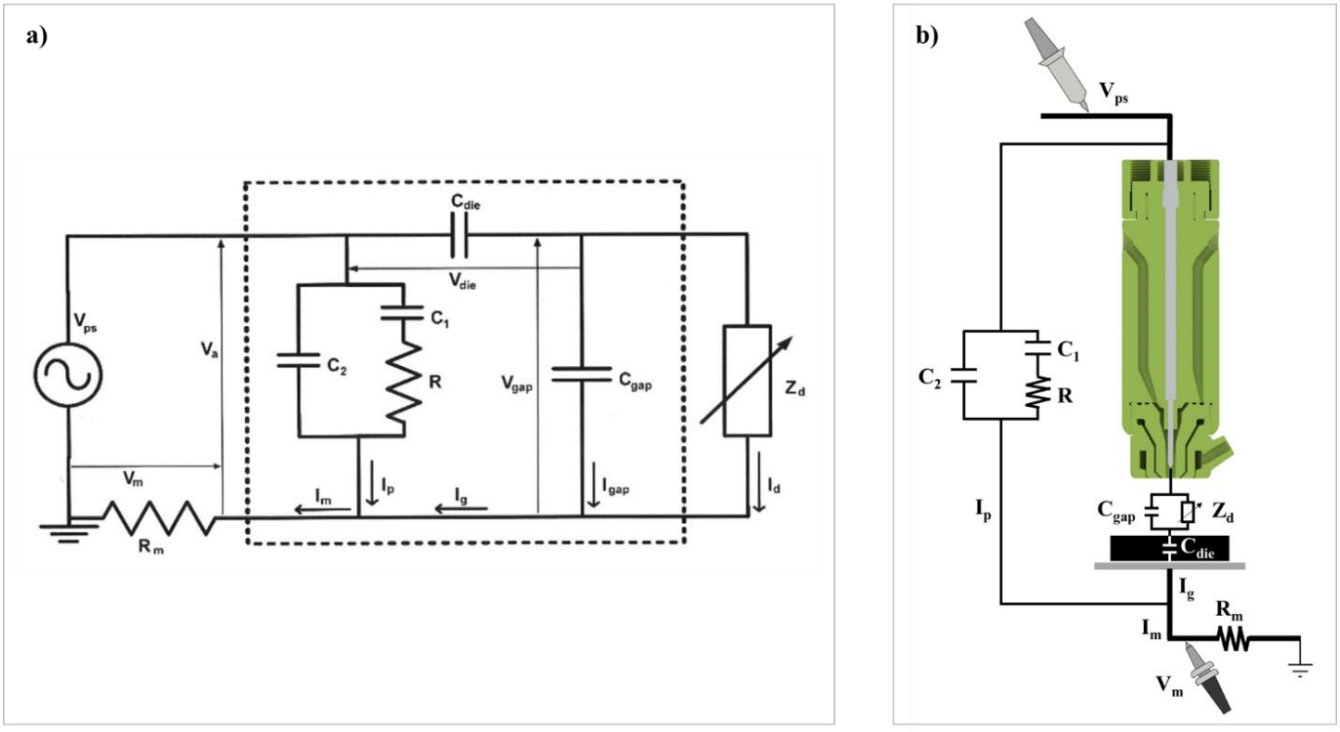

Figure 4.2: a) Equivalent electrical circuit model for a planar DBD plasma source [5]; b) Equivalent electrical circuit model applied to the single electrode plasma jet.

For the calculation of C_{die} and C_{gap}, the vertical development of the plasma column (plume) in the gas gap and its subsequent almost circular spreading by means of the filaments on the dielectric surface needs to be considered (Figure 4.3).

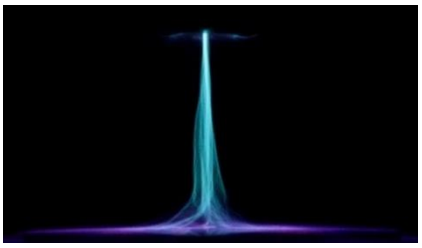

Figure 4.3: Example of a typical discharge produced with the AP single electrode plasma jet.

As a first approximation, the characteristic capacitances can be estimated using the formulas for condensers with flat planar faces ($C = \varepsilon_0 k' A/d$, where ε_0 is the vacuum permittivity, k' is the relative permittivity, $A = \pi r^2$ is the area, and d is the thickness of the dielectrics). In this case, the two dielectric materials involved are:

- air (C_{gap}): k' = 1, r = 1.5 mm, d = 13 mm;
- PVC (C_{die}): k' = 4, r = 10 mm, d = 8 mm.

The values obtained for C_{gap} and C_{die} were 0.005 pF and 1.39 pF, respectively.

To derive the components of the parasitic group (C_1, C_2, and R), measurements of V_{ps} and V_m were performed in conditions where the plasma discharge is not present, namely in atmospheric air and at applied voltage of 5.5 kV_{p-p}, for frequencies varying from 0.5 up to 40 kHz. From these V_{ps} and V_m measurements, $V_a = V_{ps} - V_m$, $I_m = V_m/R_m$, and $Z_{eq} = V_a/I_m$ were calculated. The plot of Z_{eq} amplitude and phase as a function of the frequency is reported in Figure 4.4 (blue markers). From the best fit of the experimental data, shown as continuous black curve in Figure 4.4, values of C_1 = 5.69 pF, C_2 = 1.58 pF and R = 14.55 MΩ were obtained. In the proposed model, the values of C_1, C_2 and R are assumed to remain constant even in presence of the plasma discharge and regardless to the operating condition.

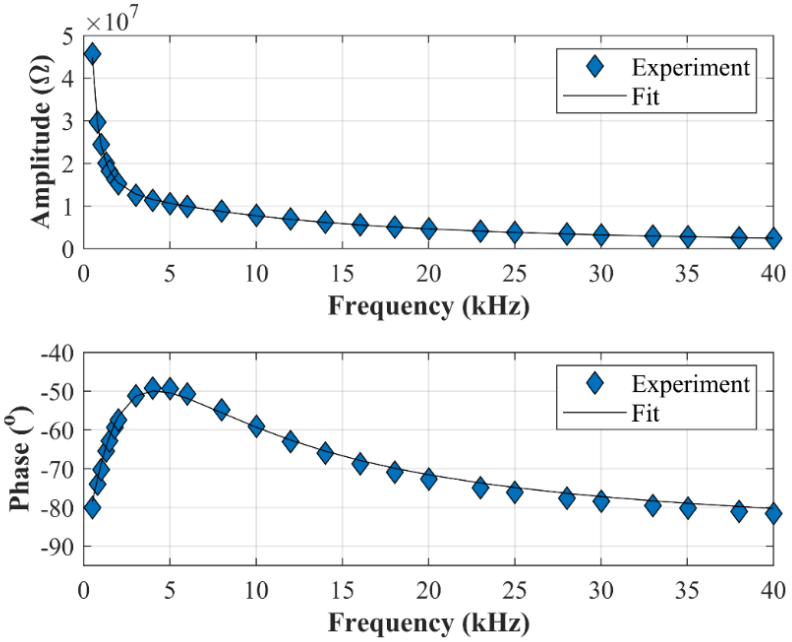

Figure 4.4: Z_{eq} amplitude and phase as a function of the frequency in absence of plasma discharge. Blu markers: experimental data, black continuous curve: best fit.

The equivalent circuit in Figure 4.2b was solved by applying the Kirchhoff's Laws and the electrical energy dissipated in the discharge per cycle (E_g) was calculated according to the following formula:

$$E_g = \frac{\int V_{gap} I_d dt}{n}, \tag{4.1}$$

where V_{gap} is the effective voltage across the gas gap, I_d is the discharge current, and n is the number of complete cycles at the applied voltage frequency. Since all the experiments were performed at least in triplicate, the results in terms of dissipated energy are typically shown as mean value ± standard deviation.

The values of delta of energy (ΔE_g) were derived as the difference between the E_g values measured in pure argon and those obtained in presence of precursor, and they were used to calculate the energy absorbed per precursor molecule (E_m) using the following formula:

$$E_m \left[\frac{eV}{molecule}\right] = \frac{\Delta E_g[\mu J] * 10^{-6}\left[\frac{J}{\mu J}\right] * f\left[\frac{1}{s}\right] * 6.24e^{18}\left[\frac{eV}{J}\right]}{N\left[\frac{molecules}{s}\right]} \tag{4.2}$$

where f is the operating frequency and N is the number of precursor molecules introduced in the discharge per second. N was calculated according to equation 4.3:

$$N\left[\frac{molecules}{s}\right] = F_d[sccm] * 10^{-3}\left[\frac{L}{cm^3}\right] * \frac{1}{24}\left[\frac{mol}{L}\right] * N_A\left[\frac{molecules}{mol}\right] * \frac{1}{60}\left[\frac{min}{s}\right] \tag{4.3}$$

where F_d is the precursor flow rate and N_A is the Avogadro's Number.

4.2.3 Surface characterization of the deposited coatings

To correlate the characteristics of the deposited coatings to the E_m values, the chemical structure of the coatings was analyzed by means of ATR-FTIR spectroscopy. Coatings were deposited on KBr disc substrates (thickness ca. 0.5 mm, diameter ca. 13 mm) prepared from 99+% IR grade powder (Fisher Scientific), which are transparent in the infrared range and consequently facilitate the interpretation of the acquired spectra. To ensure a uniform thickness of the coatings, the deposition was performed under dynamic conditions, automatically moving the substrate at a speed of 5 mm/s. The instrument employed for the analysis was a Perkin Elmer infrared spectrometer with an ATR sampling accessory. Spectra were acquired in absorbance mode, from 4000 to 600 cm^{-1} with a resolution of 4 cm^{-1}. A total of 32 scans were recorded for each spectrum.

The thickness profile of the deposited coatings was investigated by means of a profilometer (Bruker, DektakXT). For this analysis, coatings were deposited on single-crystal silicon (c-Si) substrates in static mode for 15 minutes. The thickness to be associated to each deposition condition was identified as the mean of the thickness values in correspondence of the centre of the deposition spot, where the

thickness reaches a plateau. The DR was calculated by dividing the resulting thickness for the deposition time.

4.3 Results

4.3.1 Energy measurements

Figure 4.5 shows a comparison between the E_g values in pure Ar (1.5 slpm) and in presence of HMDSO (0.1 sccm) for applied voltages (V_a) ranging from 5.5 kV_{p-p} to 9.5 kV_{p-p} at a fixed frequency of 20.5 kHz. As V_a increases, the E_g values in pure Ar increase. Nonetheless, a flat region in the energy values from 6.5 kV_{p-p} to 7.25 kV_{p-p} can be noticed. As the precursor molecules are introduced in the discharge, lower E_g values can be observed, except for the region around 7.25 kV_{p-p}, where there are no significant differences between the upper (pure Ar) and the lower (doped Ar) branches.

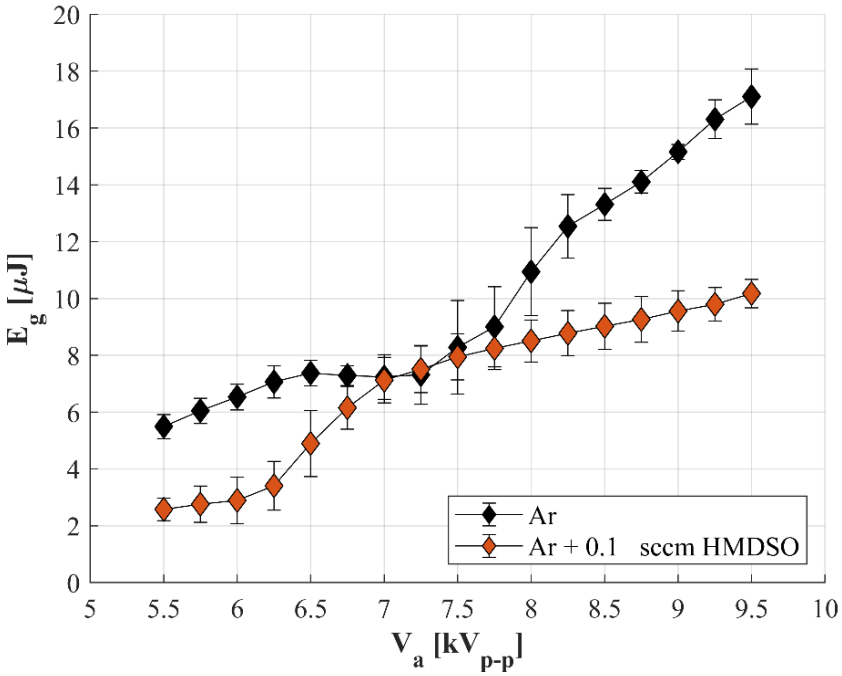

Figure 4.5: Comparison of the energy dissipated per cycle in pure Ar and in presence of HMDSO (0.1 sccm) as a function of the applied voltage (20.5 kHz).

The E_g values at 5.5 kV_{p-p} and 9 kV_{p-p} (applied voltages belonging to the regions where the effect of the precursor can be clearly distinguished) for precursor flow rates from 0.01 to 2 sccm are reported in Figure 4.6. From the curves, it can be noticed that even the addition of the lowest F_d (0.01 sccm) in the discharge is sufficient to determine a sharp drop in the E_g values for both the applied voltages. As F_d further increases, E_g tends to slightly decrease. This behaviour can be easily appreciated at 9 kV_{p-p}, while is less pronounced at 5.5 kV_{p-p} (mild increase in E_g around 0.4 sccm).

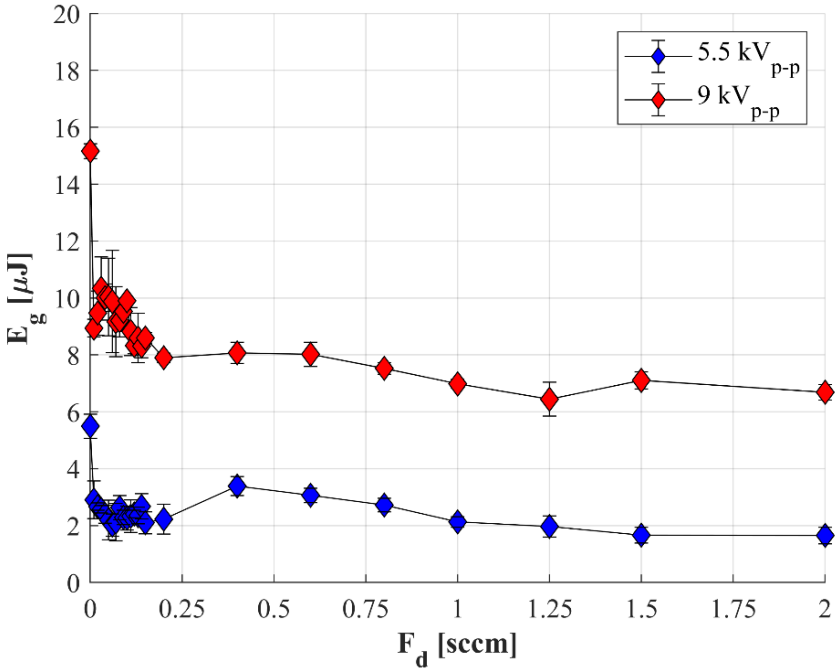

Figure 4.6: E_g as a function of F_d at 5.5 kV_{p-p} and 9 kV_{p-p} (20.5 kHz).

The values of energy absorbed per precursor molecule, E_m, were calculated starting from the deltas of energy between the E_g values in pure argon (5.5 ± 0.4 μJ at 5.5 kV_{p-p} and 15.2 ± 0.3 μJ at 9 kV_{p-p}) and those in presence of HMDSO (variable values depending on F_d). The results are shown in Figure 4.7 (logarithmic scale).

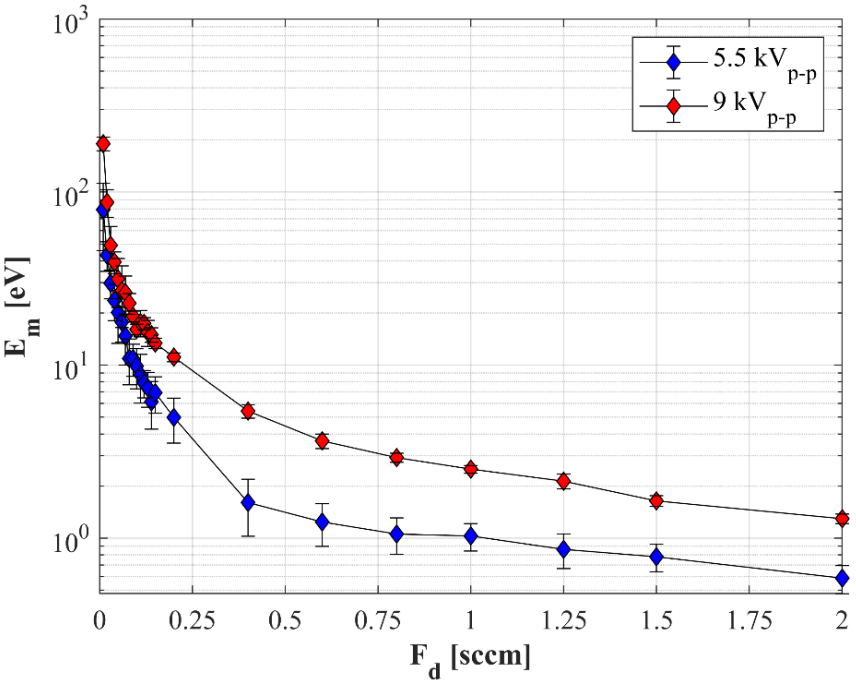

Figure 4.7: E_m as a function of F_d at 5.5 kV_{p-p} and 9 kV_{p-p} (20.5 kHz). Results are presented in logarithmic scale.

For both the applied voltages, as F_d in the discharge increases, E_m monotonically decreases. Therefore, the maximum values can be observed at 0.01 sccm (~ 80 eV per molecule for 5.5 kV_{p-p} and ~ 190 for 9 kV_{p-p}), while the minimum ones at 2 sccm (~ 0.6 eV per molecule for 5.5 kV_{p-p} and ~ 1.3 for 9 kV_{p-p}). For sake of conciseness, in the following the wording "eV per molecule" will be sometimes shortened in "eV/mol".

4.3.2 Surface characterization results

4.3.2.1 ATR-FTIR results

The ATR-FTIR spectra of coatings deposited at 9 kV_{p-p} for precursor flow rates of 0.01, 0.08, 0.15 and 1 sccm (corresponding to 190.2 ± 17.4 eV, 22.8 ± 3.2 eV, 13.4 ± 0.9 eV, 2.5 ± 0.1 eV per molecule, respectively) are shown in Figure 4.8.

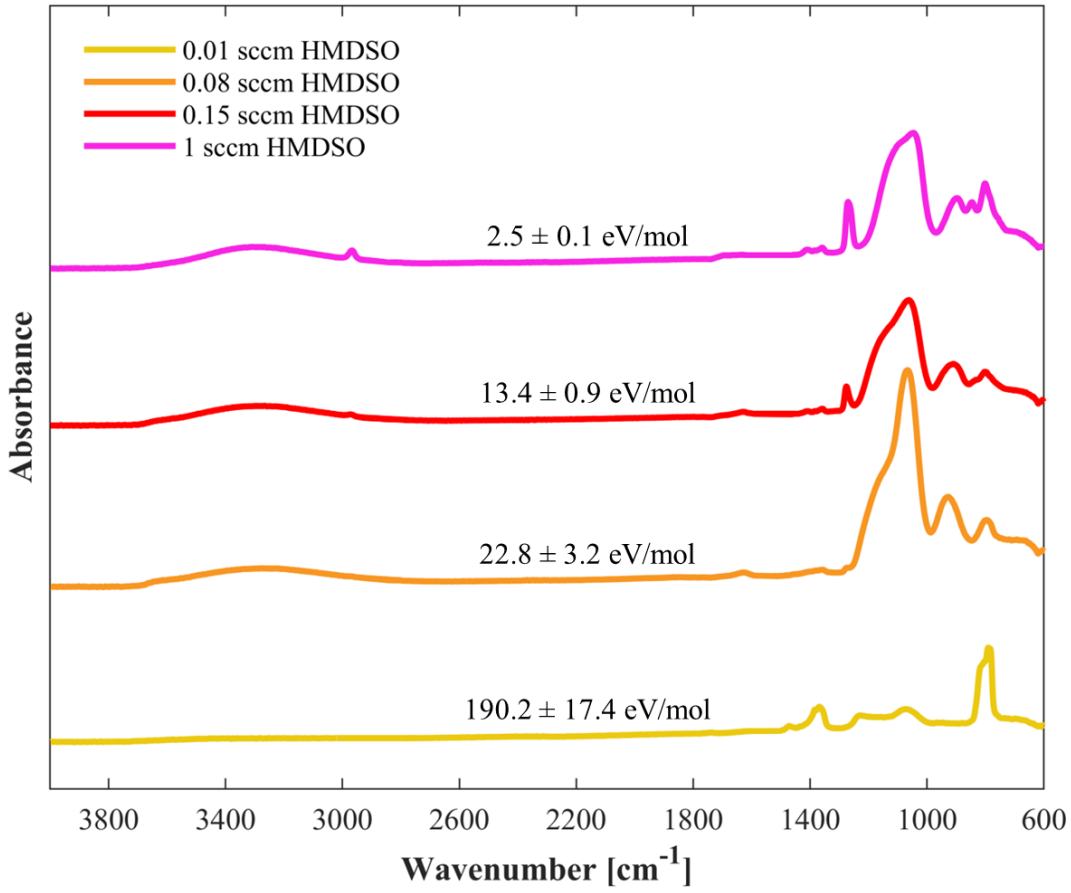

Figure 4.8: ATR-FTIR spectra of coatings deposited at 9 kV_{p-p} for different E_m values (20.5 kHz)

To ease the interpretation of these spectra, a list of possible peak assignments is reported in Table 4.1.

Wavenumbers [cm^{-1}]	Possible assignment	References
3700-3100	Si-OH stretching	[6], [7]
2965	CH_3 stretching	[6], [8]
1265	CH_3 deformation in Si-CH_3	[1], [8], [9]
	Si-$(CH_3)_x$ stretching (x = 1,2,3)	[2]
1200-1000	Si-O-Si asymmetric stretching	[2], [6], [8], [10]–[12]
930	Si-OH stretching	[8], [11], [13], [14]
840	CH rocking	[6], [15]
	Si$(CH_3)_3$ stretching	[13]
800	Si-O-Si bending	[16], [17], [13]
	Si-O-Si stretching	[1], [10]
	Si-C stretching	[18]
	Si-$(CH_3)_2$ stretching	[17]
	CH_3 rocking	[1]

Table 4.1: Assignment of the peaks.

At 22.8 eV per molecule, the spectrum exhibits numerous peaks associated to the silicon presence in the coating, such as the Si-O-Si bending or stretching at 800 cm^{-1}, the Si-OH stretching at 930 cm^{-1}, the Si-O-Si asymmetric stretching at 1200-1000 cm^{-1}, and the Si-OH stretching at 3100-3700 cm^{-1}. In the band related to the Si-O-Si asymmetric stretching, the presence of two superimposed peaks can be clearly distinguished: the in phase asymmetric stretching AS1 at around 1070 cm^{-1} and the out-of-phase asymmetric stretching at around 1150 cm^{-1}. The weak peak at 1265 cm^{-1}, related to the CH_3 stretching in Si-$(CH_3)_x$ (x=1,2,3), is the only peak associated to the presence of methyl groups in the spectrum, thus suggesting an almost negligible presence of carbon in coatings deposited in this condition.

As E_m decreases, new methyl-related peaks appear in the spectra: the CH_3 rocking or the Si-$(CH_3)_2$ stretching at 800 cm^{-1}, the CH_3 rocking or the Si-$(CH_3)_3$ stretching at 840 cm^{-1}, and the CH_3 stretching. These peaks, along with the one at 1265 cm^{-1}, become progressively more pronounced as the energy per molecule diminishes. Contextually, the "shoulder" in the band 1000-1200 cm^{-1} associated to AS2 tends to become less pronounced, leading the band to assume a "single peak" shape. The AS1 peak, in turn, shifts towards lower wavenumbers (from 1070 cm^{-1} to 1040 cm^{-1}). The described changes in the spectra have already been observed in literature [6] and can be ascribed to a transition towards coatings with a more pronounced organic character.

The spectrum at 190 eV/mol exhibits different features from the ones typically associated to spectra from PP of HMDSO, thus making its interpretation not obvious and requiring a separate description in this section. Few peaks can be observed in the spectrum, such as the CH_3 bending at 1370

cm^{-1} [19], the Si-CH_2CH_3 vibration [20] or the Si-O stretching [21] at 1220 cm^{-1}, the asymmetric stretching AS1 at 1070 cm^{-1}, and the Si-O-Si bending or stretching or the CH_3 rocking or the Si-$(CH_3)_2$ stretching at 800 cm^{-1}.

4.3.2.2 Profilometer results

Figure 4.9 shows, as an example, the picture of a coating deposited on a c-Si substrate under static conditions for 15 minutes at 9 kV_{p-p} and in presence of 0.15 sccm of HMDSO. This picture is reported along with the corresponding thickness profile (symmetric profile). The thickness to be associated to this operating condition was extracted from this profile, considering the mean of the thickness in the region where the thickness reaches a plateau.

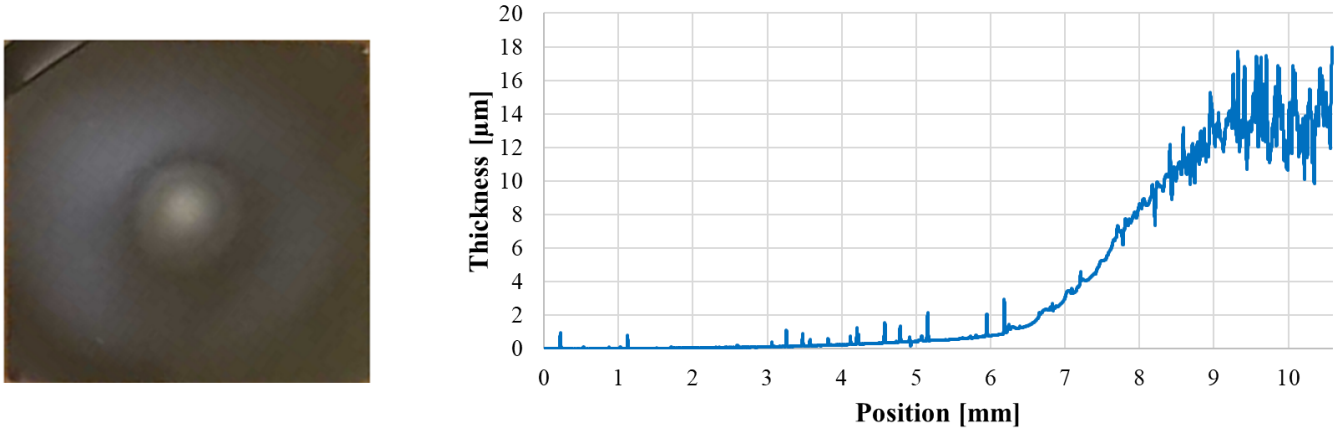

Figure 4.9: Left: picture of a coating deposited on a c-Si substrate under static conditions for 15 minutes at 9 kV_{p-p} and in presence of 0.15 sccm of HMDSO; right: corresponding thickness profile.

The thickness was investigated for coatings deposited at 9 kV_{p-p} for F_d values of 0.01, 0.08, 0.15 and 1 sccm (corresponding to 190.2 ± 17.4 eV, 22.8 ± 3.2 eV, 13.4 ± 0.9 eV, 2.5 ± 0.1 eV per molecule, respectively). The corresponding values of deposition rate (DR), calculated by dividing the measured thickness for the deposition time (15 minutes), are reported in Table 4.2.

F_d [sccm]	E_m [eV]	Thickness [µm]	DR [µm/min]
0.01	190.2 ± 17.4	0.71	0.05
0.08	22.8 ± 3.2	5.68	0.38
0.15	13.4 ± 0.9	13.58	0.91

Table 4.2: Deposition rates for coatings deposited on c-Si under different precursor flow rates.

As F_d increases (and E_m decreases), the DR increases following a quadratic behavior. Data related to a flow rate of 1 sccm are not reported in Table 4.2 since the coatings were too powdery to obtain reliable thickness values with the profilometer.

4.4 Discussion

The resulting values of energy dissipated per cycle, E_g, in pure argon increase as a function of the applied voltage except for the flat region from 6.5 kV_{p-p} to 7.25 kV_{p-p}. A tentative explanation of this behaviour can be provided by analysing the voltage (V_a) and current (I_m) waveforms reported in Figure 4.10a (5.5 kV_{p-p}), 4.10b (7.25 kV_{p-p}), and 4.10c (9 kV_{p-p}).

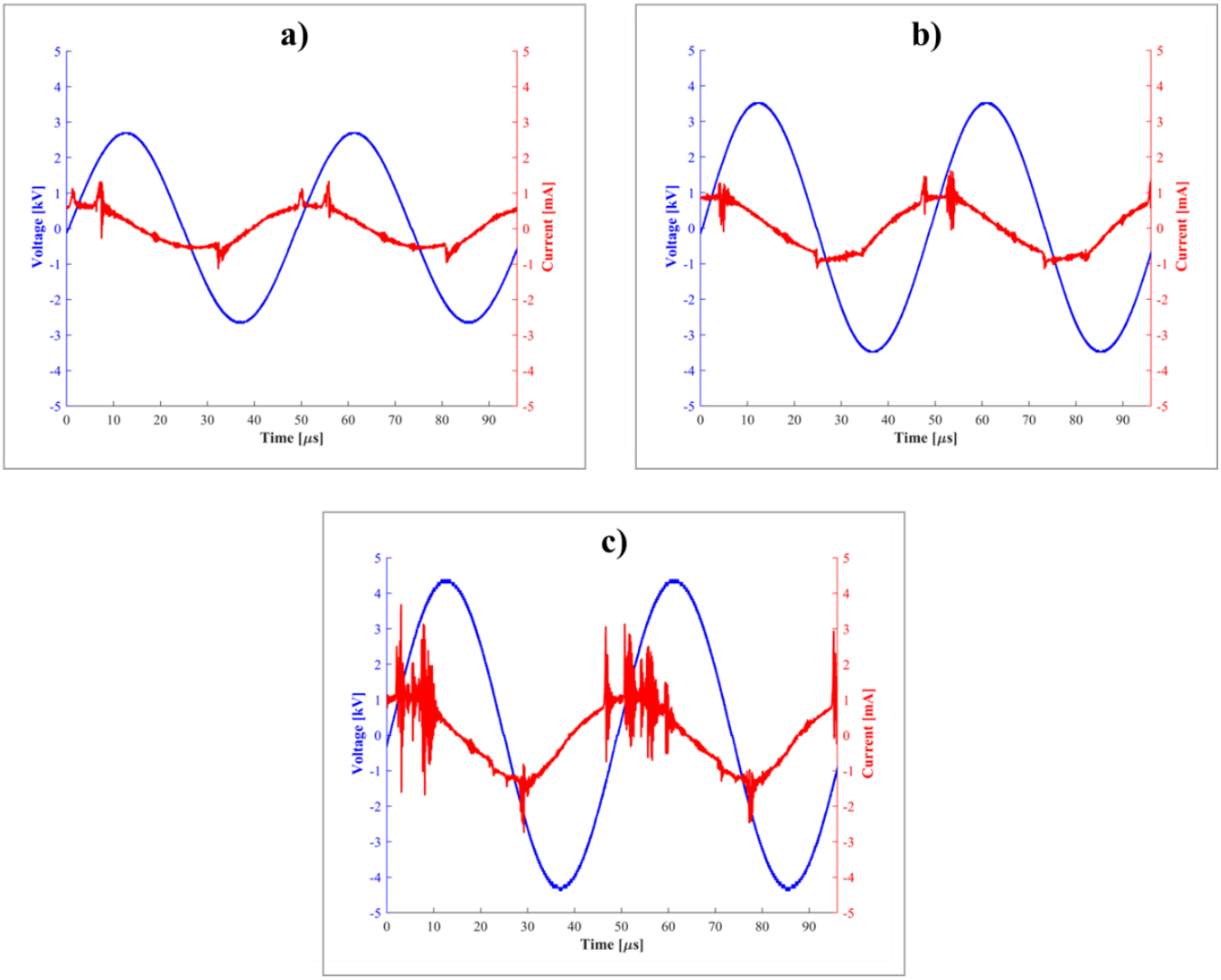

Figure 4.10: Voltage and current waveforms at 5.5 kV_{p-p} (a)), 7.25 kV_{p-p} (b)), and 9 kV_{p-p} (c)) at 20.5 kHz. These waveforms are examples of single voltage and current waveforms: the data effectively processed for the calculation of the energy values are the average of numerous acquisitions like these obtained over 1 minute.

While the current waveform at 5.5 kV_{p-p} is characterized by the presence of few wide peaks superimposed on the displacement current waveform (two on the positive half-cycle, one on the negative one), typical of a pseudo-glow regime, the current waveform at 9 kV_{p-p} exhibits numerous spikes of nanosecond duration which generally characterize a filamentary discharge. [6], [22], [23] The current waveform at 7.25 kV_{p-p} highlights peculiar characteristics: the peaks on the positive half cycle show a

more filamentary nature than the case at 5.5 kV_{p-p} (but still not comparable with the ones at 9 kV_{p-p}), while the peaks on the negative half cycle are almost negligible. The described current behaviour suggests attributing the observed flat region to a region where the discharge regime is changing.

The introduction of a flow rate of 0.1 sccm of vaporized HMDSO in the discharge determines a general decrease in the energy values. Again, an in-depth analysis of the voltage and current waveforms can be useful to interpret this behaviour. Figure 4.11 shows the voltage and current waveforms in presence of precursor molecules for applied voltages of 5.5 kV_{p-p} (Figure 4.11a) and 9 kV_{p-p} (Figure 4.11b). The curves at 7.25 kV_{p-p} are not presented since no significant differences between pure Ar and doped Ar can be observed in that case.

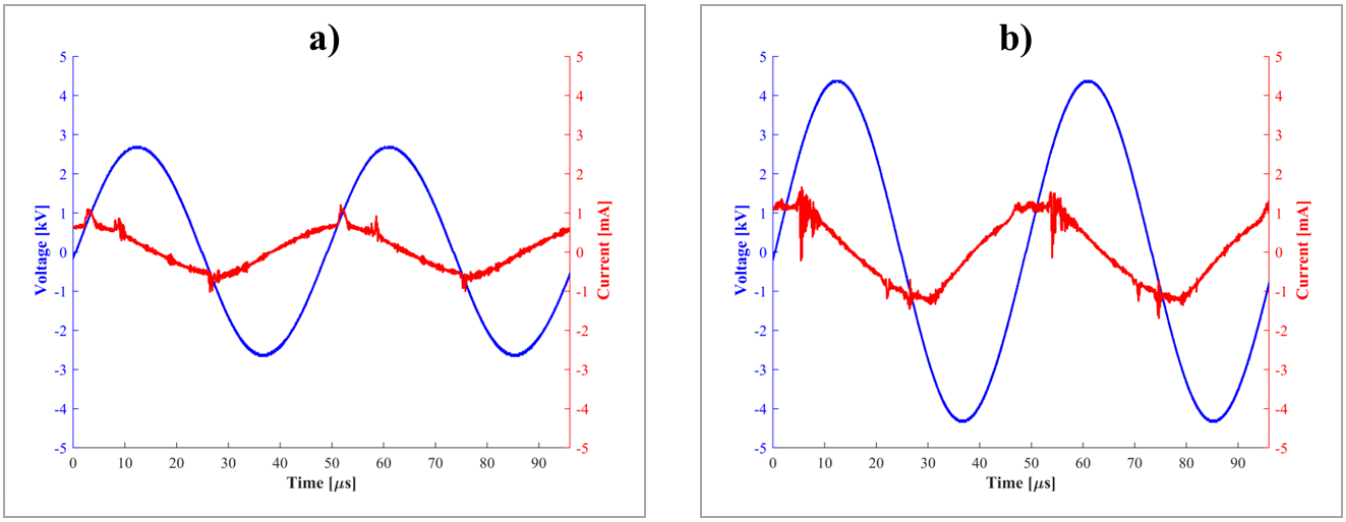

Figure 4.11: Voltage and current waveforms at 5.5 kV_{p-p} (a)) and 9 kV_{p-p} (b)) in presence of 0.1 sccm of HMDSO at 20.5 kHz.

By comparing the waveforms with those obtained in pure Ar (Figure 4.10a and 4.10c), it can be noticed that the current waveforms are significatively affected by the presence of precursor. Indeed, for both the V_a values, the number of current peaks (and their intensity) tends to decrease, thus implying a more homogeneous discharge. This decrease in the total current, already observed also by Mertens et al. in the case of a planar DBD [24], can be ascribed to the different interactions to which electrons are subjected in the discharge in presence of precursor molecules. As E_g is calculated starting from the applied voltage and current waveforms, the decrease in E_g values appears reasonable.

From the differences of energy between pure Ar and doped Ar, ΔE_g, E_m has been calculated for F_d values ranging from 0.01 to 2 sccm and applied voltages of 5.5 kV_{p-p} and 9 kV_{p-p}. For both the applied voltages, it was shown that E_m monotonically decreases as F_d increases. To correlate the values of energy per molecule obtained with the methodology to the chemical characteristics of the coatings, ATR-FTIR analysis of thin films deposited under different precursor flow rate was performed. As F_d increases from 0.08 sccm to 1 sccm, the chemical composition evolves from almost purely inorganic ("silica-like") to organic ("PDMS-like"). Indeed, the spectra reveal a gradually higher presence in the coatings of

functional groups of the starting monomer (i.e. methyl groups) and exhibit features typically associated in the literature of coatings from HMDSO to an organic behaviour (i.e. peak related to Si-O-Si asymmetric stretching towards lower wavenumbers). This behaviour is coherent with the progressive reduction of E_m (from 22.8 to 2.5 eV) which determines a less intense fragmentation of the organosilicon precursor in the discharge.

The lowest F_d value which was investigated (0.01 sccm), kept out from the above reasoning for simplicity, leads to the highest E_m value (190.2 eV). Being this value of energy per molecule higher than 22.8 eV, a higher degree of fragmentation of the precursor in the discharge and a consequent lower retention of functional groups in the coating should be expected (e.g. total disappearance of the only peak related to methyl groups at 1265 cm^{-1}). Nonetheless, the ATR-FTIR spectrum of coating deposited at 0.01 sccm of HMDSO does not exhibit the typical features of a purely inorganic coating but shows few and not very intense peaks in some cases related to silicon and in some cases related to carbon. This behaviour suggests an extremely higher degree of fragmentation of the precursor in the discharge and the consequent creation of a thin layer made from the recombination of small fragments.

The trend of the E_m values appears to be in good agreement with the chemical properties of the coatings, thus supporting the validity of the methodology for the AP single electrode plasma jet. Nonetheless, to test the reliability of the methodology, it is worthy to add some considerations about the relation between the obtained energy values and the energies required to break the bonds in the HMDSO molecule. For sake of simplicity, the following discussion will not take into account the possible evolution of the bond energies in a highly reactive and dynamic environment like the plasma discharge and the statistical nature of the processes of bond dissociation. Furthermore, possible contributions in the breaking of the chemical bonds due to VUV (vacuum ultraviolet) photons typically present in AP argon discharges will be neglected. [25]

The main bond energies in the HMDSO molecule are 3.5 eV for the C-H bond, 4.53 eV for the Si-C bond, and 8.31 eV for the Si-O bond. [26], [27] This means that E_m values of 22.8 eV, 13.4 eV, and 2.5 eV (obtained for precursor flow rates of 0.08, 0.15, and 1 sccm, respectively) are roughly in the same order of magnitude of the bond energies and can be used to interpret the mechanisms of fragmentation. Despite a detailed dissertation on the fragmentation pathways of HMDSO molecules in AP PP is beyond the purposes of this work, some information can be provided in this context.

An energy of 22.8 eV/mol is sufficient to provide the dissociation of all the above-mentioned bonding types thus justifying the presence in the coatings of features mostly related to pure inorganic coatings. As the energy decreases to 13.4 eV/mol, the bond dissociation is less intense, and more methyl groups can be conserved in the final coating. Coatings deposited for an E_m of 2.5 eV exhibit the most organic character, suggesting an extremely low fragmentation of the precursor in the coating. This is coherent with the bond energies in the HMDSO molecules, since 2.5 eV is around the minimum values which are needed to abstract hydrogen or methyl groups.

Among the values of E_m investigated in this work, 190.2 eV corresponds to the condition where the maximum transfer of energy from the plasma discharge to the precursor molecules occurs. Since the sum of all the bond energies in the HMDSO molecule is around 105 eV, the ATR-FTIR spectrum observed at 190.2 eV/mol can be reasonably explained as a consequence of the total breakage of all the constituent bonds. In this perspective, the value of E_m which confers a purely inorganic chemical composition to the coating should be comprised between 22.8 eV and 190.2 eV.

Besides their chemical composition, coatings were characterized also in terms of thickness using a profilometer, to gather information about the deposition kinetics. It was observed that the DR increases as F_d increases from 0.01 to 0.15 sccm. This behaviour can be explained by considering that conditions of higher fragmentation in the polymerization process are usually associated to higher degree of crosslinking and densification in the resulting coatings (i.e. lower thickness) [28]. Therefore, as E_m decreases, the coating progressively assumes a higher thickness and a less compact structure. The coating obtained at 1 sccm, too powdery for being characterized with a profilometer, further supports this hypothesis.

According to the above discussion, this methodology, for the first time applied to the case of APPJs, provides reasonable and promising results in terms of energy per precursor molecule. To this point, it seems worthy to compare the data obtained from the methodology with those from a known method for the calculation of the energy dissipated per cycle: the Lissajous method.

Firstly proposed by Manley [29] for DBD plasma sources driven by sinusoidal signals, the Lissajous method is based on:

- the addition of a monitor capacitor (C_m) of known value between the source and the ground. As a rule of thumb, the value of the monitor capacitor should be 100-10000 times the one of C_{cell}; [30]
- the measurement of the voltage across the monitor capacitor (V_m).

In this way, the charge deposited in the dielectric surfaces can be calculated as $Q(t) = C_m V_m(t)$. The plot of the charge in function of the applied voltage (V) constitutes the so-called Lissajous figure (or voltage-charge plot). The average discharge power dissipated over the period T can be determined from the area of the Lissajous figure multiplied for the frequency (inverse of the period), using the equation 4.4:

$$P = \frac{1}{T} \oint_T V(t)\, dQ(t) \tag{4.4}$$

Considering the measurement units, it appears clear that the integral itself in equation 4.4, namely the area of the Lissajous figure, represents the energy dissipated per cycle in the discharge (E_g).

The slopes of the sides of the Lissajous figure corresponding to the active and passive phases represent the characteristic capacitances C_{cell} and C_d, respectively. Using this capacities (whose evaluation is not always obvious [31]), the equivalent circuit typically associated to this method (Figure

4.12) can be solved, and the gas gap voltage $U_g(t)$ and the active current $j_R(t)$ can be obtained [32]. Therefore, E_g can be calculated also as the integral over the period of the product of these two quantities.

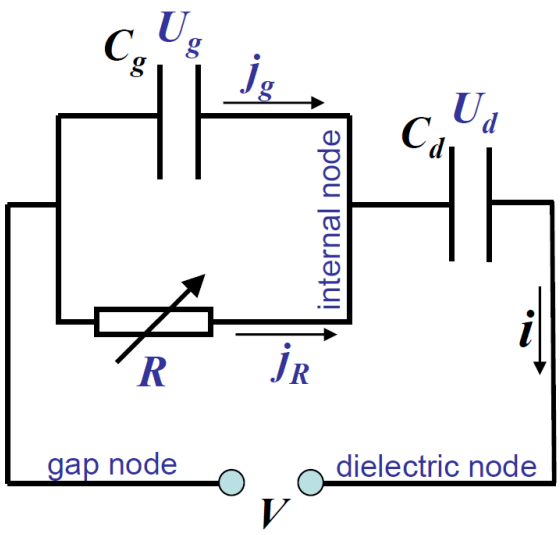

Figure 4.12: Equivalent circuit typically associated to the Lissajous method. [32]

As pointed out earlier in the text, the determination of E_g does not require knowledge about the equivalent circuit, as calculating the area of the Lissajous figure is sufficient for this purpose. Nonetheless, the resolution of the standard circuit is still necessary to gather information about the evolution in time of the gas gap voltage and the active current.

Despite being interesting for the calculation of E_g, the classical equivalent circuit associated to the Lissajous method usually does not include the presence of parasitic effects. On the other hand, the methodology proposed here is based on a more complex equivalent circuit which models and estimates the parasitic components. Therefore, it looks interesting to compare the results from both the methods, thus having information on the importance of the parasitic effects on the calculated values of energy per molecule.

In this work, the application of the Lissajous method has been performed by replacing the precision resistor with a monitor capacitor of 470 pF and by measuring the voltage across the capacitor with the same low voltage probe used in the rest of the work for the measurement of the current. Results were obtained in pure argon (1.5 slpm) and in presence of 0.15 sccm of HMDSO for values of V_a ranging from 5.5 kV_{p-p} to 9.5 kV_{p-p} and, as for the methodology, values of ΔE_g between the pure and doped Ar branches were used to calculate E_m.

Figure 4.13 shows a comparison between the results obtained using the equivalent circuit proposed in this work (4.13a) and the ones from the Lissajous methods (4.13b) with pure and doped Ar.

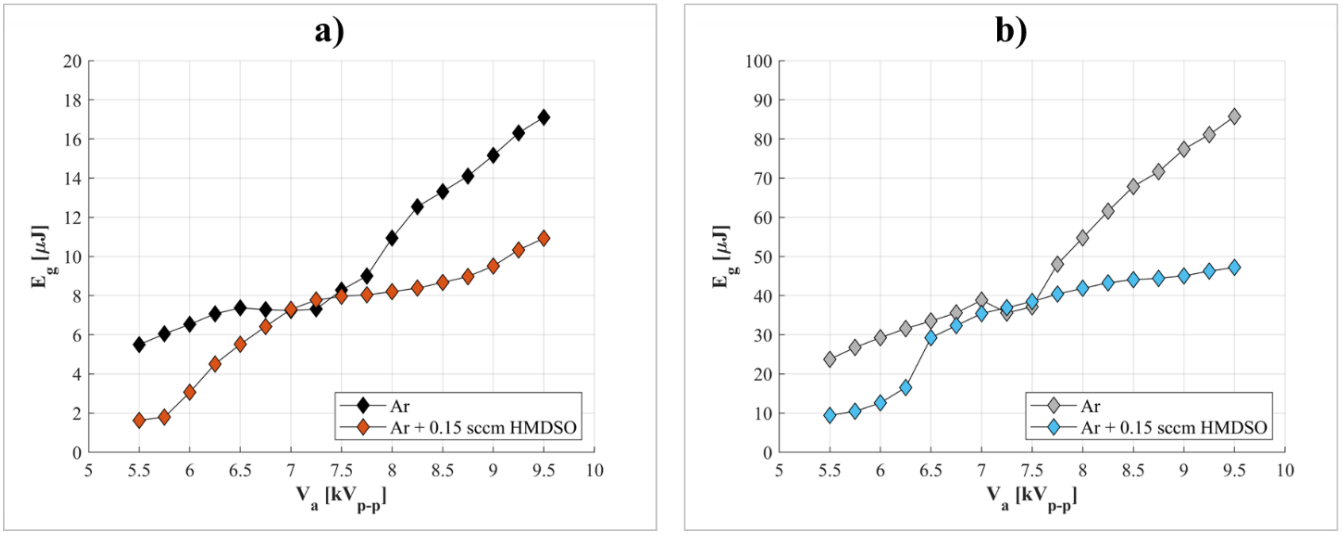

Figure 4.13: Comparison of the values of E_g obtained with the methodology (a) and the Lissajous method (b) in pure Ar and in presence of HMDSO (0.15 sccm) as a function of the applied voltage (20.5 kHz).

The overall trend is the same with both the methods, as can be clearly highlighted by the graph in Figure 4.14, where data are normalized on the maximum value of energy per cycle (17.11 µJ for the methodology and 85.75 µJ for the Lissajous method).

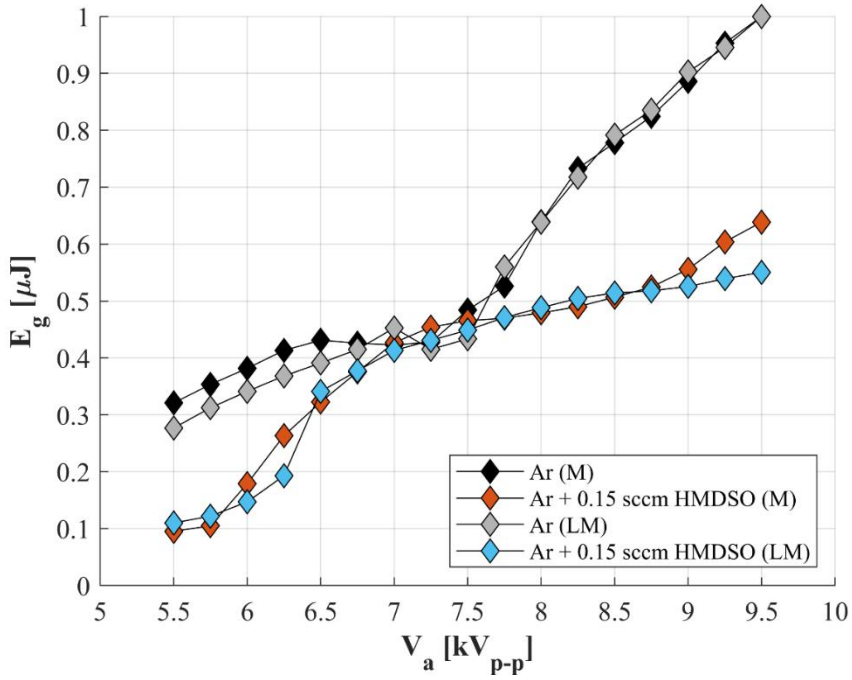

Figure 4.14: Comparison of the values of E_g obtained with the methodology (M) and the Lissajous method (LM) in pure Ar and in presence of HMDSO (0.15 sccm) as a function of the applied voltage (20.5 kHz). Data are normalized on the maximum value of energy per cycle.

Nonetheless, the actual E_g values are much larger in the case of the Lissajous method, thus leading to significatively different ΔE_g values. For comparison, the values of ΔE_g at 5.5 kV_{p-p} and 9 kV_{p-p} obtained with both the methodologies are reported in Table 4.3.

V_a [kV_{p-p}]	ΔE_g [µJ]	
	Methodology proposed in this work	Lissajous method
5.5	3.86	14.31
9	5.65	32.35

Table 4.3: Values of deltas of energy at 5.5 kV_{p-p} and 9 kV_{p-p} obtained with the methodology proposed in this work and with the Lissajous method (0.15 sccm)

As can be noticed from Table 4.3, the values obtained with the Lissajous method about 4 (for 5.5 kV_{p-p}) and 6 (for 9 kV_{p-p}) times larger than those obtained with the methodology proposed in this work. Therefore, the E_m values resulting from the ΔE_g related to the Lissajous method (around 70 eV/mol at 9.9 kV_{p-p}) are significatively larger than those obtained with the methodology (around 15 eV/mol at 9.9 kV_{p-p}). Considering that the results obtained with the methodology can be plausibly interpreted, as shown earlier in this section, the values from the Lissajous methods are clearly too large to be physically meaningful. This shows the importance to proper modelling the parasitic effects in the circuit, thus suggesting a higher accuracy in the energy values obtained from the methodology proposed in this work. As a final remark, it can be highlighted that the greater resolution complexity required by the presented methodology (compared to the Lissajous method) represents a good compromise to obtain more reliable results and advance the understanding of polymerization processes.

4.5 Conclusions

In this work, the development of a methodology for measuring the energy of reactions in a plasma polymerization process assisted by an AP single electrode plasma jet and vaporized HMDSO is presented. The values of energy per precursor molecule are calculated through the identification and resolution of a proper equivalent electrical circuit model. To validate the methodology, these energy values are correlated to the chemical and physical properties of deposited thin films assessed by means of ATR-FTIR spectroscopy and profilometry.

It was demonstrated that values of energy dissipated per cycle (E_g) can be successfully calculated both in pure Ar and in presence of HMDSO. The introduction of precursor molecules leads to a decrease in the E_g values because electrons are subjected to different interactions in presence of precursor molecules, thus reducing the total measured current. Starting from the difference of energy detected between pure Ar and doped Ar, the energy per precursor molecule (E_m) was calculated at 5.5. kV_{p-p} and 9 kV_{p-p} for several values of the precursor flow rate (F_d): a monotonical decrease of E_m as a function of F_d was observed for both the applied voltages.

ATR-FTIR spectra of coatings deposited under different precursor flow rates exhibit features consistent with the trend of E_m: as E_m decreases, the fragmentation of the precursor in the discharge is

reduced, and the conservation of the functional groups of the starting precursor (i.e. methyl groups) in the coating is higher. The DR of the deposited coatings, analyzed through profilometry, is coherent as well since a higher degree of crosslinking and densification usually follow a higher fragmentation of the precursor in the discharge. The promising results obtained by correlating the E_m values to the characteristics of the deposited coatings support the validity of the methodology.

To verify the importance of the parasitic effects in the circuit on the energy values, the results from the methodology were compared to those derived from the Lissajous method, whose circuit typically does not include parasitic components. It is shown that, while the methodology leads to energy values which can plausibly interpreted according to the properties of the coatings, the ones from the Lissajous method are too large to be physically meaningful. The comparison with the Lissajous method is an encouraging confirmation of the potentialities of the methodology developed for APPJs.

4.6 References

[1] R. Morent, N. De Geyter, T. Jacobs, S. Van Vlierberghe, P. Dubruel, C. Leys, and E. Schacht, "Plasma-polymerization of HMDSO using an atmospheric pressure dielectric barrier discharge," *Plasma Process. Polym.*, vol. 6, no. SUPPL. 1, pp. 537–542, 2009, doi: 10.1002/ppap.200931101.

[2] U. Lommatzsch and J. Ihde, "Plasma polymerization of HMDSO with an atmospheric pressure plasma jet for corrosion protection of aluminum and low-adhesion surfaces," *Plasma Process. Polym.*, vol. 6, no. 10, pp. 642–648, 2009, doi: 10.1002/ppap.200900032.

[3] J. Petersen, R. Bechara, J. Bardon, T. Fouquet, F. Ziarelli, L. Daheron, V. Ball, V. Toniazzo, M. Michel, A. Dinia, and David Ruch, "Atmospheric plasma deposition process: A versatile tool for the design of tunable siloxanes-based plasma polymer films," *Plasma Process. Polym.*, vol. 8, no. 10, pp. 895–903, 2011, doi: 10.1002/ppap.201100022.

[4] J. Pulpytel, V. Kumar, P. Peng, V. Micheli, N. Laidani, and F. Arefi-Khonsari, "Deposition of organosilicon coatings by a non-equilibrium atmospheric pressure plasma jet: Design, analysis and macroscopic scaling law of the process," *Plasma Process. Polym.*, vol. 8, no. 7, pp. 664–675, 2011, doi: 10.1002/ppap.201000121.

[5] B. Nisol, H. Gagnon, S. Lerouge, and M. R. Wertheimer, "Energy of Reactions in Atmospheric-Pressure Plasma Polymerization with Inert Carrier Gas," *Plasma Process. Polym.*, vol. 13, no. 3, pp. 366–374, 2016, doi: 10.1002/ppap.201500068.

[6] R. Morent, N. De Geyter, S. Van Vlierberghe, P. Dubruel, C. Leys, and E. Schacht, "Organic-inorganic behaviour of HMDSO films plasma-polymerized at atmospheric pressure," *Surf. Coatings Technol.*, vol. 203, no. 10–11, pp. 1366–1372, 2009, doi: 10.1016/j.surfcoat.2008.11.008.

[7] A. S. Meshkova, Y. Liu, F. M. Elam, S. A. Starostin, M. C. M. van de Sanden, and H. W. de Vries, "The role of the gradient film properties in silica moisture barriers synthesized in a roll-to-roll atmospheric pressure plasma enhanced CVD reactor," *Plasma Process. Polym.*, vol. 15, no. 1, pp. 1–10, 2018, doi: 10.1002/ppap.201700093.

[8] J. Petersen, J. Bardon, A. Dinia, D. Ruch, and N. Gherardi, "Organosilicon coatings deposited in atmospheric pressure townsend discharge for gas barrier purpose: Effect of substrate temperature on structure and properties," *ACS Appl. Mater. Interfaces*, vol. 4, no. 11, pp. 5872–5882, 2012, doi: 10.1021/am3015229.

[9] D. P. Dowling, C. E. Nwankire, M. Riihimäki, R. Keiski, and U. Nylén, "Evaluation of the anti-fouling properties of nm thick atmospheric plasma deposited coatings," *Surf. Coatings Technol.*, vol. 205, no. 5, pp. 1544–1551, 2010, doi: 10.1016/j.surfcoat.2010.10.010.

[10] A. Fidalgo and L. M. Ilharco, "The defect structure of sol-gel-derived silica/polytetrahydrofuran hybrid films by FTIR," *J. Non. Cryst. Solids*, vol. 283, no. 1–3, pp. 144–154, 2001, doi: 10.1016/S0022-3093(01)00418-5.

[11] S. A. Starostin, M. Creatore, J. B. Bouwstra, M. C. M. Van De Sanden, and H. W. De Vries, "Towards roll-to-roll deposition of high quality moisture barrier films on polymers by atmospheric pressure plasma assisted process," *Plasma Process. Polym.*, vol. 12, no. 6, pp. 545–554, 2015, doi: 10.1002/ppap.201400194.

[12] H. Sanaeishoar, M. Sabbaghan, and F. Mohave, “Synthesis and characterization of micro-mesoporous MCM-41 using various ionic liquids as co-templates,” *Microporous Mesoporous Mater.*, vol. 217, pp. 219–224, 2015, doi: 10.1016/j.micromeso.2015.06.027.

[13] X. Zhu, F. Arefi-khonsari, C. Petit-etienne, and M. Tatoulian, “Open Air Deposition of SiO_2 Films by an Atmospheric Pressure Line-Shaped Plasma,” *Plasma Process. Polym.*, pp. 407–413, 2005, doi: 10.1002/ppap.200400049.

[14] B. Shokri, M. A. Firouzjah, and S. I. Hosseini, “FTIR analysis of silicon dioxide thin film deposited by metal organic-based PECVD,” *Proc. 19th Int. Plasma Chem. Soc.*, pp. 1–4, 2009.

[15] J. Fang, L. Zhang, D. Sutton, X. Wang, and T. Lin, “Needleless Melt-Electrospinning of Polypropylene Nanofibres,” *Journal of nanomaterials*, vol. 2012, pp. 1–9, 2012, doi: 10.1155/2012/382639.

[16] M. T. Kim, “Deposition behavior of hexamethydisiloxane films based on the FTIR analysis of Si-O-Si and Si-CH_3 bonds,” *Thin Solid Films*, vol. 311, no. 1–2, pp. 157–163, 1997, doi: 10.1016/S0040-6090(97)00683-4.

[17] F. Babonneau, K. Thorne, and J. D. Mackenzie, “Dimethyldiethoxysilane/Tetraethoxysilane Copolymers: Precursors for the Si-C-O System,” *Chemistry of Materials*, no. 10, pp. 554–558, 1989.

[18] J. H. Yim, V. Rodriguez-santiago, A. A. Williams, T. Gougousi, D. D. Pappas, and J. K. Hirvonen, “Atmospheric pressure plasma enhanced chemical vapor deposition of hydrophobic coatings using fluorine-based liquid precursors,” *Surf. Coat. Technol.*, vol. 234, pp. 21–32, 2013, doi: 10.1016/j.surfcoat.2013.03.028.

[19] S. Zanini, E. Grimoldi, and C. Riccardi, “Development of controlled releasing surfaces by plasma deposited multilayers,” *Mater. Chem. Phys.*, vol. 138, no. 2–3, pp. 850–855, 2013, doi: 10.1016/j.matchemphys.2012.12.070.

[20] P. J. Launer, “Infrared analysis of organosilicon compounds: spectra-structure correlations,” *Silicon Compd. Silanes Silicones*, 2013, doi: 10.1080/01919519008552219.

[21] G. B. Alers, D. J. Werder, and Y. Chabal., “Intermixing at the tantalum oxide/silicon interface in gate dielectric structures,” *Appl. Phys. Lett.*, vol. 73, no. 11, pp. 1517–1519, 1998, doi: 10.1063/1.122191.

[22] F. Massines and G. Gouda, “A comparison of polypropylene-surface treatment by filamentary, homogeneous and glow discharges in helium at atmospheric pressure,” *J. Phys. D. Appl. Phys.*, vol. 31, no. 24, pp. 3411–3420, 1998, doi: 10.1088/0022-3727/31/24/003.

[23] Z. Fang, T. Shao, J. Yang, and C. Zhang, “Discharge processes and an electrical model of atmospheric pressure plasma jets in argon,” *Eur. Phys. J. D*, vol. 70, no. 1, 2016, doi: 10.1140/epjd/e2015-60437-4.

[24] J. Mertens, J. Baneton, A. Ozkan, E. Pospisilova, B. Nysten, A. Delcorte, F. Reniers, “Atmospheric pressure plasma polymerization of organics: effect of the presence and position of double bonds on polymerization mechanisms, plasma stability and coating chemistry,” *Thin Solid Films*, vol. 671, no. December 2018, pp. 64–76, 2019, doi: 10.1016/j.tsf.2018.12.036.

[25] J. Golda, B. Biskup, V. Layes, T. Winzer, and J. Benedikt, “Vacuum ultraviolet spectroscopy of

cold atmospheric pressure plasma jets," *Plasma Process. Polym.*, vol. 17, no. 6, 2020, doi: 10.1002/ppap.201900216.

[26] D. Magni, C. Deschenaux, C. Hollenstein, A. Creatore, and P. Fayet, "Oxygen diluted hexamethyldisiloxane plasmas investigated by means of in situ infrared absorption spectroscopy and mass spectrometry," *J. Phys. D. Appl. Phys.*, vol. 34, no. 1, pp. 87–94, 2001, doi: 10.1088/0022-3727/34/1/315.

[27] D. Hegemann, *Plasma Polymer Deposition and Coatings on Polymers*, vol. 4. Elsevier, 2014.

[28] F. Massines, C. Sarra-Bournet, F. Fanelli, N. Naudé, and N. Gherardi, "Atmospheric pressure low temperature direct plasma technology: Status and challenges for thin film deposition," *Plasma Process. Polym.*, vol. 9, no. 11–12, pp. 1041–1073, 2012, doi: 10.1002/ppap.201200029.

[29] T. C. Manley, "The electric characteristics of the ozonator discharge," *Trans. Electrochem. Soc.*, vol. 84, no. 1, p. 83, 1943.

[30] F. Peeters and T. Butterworth, "Electrical diagnostics of dielectric barrier discharges," in *InTech*, no. Atmospheric Pressure Plasma - From Diagnostics to Applications Figure, 2018, p. 27.

[31] A. V. Pipa, J. Koskulics, R. Brandenburg, and T. Hoder, "The simplest equivalent circuit of a pulsed dielectric barrier discharge and the determination of the gas gap charge transfer," *Rev. Sci. Instrum.*, vol. 83, no. 11, 2012, doi: 10.1063/1.4767637.

[32] A. V. Pipa and R. Brandenburg, "The equivalent circuit approach for the electrical diagnostics of dielectric barrier discharges: The classical theory and recent developments," *Atoms*, vol. 7, no. 1, 2019, doi: 10.3390/atoms7010014.

Chapter 5

Conclusions and future perspectives

This PhD thesis is focused on the control strategies for a polymerization process assisted by an atmospheric pressure (AP) single electrode plasma jet. After a general overview on the plasma polymerization process (Chapter 1) and a description of the motivations behind this PhD project (Chapter 2), two main sections are presented, each related to an in-depth investigation of one specific control strategy.

In Chapter 3, a study of the validity of the Yasuda parameter (W/FM) as controlling parameter in the polymerization process assisted by the plasma jet and an aerosolized fluorinated silane precursor is proposed. The chemical and physical properties of thin films deposited under different W/FM values are characterized by means of attenuated total reflectance – Fourier transform infrared (ATR-FTIR) spectroscopy, X-ray photoelectron spectroscopy (XPS), water contact angle (WCA) measurements, and scanning electron microscopy (SEM). The results of the surface characterization techniques suggest the presence of two deposition domains as varying W/FM: one leading to coatings with chemical composition and wettability that do not change with W/FM, the other leading to coatings with higher retention of functional groups of the starting precursor (such as CH_x and CF_x, x = 1,2,3) and higher hydrophobicity as W/FM progressively decreases. The plot of the normalized deposition rate as a function of W/FM reveals that the two deposition domains observed can be associated with two regimes very well known in literature (the energy-deficient domain and the monomer-deficient domain), thus suggesting the validity of W/FM as controlling parameter in this process. In addition, the key role of the Yasuda parameter in the process is further demonstrated since coatings deposited under the same W/FM exhibit similar properties, regardless of how W/FM is obtained.

Despite the validity of W/FM as controlling parameter in this AP process has been proven, it must be pointed out that the calculated W/FM values cannot be used to make proper reasonings on the fragmentation of the precursor molecules in the discharge. First, the Yasuda parameter implicitly assumes that the entire power coupled to the discharge (whose measurement, additionally, is far from trivial) is provided to the precursor molecules. While this idea well applies to LP plasma polymerization processes, where the precursor is often introduced undiluted in the discharge, the same cannot be said for AP processes, where the precursor constitutes exclusively a minimum part of the feed mixture. Moreover, the energy exchanges in presence of aerosolized precursors, instead of gaseous or vaporized ones, are even more complex and not completely explained to date, thus further questioning the energy values per precursor molecule which can be derived from the Yasuda parameter. Nonetheless, under specific conditions, the use of W/FM can still be a good option for controlling the process and guiding it towards the production of coatings with tailored characteristics.

In Chapter 4, the development of a methodology for measuring the energy of reactions in the polymerization process assisted by the plasma jet driven by a sinusoidal power supply and from the vaporized precursor HMDSO is presented. The values of energy per precursor molecule (E_m) are calculated through the identification and resolution of a proper equivalent electrical circuit which models also the presence of parasitic effects. It is demonstrated that, as the precursor flow rate increases, a

monotonical decrease of E_m is observed. To validate the methodology, these E_m values are correlated to the chemical and physical properties of deposited thin films assessed by means of ATR-FTIR spectroscopy and profilometry. These analyses reveal that coating characteristics are consistent with the observed trend in the energies per molecule: as E_m decreases, the fragmentation of the precursor is less intense, and coatings with higher conservation of the functional groups of the starting precursor (i.e. methyl groups) and higher deposition rate can be obtained. Furthermore, these energy values can be reasonably used to gather information on the fragmentation of the precursor molecule in the discharge since they are in the same order of magnitude of the bond energies in the molecule. To verify the importance of the parasitic effects in the circuit on the obtained energy values, the results from the methodology are compared to those derived from the Lissajous method, a known method for the calculation of the energy dissipated in the discharge (whose standard equivalent circuit does not include the parasitic effects). It is shown that, while the methodology leads to E_m values which can plausibly interpreted according to the properties of the coatings, the values provided by the Lissajous method are too large to be physically meaningful.

Overall, the correlation between the energy values and the characteristics of the coating and the comparison with the Lissajous method emphasize the potentialities of this methodology developed for atmospheric pressure plasma jets (APPJs). Nevertheless, some considerations are needed also in this case. Firstly, the presented methodology has not been tested yet for precursors with different chemical composition or physical state, hence further investigations still need to be performed in this perspective. Moreover, to apply the methodology also to other kind of power supplies (e.g. pulsed ones), a change of approach in the processing of the signals would be required. Finally, it must be highlighted that the application of this methodology is not straightforward since both a thorough study of the electrical characteristics of the specific plasma source and the use of a complex code to process the data are necessary. However, the greater resolution complexity is a good compromise to obtain more reliable energy per molecule values, which can be used to advance the comprehension of the entire plasma polymerization process.

According to the results obtained in this thesis, it can be inferred that both the discussed control strategies for the polymerization process assisted by an APPJ can be helpful in depositing coatings with tailored characteristics. The Yasuda parameter has a more transversal character since, at least in principle, it can be applied in a straightforward manner to all the AP polymerization setups (the type of power supply, the plasma source, the chemical structure, and the physical state of the precursor are not taken into account). Nonetheless, as pointed out earlier in the text, its validity as controlling parameter needs to be tested on a case-by-case basis. Once validated, it still must be considered that the values of energy per molecule cannot be used to interpret the fragmentation mechanisms but exclusively to have a qualitative interpretation of the phenomena in the discharge. For this reason, it can be said that the control which can be reached at AP using the Yasuda parameter is a “coarse” control. Despite being “coarse”, this kind of control can still be accurate enough to identify the region of interest which leads to coatings

with properties suitable for the specific application. Furthermore, for those processes where it is proven that coatings deposited under similar W/FM exhibit similar properties, it is possible to obtain coatings with the desired properties by adopting the less expensive solution in terms of electrical and precursor consumption. This aspect certainly represents an attractive point from an industrial perspective. On the other hand, the methodology proposed in this work requires a more in-depth analysis of the electrical aspects related to plasma the polymerization process but leads to more reliable values of energy per molecule. Thanks to this methodology, a finer control of the process can be enabled and reasonings on the fragmentation of the precursor molecule can be performed, thus increasing the possibility to gather specific information about PP reactions. In a future perspective, the proposed methodology can help to shed the light on some of the mechanisms involved in the complex polymerization process assisted by APPJs, also for power supplies different from the sinusoidal ones and aerosolized precursors. As a final remark, it must be stressed that both control strategies could be combined with other plasma diagnostic techniques in order to obtain a more robust comprehension of the process.

To conclude, this thesis provides useful insights into the control of polymerization processes assisted by atmospheric pressure plasma jets, which can be valuable to support the advancing of the understanding of these unique processes and promote their implementation at industrial level. Furthermore, it highlights the potentialities of these processes along with the scientific open points, thus stimulating the research in this field.

Acknowledgments

The enthusiasm of performing a successful experiment after weeks of failures, the satisfaction of presenting the results of your research activities at international schools and conferences, the pleasure to collaborate with extremely valuable people from the academic and non-academic world, the emotion of living from the other side of the world for 4 months, the opportunity to teach to students and help them in discovery science... this is what I see when I look back to my PhD journey. These three years have been one of the most intense chapters of my life, which made me grow in a way I never imagined from a working and personal point of view. If there is a thing I clearly understood in these years is that, as control strategies are crucial for a successful plasma polymerization process, people that surround you are crucial for a successful PhD. Many great people took part to my PhD and the end of the last thesis of my life looks like a nice place where to thank them all. Be prepared because what follows is basically a second thesis!

The first person I would like to thank is my supervisor-since-the-master-degree Professor Matteo Gherardi. Thank you, Matteo, for all the times that, without even realizing it, we turned what was supposed to be a quick meeting in a discussion about science of hours and hours, for inspiring me to never stop asking questions, for always being present and available to listen to my ideas, for introducing me to all the aspects of the academic life, for your love for irony and puns. You had a key role in defining the researcher I am now, and I could never really ask for a better supervisor.

Talking about supervisors, I would take the opportunity to express my full gratitude also to my "supervisors overseas" Professors Michael Wertheimer and Stephan Reuter, who warmly welcomed me in their research group during my 4 months abroad at the Polytechnique Montréal (Canada). Thank you for your great kindness, for actively taking part to the challenging project related to the energy measurements in plasma jets, for transmitting to me your love for science, for sharing with me your precious experience and knowledge. It was a real pleasure working with you and the months in Montréal will be forever in my hearth. If I have such a nice memory of my period in Montréal, part of the merit is for sure also of my "Lab mate overseas" Sean Watson. Thank you, Sean, for being one of the politest people I've ever met, for being always available to help me during my Lab activities, for all the lunches we had together, for our long but always fruitful discussions about science and PhD life, for making every day in the laboratory enjoyable.

Since my master's degree, I spend my days in Via Terracini 24, in the Lab of the Research Group for Industrial Applications of Plasmas (IAP Group). The "Lab" has always been special for me: it represented a safe and peaceful place when in the past my world outside was falling apart and represents everyday a super dynamic and stimulating environment. But for sure it's not the walls and the instrumentation to make this place so unique… it's the people who work there: the members of the IAP Group.

If I think to the IAP Group, the first who comes to my mind is Professor Vittorio Colombo. Thank you, Prof, for creating such a great group, for your always interesting point of views, for your ability to stimulate people in doing their better, for demonstrating to me that, in science as in literature, is the enthusiasm that you put in things that makes the difference. Your charism and expertise are the reasons why in 2018 I decided that the plasma technology was fascinating and basically the reasons why I joined the IAP Group. I can't thank you enough for that.

But there are many other people which I would like to thank.

Thank you, Romolo, for the time spent together in front of the scanning electron microscope, for proving me how much commitment and passion it takes to teach students, for showing me the strength of working in a team, but, most of all, thank you for being the Number 1 Fan of my husky-puns.

Thank you, Filippo and Pasquale. You are the sun rays in the darkest days, the pleasant silence when the heating system is turned off in the Tesla Lab, the fresh beer after a day of work, the hot dish of "tortellini in brodo" on a cold winter day. Thank you for our continuous laughs, for the uncountable breakfasts together, for our love for betting on everything, for our trips to the train station, for the high-quality beach volleys, for always giving me a sincere opinion whether it was about science or about other, for all the times that a glance is enough to understand each other. You are the best colleagues I could ask for.

Thank you, Cristiana, for being my companion during these three years. We started this journey together and we close it together. As they say, what is most important is not what we find at the end, but what we do feel during the journey. And of our journey I will never forget our photos together at the beginning of each year, our long discussions about cytokines, your annual gift to me of writing the email for activating the badge to have access to the Lab, our laughs about my adventures in the life, our update calls from Canada to Spain at crazy times. Thank you.

Thank you, Roberto, for your self-irony and your genuine enthusiasm, for the super cheap soups we ate together in Szczecin, for always catching my quotes from the Ciclone movie. If you are like this, it's definitively because you were born in Torino but then you moved to Empoli.

I would like to also thank the youngest PhD students of the IAP Group: Andrea, Mariachiara, and Caterina. It's a pleasure to see how well you already are integrated into the group. Your sense of humor, your brightness, your projects on challenging topics are an incredible added value for our group and I am sure you'll enjoy this PhD experience as much as I did.

As a mentioned before, the lab is a dynamic environment… and as new people have recently joined the group, others have left it over the years to start another adventure.

Thank you, Alina, for all the "torte salate col porro" that you prepared for the group in these years, for always helping me in the Lab stuff whenever I needed it, for our shared talent of losing things, for being my great ping pong mate in Slovakia. I did not yet fully realize that you are not in the Lab anymore, but I am sure that your new job will give you a lot of satisfactions and amazing experiences.

Thank you, Federica, Emanuele, and Tommaso. You are the people I bonded with the most when I arrived in the Lab for my master thesis. Thank you for explaining to me how to behave in a research lab, for supporting me when I was doing my first experiments, for transmitting to me your love for research, for being always present when I needed some advice, for participating with me to wonderful conference which has been ISPC24 in Naples. Few years ago, our working paths have separated but continuing to be part of your lives is wonderful.

But we know, a PhD is not just unicorns and rainbows: it's not giving up after weeks of unsuccessful experiments, it's being responsible of your own activities and of those of the students which are assigned to you, it's working on the weekend to meet the deadlines, and much more. A PhD requires sacrifice, perseverance… but mostly people outside the workplace who can support you by making you think of something different than the work or by listening to your lab stories or by just being there.

And outside the workplace for me during these years there were definitively Pola e Saglio. Thank you, my beloved Palette, for our holidays together, for being the persons to which I could talk about everything, for our love for trash songs and fat food (especially before dinner). We've been through so many hilarious adventures that another thesis would not be sufficient to mention them all ("With what!?!?!?"). Thank you for always being a constant and crucial presence in my life.

Thank you, Devis, for all the times that while drinking at the bar or from the other side of the world with 6 hours of time zone you carefully listened to my doubts about electrical circuits and solved them. You are absolutely the most brilliant and fun teacher of electrotechnics that I've ever met. I owe you one!

Thank you, Lonfi. You are the most crazy and solid group of friends that I've ever had. Thank you for all the nights spent together "da Nelson", for the birthday dinners, for the fun we have together after all these years. It is great to see how we still do care of each other even we are all growing and finding our way in the world. I really couldn't ask for better friends.

Coming to an end, I think that I am missing in the list the family squad, which was fundamental more than anyone else in these years. So, here we are.

Thank you, Stefania, for being the smartest and strongest woman (but also teacher, cook, plumber, electrician, thermo-technical…) that I know, for your curiosity in wanting to know how my PhD life was going when I came home after a week of work, for always giving me useful and wise advices in every aspect of life, for having transmitted to me wonderful gifts like stubbornness, irony… and ability to lose everything. You've always been a brilliant mother.

Thank you, Mattia e Laura, for being my first supporters since the times of my bachelor's degree, for the quality time we spend together during summer at San Benedetto del Tronto, for visiting me in Canada when I was doing my research period abroad. It's hard to believe that when I took your picture together at the Belvedere in Mont Royal (and also when I brought you to eat tons of parsley at the Lebanese restaurant…ops!) you were already three. The future is bright, and I couldn't be happier to become Aunt Giulia.

Thank you, Tommy, for being my favorite person in the world. You are the one who knows that I am going to say a sad joke before I even opened my mouth, the one I want to tell what happened to me during the day once back home, and the one who helps me in looking at things from the right perspective. In these three years you supported me in ways I could never imagined, from giving me feedback on what I had written (you should thank me: you are almost a plasma expert now!), to taking care of me and leaving me space when I was overloaded of things to do, to making special every activity we organized in our free time. Thank you for all the places we visited, for all the restaurants we tried, for all the Lego Sets we assembled, for all the escape rooms we played, but most of all… for those French fries we ate at 550 m at the top of the CN tower in Toronto. This PhD, as my entire life, would certainly not have been the same without you.

To all the people that I've met during this journey, the friends, the family members who I did not mention: a huge thank you.

Now it's really time to conclude: I swear this is the very end. Like a famous book writer, I would like to dedicate this PhD thesis to my Dad. He is no longer with us, but I am pretty sure that he would have laughed a lot in these three years: when I tried to screw plastic screws for the first time, when I burst out laughing during AlmaOrienta seeing a sign with the inscription BRAVI TUTTI, when I hardly worked to create the "Asporto del venerdì" tradition in the Lab, when I lost my subway pass in Montréal after 5 minutes I bought it, when I left my trolley (with my poster inside) on the train directed to Frankfurt once I got off in Erfurt for a conference…